New Astronomy Reviews 80 (2018) 1–28

Contents lists available at ScienceDirect

New Astronomy Reviews

journal homepage: www.elsevier.com/locate/newastrev

The State-of-Play of Anomalous Microwave Emission (AME) research

Clive Dickinson[*,a], Y. Ali-Haïmoud[b], A. Barr[a], E.S. Battistelli[c], A. Bell[d], L. Bernstein[e], S. Casassus[f], K. Cleary[g], B.T. Draine[h], R. Génova-Santos[i,j], S.E. Harper[a], B. Hensley[g,k], J. Hill-Valler[l], Thiem Hoang[m], F.P. Israel[n], L. Jew[l], A. Lazarian[o], J.P. Leahy[a], J. Leech[l], C.H. López-Caraballo[p], I. McDonald[a], E.J. Murphy[q], T. Onaka[d], R. Paladini[r], M.W. Peel[s,a], Y. Perrott[t], F. Poidevin[i,j], A.C.S. Readhead[g], J.-A. Rubiño-Martín[i,j], A.C. Taylor[l], C.T. Tibbs[u], M. Todorović[v], Matias Vidal[f]

[a] Jodrell Bank Centre for Astrophysics, School of Physics and Astronomy, The University of Manchester, Oxford Road, Manchester, Manchester, M13 9PL, UK
[b] Center for Cosmology and Particle Physics, Department of Physics, New York University, New York, NY, 10003, USA
[c] Sapienza, University of Rome, Italy
[d] Department of Astronomy, Graduate School of Science, The University of Tokyo, Tokyo, 113-0033, Japan
[e] Spectral Sciences Inc., 4 Fourth Ave, Burlington, MA, 01803-3304, USA
[f] Universidad de Chile, Santiago, Chile
[g] California Institute of Technology, Pasadena, CA, 91125, USA
[h] Princeton University Observatory, Peyton Hall, Princeton, NJ, 08544-1001, USA
[i] Instituto de Astrofisíca de Canarias, 38200 La Laguna, Tenerife, Canary Islands, Spain
[j] Departamento de Astrofísica, Universidad de La Laguna (ULL), 38206 La Laguna, Tenerife, Spain
[k] Jet Propulsion Laboratory, Pasadena, CA, 91109, USA
[l] Sub-department of Astrophysics, University of Oxford, Denys Wilkinson Building, Keble Road, Oxford, OX1 3RH, UK
[m] Korea Astronomy and Space Science Institute, Daejeon, 305-348, Korea
[n] Sterrewacht, Leiden, The Netherlands
[o] Department of Astronomy, University of Wisconsin-Madison, 475 Charter St., Madison, WI, 53705, USA
[p] Instituto de Astrofísica and Centro de Astro-Ingeniería, Facultad de Física, Pontificia Universidad Católica de Chile, Av. Vicuña Mackenna 4860, 7820436 Macul, Santiago, Chile
[q] NRAO, USA
[r] Infrared Processing and Analysis Center, California Institute of Technology, Pasadena, California, USA
[s] Departamento de Física Matematica, Instituto de Física, Universidade de São Paulo, Rua do Matão 1371, São Paulo, Brazil
[t] Cavendish Laboratory, University of Cambridge, Madingley Road, Cambridge, CB3 0HA, UK
[u] Directorate of Science, European Space Research and Technology Centre (ESA/ESTEC), Noordwijk, The Netherlands
[v] University of South Wales, Wales, UK

ARTICLE INFO

Keywords:
Radiation mechanisms
Spinning dust
Diffuse radiation
Radio continuum
Cosmic microwave background
Interstellar medium

ABSTRACT

Anomalous Microwave Emission (AME) is a component of diffuse Galactic radiation observed at frequencies in the range ≈ 10–60 GHz. AME was first detected in 1996 and recognised as an additional component of emission in 1997. Since then, AME has been observed by a range of experiments and in a variety of environments. AME is spatially correlated with far-IR thermal dust emission but cannot be explained by synchrotron or free–free emission mechanisms, and is far in excess of the emission contributed by thermal dust emission with the power-law opacity consistent with the observed emission at sub-mm wavelengths. Polarization observations have shown that AME is very weakly polarized ($\lesssim 1$ %). The most natural explanation for AME is rotational emission from ultra-small dust grains ("spinning dust"), first postulated in 1957. Magnetic dipole radiation from thermal fluctuations in the magnetization of magnetic grain materials may also be contributing to the AME, particularly at higher frequencies ($\gtrsim 50$ GHz). AME is also an important foreground for Cosmic Microwave Background analyses. This paper presents a review and the current state-of-play in AME research, which was discussed in an AME workshop held at ESTEC, The Netherlands, June 2016.

[*] Corresponding author.
E-mail address: clive.dickinson@manchester.ac.uk (C. Dickinson).

https://doi.org/10.1016/j.newar.2018.02.001
Received 10 November 2017; Accepted 22 February 2018
Available online 23 February 2018
1387-6473/

1. Introduction

Anomalous Microwave Emission (AME) is a dust-correlated component of Galactic emission that has been detected by cosmic microwave background (CMB) experiments and other radio/microwave instruments at frequencies $\approx$ 10–60 GHz since the mid-1990s (Kogut et al., 1996; Leitch et al., 1997). It is thought to be due to electric dipole radiation from small spinning dust grains in the interstellar medium (ISM), although the picture is still not clear. The emission forms part of the diffuse Galactic foregrounds that contaminate CMB data in the frequency range $\approx$ 20–350 GHz, and hence knowledge of their spatial structure and spectral shape can be exploited during CMB component separation (Dunkley et al., 2009a; Bennett et al., 2003; Planck Collaboration et al., 2016b). Since spinning dust emission depends critically on the dust grain size distribution, the type of dust, and the environmental conditions (e.g., density, temperature, interstellar radiation field), precise measurements of AME can also provide a new window into the ISM, complementing other multi-wavelength tracers.

The first mention of spinning dust grains in the literature was by Erickson (1957), who proposed this non-thermal emission as a contributor at high radio frequencies (GHz and above). The same basic mechanism of radio emission from rapidly spinning dust grains was also discussed by Hoyle and Wickramasinghe (1970) in the context of converting optical photons from stars into radio/microwave emission. Ferrara and Dettmar (1994) further developed the theory, estimating the contribution from radio-emitting dust in spiral galaxies. These earlier works outlined the basic mechanisms of how small dust grains with finite electric dipole moments can be spun up to high rotational frequencies, thus producing radio emission. They also understood that such emission would predominantly arise at relatively high frequencies. However, it was not until the late 1990s, after when observations detected excess emission at frequencies $\approx$ 10–60 GHz (Section 3), that detailed predictions of spinning dust emission were made by Draine and Lazarian (1998a,b). The field of AME research then became important, particularly since AME was known to be a significant CMB foreground (Section 4). Magnetic dust emission (MDE) on the other hand had not been discussed in the literature until the seminal work of Draine and Lazarian (1999) who proposed it as an alternative to spinning dust.

In this article, we provide a comprehensive review the state-of-play of AME research. For a previous review, see Dickinson et al. (2013) and articles within. Section 2 provides an overview of the theory of spinning dust, magnetic dust, and other emission mechanisms that may be contributing to AME. Observations of AME are summarised in Section 3. Section 4 discusses AME as a CMB foreground while in Section 5 we discuss various methodologies and goals for future research. Concluding remarks are made in Section 6. This article is partially an outcome of the discussions at the AME workshop[1] held 22–23 June 2016 at ESTEC (Noordwijk, The Netherlands). Previous AME workshops were held at Manchester[2] in 2012 and at Caltech[3] in 2013.

2. Models of candidate AME mechanisms

2.1. Spinning dust

2.1.1. Basic theory

A dust grain with electric or magnetic dipole moment μ rotating with angular frequency ω will produce emission according to the Larmor formula

$$P = \frac{2}{3}\frac{\omega^4 \mu^2 \sin^2\theta}{c^3}\,, \tag{1}$$

where P is the total power emitted at frequency $\nu = \omega/2\pi$ and θ is the angle between ω and μ. A schematic diagram of a single dust grain is shown in Fig. 1. It is immediately evident that the spinning dust emission spectrum will depend sensitively on the distribution of rotational frequencies attained by the grains as well as their distribution of dipole moments. Indeed, much of the theoretical modelling efforts have been toward accurate calculation of the distribution of rotation rates as a function of grain size and composition in various interstellar environments.

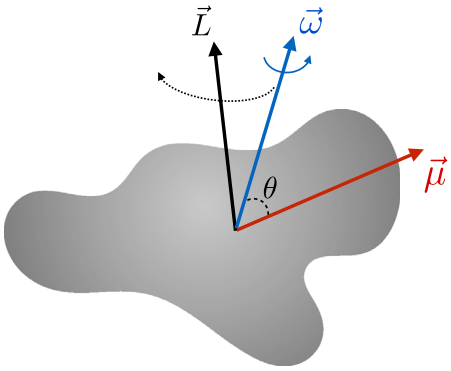

Fig. 1. Schematic spinning dust grain, with its permanent electric dipole moment $\vec{\mu}$, its instantaneous angular velocity $\vec{\omega}$, and its angular momentum $\vec{L}$, about which $\vec{\omega}$ precesses.

A spherical grain of radius a and mass density ρ rotating thermally in gas of temperature T will have a rotational frequency of

$$\frac{\omega}{2\pi} = 21\,\mathrm{GHz}\left(\frac{T}{100\,\mathrm{K}}\right)^{1/2}\left(\frac{\rho}{3\,\mathrm{g\,cm^{-3}}}\right)^{-1/2}\left(\frac{a}{5\,\text{Å}}\right)^{-5/2}. \tag{2}$$

To emit appreciably in the 20–30 GHz range as required to reproduce the observed AME, the grains must be very small, $a \lesssim 1$ nm.

2.1.2. Rotational dynamics

An interstellar dust grain is subject to a number of torques arising from its interactions with the ambient interstellar matter, which can both excite and damp rotation. Collisions with ions and neutral atoms, photon emission, H_2 formation, photoelectric emission, and interaction with the electric fields of passing ions ("plasma drag") have all been identified as contributing to grain rotation. The distribution of grain rotational velocities will generally be non-thermal resulting from the interplay of a number of different excitation and damping processes, including collisions with atoms and ions, and absorption and emission of radiation. Systematic torques (i.e., torques that do not have a time average of zero in grain coordinates), and impulsive torques (i.e., impacts that produce large fractional changes in the grain angular momentum) can be important.

Draine and Lazarian (1998b) presented the first comprehensive model of spinning dust emission taking most of these processes into account. For simplicity, they assumed $\langle\omega^4\rangle = 5/3\langle\omega^2\rangle^2$, consistent with a Maxwellian distribution. Recognizing that ultrasmall grains could simultaneously furnish an explanation for AME and the infrared emission bands, they focused their analysis on electric dipole emission from PAHs.

Ali-Haïmoud et al. (2009) improved on the treatment of the rotational dynamics by employing the Fokker–Planck equation to compute the angular velocity distribution. Notably, they found significantly less power in the tails of the distribution, particularly toward high values of

[1] http://www.cosmos.esa.int/web/ame-workshop-2016/schedule.
[2] http://www.jb.man.ac.uk/~cdickins/Man_AMEworkshop_July2012.html.
[3] https://wikis.astro.caltech.edu/wiki/projects/ameworkshop2013/AME_Workshop_2013.html.

Table 1
Key developments in the theory of spinning dust emission with associated references.

Development	Reference
First proposal for electric dipole radiation from spinning dust grains	Erickson (1957)
First full treatment of spinning dust grain theory	Draine and Lazarian (1998b)
Quantum suppression of dissipation and alignment	Lazarian and Draine (2000)
Factor of two correction in IR damping coefficient	Ali-Haïmoud et al. (2009)
Fokker–Planck treatment of high-ω tail	Ali-Haïmoud et al. (2009)
Quantum mechanical treatment of long-wavelength tail of PAHs	Ysard and Verstraete (2010)
Rotation around non-principal axis	Hoang et al. (2010); Silsbee et al. (2011)
Transient spin-up events	Hoang et al. (2010)
Effect of tri-axiality on rotational spectrum	Hoang et al. (2011)
Effects of transient heating on emission from triaxial grains	Hoang et al. (2011)
Magnetic dipole radiation from ferromagnetic spinning dust	Hoang and Lazarian (2016a); Hensley and Draine (2017)
Improved treatment of quantum suppression of dissipation and alignment	Draine and Hensley (2016)

ω, relative to a Maxwellian. Theoretical emissivity[4] curves, as a function of frequency, can be calculated using the publicly available[5] SPDUST code, written in the Interactive Data Language (IDL).[6] Ysard and Verstraete (2010) presented a quantum mechanical analysis of the grain excitation and damping processes, finding good agreement with classical models. Hoang et al. (2010) and Silsbee et al. (2011) further refined models of the rotational dynamics by considering asymmetric grains that rotate about a non-principal axis, incorporating this into the updated SPDUST2 code.

Both studies concluded that this grain "wobbling" could increase both the peak[7] frequency and the emissivity of the spinning dust emission spectrum. Additionally, Hoang et al. (2010) computed the angular velocity distribution via the Langevin equation, which, unlike the approach based on the Fokker–Planck equation, can account for impulsive torques. Subsequent improvements accounting for the effects of irregular grain shapes, stochastic heating, and emissivity enhancements due to compressible turbulence were made by Hoang et al. (2011). Table 1 lists the most important developments in spinning dust theory and the associated references.

Fig. 2 shows spinning dust spectra for various phases (environments) of the interstellar medium: cold neutral medium (CNM), warm neutral medium (WNM), warm ionized medium (WIM), molecular clouds (MC), dark clouds (DC), reflection nebulae (RN), and photodissociation regions (PDR). The curves were produced using the SPDUST2 code using the same parameters used by Draine and Lazarian (1998b) for idealized phases of the ISM; these are listed in Table 2 for seven representative environments. These include the gas density $n_{\rm H}$, gas temperature T, dust temperature T_d, strength of the interstellar radiation field χ, and the fraction of molecular hydrogen y, ions of hydrogen $x_{\rm H}$, and heavier ions $x_{\rm M}$. Other inputs include the dust size distribution and electric dipole moments (amongst others). The spectra can be compared with the original curves presented by Draine and Lazarian (1998b), which are similar but are slightly different in detail, due to enhancements to the code already mentioned. One can see that a peaked shape spectrum is always produced, but with considerable variations in both emissivity (by almost 2 orders of magnitude) and peak frequency ($\approx$ 30 GHz to over 100 GHz). The strongest signals and higher peak frequencies are typically produced by the densest environments, such as in PDRs and molecular clouds.

The physics of spinning dust emission is thus very well-established, with numerous mechanisms affecting the rotational velocity distribution of interstellar grains having been worked out in detail (see for example the review by Ali-Haïmoud, 2013). The primary limitation with making a theoretical prediction of the spinning dust spectral energy distribution (SED) is not the current understanding of the various excitation and damping mechanisms, but rather by the unknown sizes, dipole moments, charges, and shapes of ultra-small interstellar grains.

Table 2
Environmental parameters for various idealized phases of the ISM, as was done by Draine and Lazarian (1998a) (see text). These parameters were used to produce the emissivity curves in Fig. 2.

Parameter	Phase						
	DC	MC	CNM	WNM	WIM	RN	PDR
$n_{\rm H}$ (cm^{-3})	10^4	300	30	0.4	0.1	10^3	10^5
T (K)	10	20	100	6000	8000	100	300
T_d (K)	10	20	20	20	20	40	50
χ	0.0001	0.01	1	1	1	1000	3000
$y \equiv 2n({\rm H}_2)/n_{\rm H}$	0.999	0.99	0	0	0	0.5	0.5
$x_{\rm H} \equiv n({\rm H}^+)/n_{\rm H}$	0	0	0.0012	0.1	0.99	0.001	0.0001
$x_{\rm M} \equiv n({\rm M}^+)/n_{\rm H}$	10^{-6}	0.0001	0.0003	0.0003	0.001	0.0002	0.0002

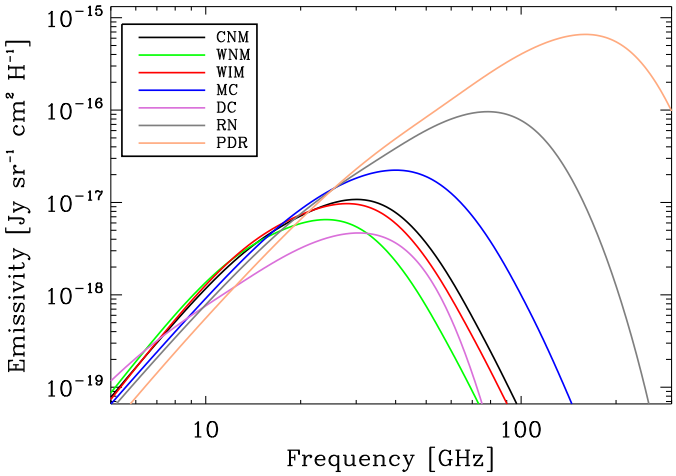

Fig. 2. Spinning dust emissivity curves as a function of frequency for different idealized phases of the interstellar medium (see text). The curves were produced using the SPDUST2 code, with parameters given in Table 2, which can be compared with the original curves presented by Draine and Lazarian (1998b).

[4] The term "emissivity" is usually defined as how well a body radiates relative to a blackbody. However, in astronomy it is used in a number of situations, including how much radiation is emitted per unit volume (or column density) as in spinning dust emissivity curves. Later, it will be used in the context of the emissivity law of dust grains (how well dust grains emit as a function of frequency) and also in terms of AME emissivities or correlation coefficients (AME brightness relative to various dust templates).

[5] http://cosmo.nyu.edu/yacine/spdust/spdust.html.

[6] http://www.harrisgeospatial.com/ProductsandTechnology/Software/IDL.aspx.

[7] The peak frequency strictly depends on whether flux density or brightness temperature is used (they are related by a factor of $1/\nu^2$). For AME, we will typically discuss the peak in flux density units at $\approx$ 30 GHz. In brightness temperature units the spinning dust spectrum does not have a clear peak; instead it has an inflection point, which turns over at $\approx$ 16 GHz.

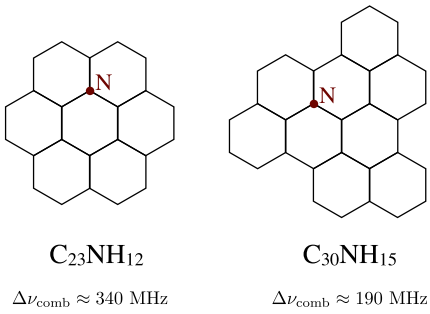

Fig. 3. Examples of two nitrogen-substituted symmetric PAHs that remain quasi-symmetric after substitution, i.e., their two smallest moments-of-inertia differ by less than a few percent. Such molecules are the target of AME searches. $\Delta\nu_{comb}$ indicates the approximate line spacing of their comb-like rotational spectrum. Figure reproduced from Ali-Haïmoud et al. (2015).

2.1.3. Line emission

An interesting consequence of the spinning-PAH model is the possibility of rotational *line* emission (Ali-Haïmoud, 2014). The rotational quantum numbers of spinning PAHs are typically of order ~ 100 (Draine and Lazarian, 1998b), large enough for a classical treatment to be accurate, but small enough for discrete rotational line transitions to be potentially distinguishable. The observability of individual transitions depends on two criteria.

The first criterion is the diversity of PAH species carrying the emission: if a very large number of species are present in small abundances, their individual rotational spectra may be buried in the quasi-continuum total emission. Ali-Haïmoud (2014) argued that it is likely that a few select, highly stable PAH species are more resistant to the harsh ISM conditions, making them over-abundant. This "grandPAH" hypothesis, first put forward by Tielens (2013), was recently studied more quantitatively by Andrews et al. (2015). These authors showed that available infrared data suggest that a limited number of compact, highly symmetric PAHs dominate the interstellar PAH family.

The second criterion for the observability of PAH lines is the degree of symmetry of the emitting molecules: large triaxial molecules have complex rotational spectra, with many weak individual transitions, making them impractical for spectroscopic identification. On the other hand, perfectly symmetric PAHs, such as coronene ($C_{24}H_{12}$) or circumcoronene ($C_{54}H_{18}$), which are likely to be among the "grandPAHs", have no permanent dipole moment hence no rotational emission. Ali-Haïmoud (2014) argued that Nitrogen substitution, a process likely to lead to large dipole moments in interstellar PAHs (Hudgins et al., 2005), breaks the symmetry of the moment-of-inertia matrix by a small enough amount that the rotational spectrum has the appearance of a "comb" of intense lines if observed with a resolution of ~ 1 MHz. Fig. 3 shows two possible symmetric PAHs that may be responsible for part of the AME and their approximate line spacing. The spacing of the "teeth" of the comb is inversely proportional to the moment of inertia of the carrier, hence providing a clear discriminative test of individual PAHs. The comb pattern moreover allows for blind searches with matched filtering.

Ali-Haïmoud et al. (2015) performed an observational test of this idea by taking a spectrum of the Perseus molecular cloud at 25 GHz, over a 3 GHz bandwidth and with a 0.4 MHz resolution. They matched-filtered the spectrum to search for comb patterns, though did not make a detection, and set upper limits on the abundance of individual PAHs assuming that the AME from Perseus is entirely due to spinning PAHs. A detection of PAH lines would not only be a smoking-gun signature of the spinning PAH hypothesis, but would also provide the long-awaited identification of specific planar PAHs.

2.1.4. Non-PAH carriers

Each of the aforementioned studies focused on electric dipole emission from PAHs, which are known to be a significant component of interstellar dust due to their prominent mid-infrared features. Hensley et al. (2016) found no correlation between PAH emission fraction (presumably proportional to PAH abundance) and AME emission fraction (presumably proportional to AME carrier abundance). As a result, there has been interest in other potential carriers of spinning dust emission. The spinning dust theory developed for PAHs is equally applicable to nanoparticles of other compositions that have electric (or magnetic) dipole moments and thus most of the predictions based on models of spinning PAHs hold for other carriers.

Hoang and Lazarian (2016b) and Hensley and Draine (2017) considered spinning dust emission arising from the rotation of a *magnetic* dipole in interstellar iron grains. Both studies concluded that such particles may constitute a portion of the observed AME, but that constraints on the solid-phase abundance of interstellar iron preclude a population of such particles large enough to account for the entirety of the observed emission. Rotational emission from nanosilicate grains was considered by Hoang et al. (2016) and Hensley and Draine (2017), who determined that such grains could account for the entirety of the observed emission without violating other observational constraints provided that the grains have a suitable electric dipole moment.

2.1.5. Polarization

Electric (or magnetic) dipole emission from a single rotating grain is perfectly polarized. Thus, the spinning dust emission spectrum could be highly polarized if the ultrasmall grains, which carry the emission, are substantially aligned. However, the interstellar polarized extinction law is observed to drop rapidly in the UV with decreasing wavelength (e.g., Martin et al., 1999). Thus, on empirical grounds, it appears that the smallest grains are not systematically aligned, leading to a low level of polarization.

The physics of grain alignment is complex (for a review see e.g., Andersson et al., 2015). Small grains could attain alignment via paramagnetic relaxation as proposed by Davis and Greenstein (1951). However, paramagnetic relaxation may be suppressed at high rotation frequencies. Further, Lazarian and Draine (1999) argued that thermal flipping prevents ultrasmall grains from achieving suprathermal rotation, and so collisions with gas atoms would destroy this alignment on short timescales. Nevertheless, the very smallest grains with extremely rapid rotation rates could potentially align via "resonance relaxation" in which the rotational splitting of energy levels becomes important (Lazarian and Draine, 2000). If ultrasmall grains are able to align in this way, then spinning dust emission could be polarized at roughly the percent level (Lazarian and Draine, 2000). Hoang et al. (2013) argued that the weak polarization in the 2175 Å feature observed along two sight-lines towards HD 197770 and HD 147933-4 could be explained with weakly-aligned PAHs, and computed that the corresponding spinning dust emission from those PAHs would have a polarization fraction of $\lesssim 1\%$ for $\nu \gtrsim 20$ GHz. Hoang and Lazarian (2016b) calculated that iron nanoparticles would be highly aligned with the interstellar magnetic field due to their large magnetic susceptibilities, and that their rotational magnetic dipole radiation could be polarized at the 40–50% level.

Most recently, Draine and Hensley (2016) argued that the quantization of energy levels in ultrasmall grains would dramatically suppress the conversion of rotational kinetic energy to vibrational energy, thereby hindering all alignment processes dependent on this direct conversion. They calculated that spinning dust emission at $\nu \gtrsim 10$ GHz would be negligibly polarized with $P \lesssim 0.0001\%$ irrespective of the grain composition.

It should be noted that theoretical predictions of dust polarization are generally maximum values. The angle between the line-of-sight and the alignment axis, depolarization due to line-of-sight effects such as changing magnetic field direction, and contamination from other emission sources that may be polarized differently, may all contribute to a reduction of the polarization fraction in real observations. To mitigate some of these effects, it may be useful to compare the observed

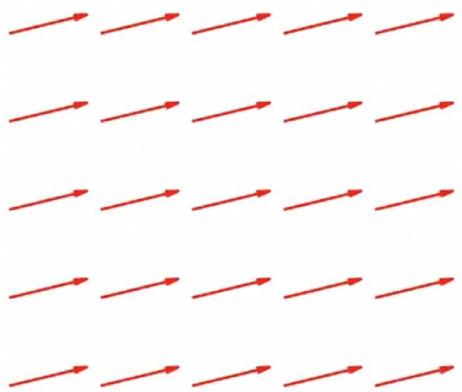

Fig. 4. Schematic representation of the electron spins within a ferromagnetic grain aligned along some preferred, energy-minimizing direction. Excitations cause the net magnetization to precess about this preferred direction, as illustrated in the animation (*electronic version only*), eventually relaxing back into alignment with this direction. The precession of the magnetization gives rise to radiation.

AME polarization (or upper bounds on it) to the observed thermal dust polarization in the same region– regions with the highest observed polarization fractions for thermal dust emission would likely have the highest spinning dust polarization fractions.

A unique way to test physics of nanoparticle alignment is through the polarization of infrared PAH emission. Theoretical calculations by Hoang (2017) found that, if PAHs are aligned with the magnetic field by paramagnetic resonance mechanism, their mid-IR emission can be polarized at a few percent for the conditions of reflection nebulae. The first detection of polarized PAH emission at 11.3 μm from the MWC 1080 nebula was recently reported by Zhang et al. (2017). The measured polarization of 1.9 ± 0.2% is much larger than the value predicted by the models with randomly oriented PAHs. PAH alignment with the magnetic field to $\sim 10\%$ can successfully reproduce this measurement. Therefore, further theoretical and observational studies in this direction are needed to achieve a convincing conclusion on the polarization of spinning dust.

In summary, if quantum effects suppress dissipation in grains spinning at $\gtrsim 10$ GHz, as suggested by Draine and Hensley (2016), the polarization from spinning dust grains is likely to be very small ($\ll 1\%$) and difficult to detect. Detailed further observations are required to confirm that this is the case.

2.2. Magnetic dust (MDE)

2.2.1. Basic theory

Most of the interstellar iron resides in dust (Jenkins, 2009), and iron inclusions (see Fig. 5) have been observed in both interplanetary dust

Fig. 5. Metallic iron inclusions may be found embedded in non-magnetic interstellar grains in much the same way that chocolate chips are embedded in chocolate chip cookies, as shown.

(Bradley, 1994) and putative interstellar grains collected in the Solar System (Westphal et al., 2014; Altobelli et al., 2016). While the chemical form of the iron in interstellar grains is unknown, it is plausible that some is in the form of magnetic materials such as ferromagnetic metallic Fe or ferrimagnetic magnetite (Fe_3O_4) or maghemite (γ-Fe_2O_3). In such materials, the spins of unpaired electrons are spontaneously ordered, giving rise to a net magnetization even in the absence of an applied field. Thermal fluctuations can excite the magnetization away from its preferred, energy-minimizing direction. As the magnetization precesses and relaxes back to the minimum energy state, radiation is emitted (see Fig. 4). Unlike spinning dust emission (see Section 2.1), the emission is thermal and is not associated with physical rotation of the grain.

Draine and Lazarian (1999) put forward the first model of thermal magnetic dipole radiation in the context of interstellar dust and as a possible explanation of the AME. They modelled the magnetic response as a damped harmonic oscillator following Morrish (2001) and noted the possible existence of a resonance feature in the absorption spectrum near 70 GHz, a magnetic analogue of a Fröhlich resonance. They concluded that magnetic materials exhibiting this resonance behaviour could possibly furnish an explanation for the entirety of AME.

Draine and Hensley (2013) revisited the dynamics of the magnetic response by employing the phenomenological Gilbert equation (Gilbert, 2004), which explicitly accounts for the precession of the electron spins, to model the time evolution of the magnetization, and resulting magnetic dipole radiation. They found that magnetic grains can produce strong, relatively grey emission from sub-millimetre to millimetre wavelengths and so could account for the apparent excess emission observed in some low-metallicity dwarf galaxies and the Small Magellanic Cloud (SMC) (Draine and Hensley, 2012). Absorption resonances associated with the precession frequency of the magnetization were also predicted between 1–30 GHz, depending on the shape of the grain. In particular, extremely elongated grains (e.g., spheroids with axial ratios greater than 2:1) exhibit resonances at $\nu \gtrsim 20$ GHz, which can more closely mimic the observed AME spectrum.

The magnetic behaviour of materials in the microwave is still poorly understood, and so direct laboratory measurements of the materials of interest in this frequency range would be of great value. We outline several key experimental tests of relevance to AME theory in Section 5.5.

2.2.2. Polarization

The polarization properties of magnetic materials depend strongly on whether they are free-flying grains or whether they are inclusions in larger, non-magnetic grains.

Draine and Lazarian (1999) and Draine and Hensley (2013) demonstrated that perfectly aligned free-flying iron nanoparticles could achieve polarization fractions of $\simeq 30\%$. Hoang and Lazarian (2016b) calculated the alignment efficiency of magnetic particles as a function of size, finding that large grains (≥ 1 nm) are poorly aligned whereas smaller grains attained high degrees of alignment and could produce emission polarized at up to 10–30% levels. Draine and Hensley (2016) showed that particles larger than ~ 2 nm could be partially aligned; if ferromagnetic, thermal emission from such particles could be linearly polarized at the percent level.

In the case of magnetic inclusions within a larger non-magnetic grain, the polarized emission depends both on the alignment of the grain and on the relative importance of the magnetic dipole emission from the inclusions and the electric dipole emission from the matrix of atoms, which are polarized orthogonally with respect to each other (Draine and Hensley, 2013). For randomly oriented magnetic inclusions in a silicate matrix, Draine and Hensley (2013) found a drop in the polarization fraction beginning at $\simeq 10^3$ GHz (300μm) and extending to lower frequencies as the magnetic dipole emission becomes comparable to the emission from the silicate material. At low frequencies (~ 10 GHz), the polarization can even undergo a reversal, provided the magnetic Fe

fraction is large enough. Thus, in the frequency range where both magnetic dipole emission and electric dipole emission from the grain are important ($\simeq$10–100 GHz), the polarization fraction of the emission is low ($\lesssim$5%). Hoang and Lazarian (2016a) investigated the alignment efficiency of grains with magnetic inclusions due to radiative torques, finding that the enhanced magnetic susceptibility due to the inclusions enabled the grain to achieve nearly perfect alignment. Thus, the polarization fraction of the emission from large grains with magnetic inclusions is likely limited only by the degree to which the magnetic dipole and electric dipole emission processes are self-cancelling.

2.3. Other emission mechanisms?

Although spinning dust and magnetic dust have received the most attention as possible explanations of AME, other mechanisms may still contribute a fraction, or even all, of the observed emission. We now briefly review some of these possibilities.

Thermal emission from interstellar grains can be written as $\epsilon(\nu)B(\nu, T)$, where $\epsilon(\nu)$ is the emissivity (= 1 for a black-body radiator) and $B(\nu, T)$ is the Planck function for a black-body at temperature T. The emissivity $\epsilon(\nu)$ is sometimes approximated as a power-law, $\epsilon(\nu) \propto \nu^{\beta_d}$ (see e.g., Draine, 2011; Martin et al., 2012). For spherical grains of radius a and internal density ρ, the emissivity is directly related to the opacity, $\kappa(\nu)$ of the dust grains, via $\epsilon(\nu) = (4\rho a/3)\kappa(\nu)$. The far-infrared opacity of nanoparticles of amorphous materials is notoriously difficult to both calculate theoretically and measure in the laboratory. As these frequencies are much lower than the known resonances in the UV and optical, it is typically assumed that the opacity should be decreasing as a power-law with $\kappa \propto \nu^{\beta_d}$ with $\beta_d = 2$. However, amorphous materials exhibit a range of β_d values depending on their composition and temperature (e.g., Agladze et al., 1996). Current measurements show a range of values depending on environment and nature of the emission, but are typically in the range $\beta_d = 1$–2, with an average value at high Galactic latitude of $\beta_d \approx 1.6$ (Planck Collaboration et al., 2014b). Given the current limited knowledge of the microwave properties of amorphous materials, it is conceivable that some materials could have an absorption resonance in the vicinity of 30 GHz and thus explain AME via thermal dust emission. However, this seems unlikely and contrived, especially given how well the simple power-law model has worked so far, to explain the low-frequency Rayleigh-Jeans (R-J) tail of thermal dust at frequencies above $\approx$ 100 GHz (e.g., Planck Collaboration et al., 2014b). Furthermore, there are good theoretical reasons[8] to assume that $\beta_d \geq 1$.

Jones (2009) suggested that AME could arise from conformational changes in groups of atoms within amorphous, low-temperature grains. If this resonant tunnelling component is associated with sub-micron-sized grains, the AME should show a good correlation with the FIR emission. They argued that the Two Level System model (TLS; Phillips, 1973; Meny et al., 2007) of this phenomenon could reproduce the general shape of the AME spectrum. However, upper limits on AME polarization require that any grains with enhanced microwave emissivity be randomly-oriented, whereas observations by *Planck* show that a substantial fraction of the sub-mm emission from dust comes from grains that are aligned (Planck Collaboration et al., 2015a). Upper limits on AME polarization are thus not supportive of large grains as the origin of AME. Jones (2009) pointed out an alternative possibility that resonant tunnelling may be associated with stochastically-heated very small grains, since they spend much of their time at low temperatures, where resonant tunnelling becomes important (Meny et al., 2007). In this case a good correlation of AME with the mid-infrared excess emission (20–60 μm) is expected. Low-temperature laboratory measurements of those materials at microwave frequencies are certainly needed to study the resonant tunnelling of these materials and draw a clear conclusion on this hypothesis.

Free–free emission from warm ionized gas could potentially contribute to excess emission above 10 GHz. Optically thin free–free emission has a well-defined spectrum that is very close to a $\beta = -2.1$ ($\alpha = -0.1$) power-law with very little variation with frequency (Draine, 2011). However, at high gas densities, the gas becomes optically thick at lower frequencies and the spectrum acts like a blackbody with a R-J spectrum ($\beta = 0$ or $\alpha = +2$) i.e., rising spectrum with frequency. This phenomena is well-known, for example, in ultracompact and hypercompact HII regions with densities of $\gtrsim 10^6$ cm^{-3} and higher, which can be optically thick up to frequencies of $\sim$ 15 GHz and higher (Kurtz et al., 1994; Kurtz, 2002, 2005); see also Dickinson (2013) for a review of AME from HII regions. However, this will only occur on small scales (typically arcsec) and along certain lines-of-sight, typically along the Galactic plane. For the majority of sight-lines across the sky, and at lower angular resolution, free–free emission is optically thin above 1 GHz. As a guide, the Orion nebula (M42) is one of the brightest diffuse HII regions, with an angular size of $\approx 5'$ and a density of $\approx 10^4$ cm^{-3} and has a turnover frequency of $\approx$ 1 GHz. Planck Collaboration et al. (2015b) evaluated the contribution of UCHII regions to the flux density as seen by WMAP and *Planck* on scales of 1° using IRAS colour ratios and high resolution 5 GHz data from the CORNISH survey (Purcell et al., 2013). They found that, for most sources in the Galactic plane, the contribution from optically thick free–free emission is minimal. The two best examples of spinning dust, Perseus and Ophiuchus, do not have substantial ongoing high-mass star formation and high resolution observations do not reveal any bright compact sources. Nevertheless, care must be taken to consider optically thick free–free emission when observing compact and dense regions.

Similarly, one can obtain a peaked synchrotron spectrum around the frequency of unit optical depth, but this requires extremely high brightness temperatures, $T_b \gg m_e c^2/k_B \sim 10^{10}$ K. In fact, if the peak is at $\approx$ 30 GHz, either the magnetic field must be far lower than typical values in the ISM, or T_b must be orders of magnitude higher. Given that the observed brightness of AME is of order mK at frequencies $\sim$ 30 GHz, this would have to be an artefact of extreme beam dilution; but high-resolution radio surveys show that the required population of compact sources peaking at 15–30 GHz does not exist. Nevertheless, AME at high Galactic latitudes is everywhere superposed on the diffuse Galactic synchrotron emission, which at $\nu > 10$ GHz can be fitted as a power-law with $\beta \approx -3$ or $\alpha \approx -1$ (e.g., Strong et al., 2011). In the frequency range 20–50 GHz where AME contributes significantly to the sky maps made by CMB experiments, in particular *WMAP* and *Planck*, synchrotron and AME spectra are usually indistinguishable, since the low-frequency tail of the AME spectrum is just out of range (see Fig. 6). This difficulty can clearly be seen in Fig. 6, which presents a summary of the separation of diffuse Galactic components on 1° scales covering 81–93% of the sky (Planck Collaboration et al., 2016b). A contributing factor to the degeneracy is that the synchrotron spectrum is not expected to have spatially-uniform spectral index, nor to be exactly a power-law. These are both rather minor effects: although maps of Galactic spectral index (e.g., Reich and Reich, 1988; Dickinson et al., 2009b) can sometimes show rather large variations in spectral index ($-2 > \beta > -3.5$)[9], these are largely due to (i) contamination by free–free emission, especially at low latitudes, and (ii) large uncertainties in

[8] According to the Kramer–Kronig relations, the real part of the dielectric constant χ of the interstellar medium is connected to an integral of the imaginary part (e.g., Tielens, 2010; Draine, 2011) as

$$\mathrm{Re}[\chi(0)] - 1 = \frac{2}{\pi}\int_0^\infty \mathrm{Im}[\chi(\nu)/\nu]d\nu \ .$$

The left-hand side is proportional to the total volume of interstellar dust (Purcell, 1969), and thus it must be finite. Then if $\mathrm{Im}(\chi) \propto \nu^{\gamma-1}$ for $\nu \to 0$, γ must be larger than zero. This can be translated to the index of the emissivity, β_d, at low frequencies being larger than unity.

[9] Brightness temperature spectral indices ($T_b \propto \nu^\beta$) are related to flux density spectral indices ($S \propto \nu^\alpha$) by $\beta = \alpha - 2$.

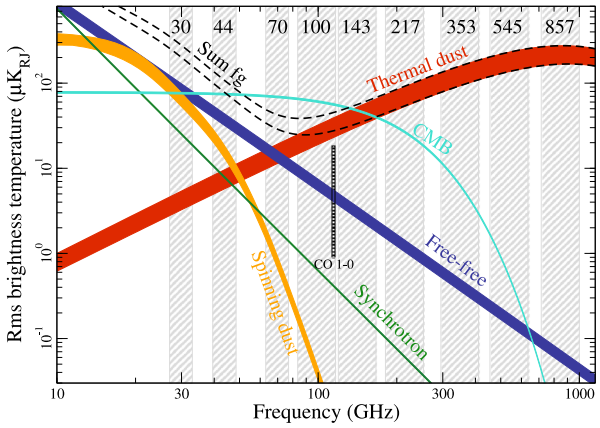

Fig. 6. Summary of the amplitude of intensity (temperature) foregrounds from the *Planck* component separation 2015 results; figure taken from Planck Collaboration et al. (2016b). The brightness temperature r.m.s. against frequency, on angular scales of 40′, is plotted for each component. The width of the curves represents the variation when using 81% and 93% of the sky.

the brightness near the minima of the all-sky synchrotron emission, due to uncertainties in the zero level. Residual variations in synchrotron β where neither of these effects are important are around $\pm$ 0.2 (e.g., Davies et al., 1996). The Galactic synchrotron spectrum steepens by about 0.4 between 1 and 10 GHz, but the models of Strong et al. (2011) suggest a return to power-law behaviour above this knee. Although models of the high-frequency AME spectrum are much more strongly curved than synchrotron, this is not a very useful discriminator because both components are rapidly swamped by CMB and thermal dust emission above about 70 GHz. This AME/synchrotron degeneracy accounts for the widely-divergent estimates of the fractional contribution of AME to the Galactic emission in the lowest-frequency *WMAP* and *Planck* bands. Nevertheless, the apparent lack of AME polarization (Section 3.4) suggests that synchrotron emission cannot account for the majority of AME.

In summary, other mechanisms including blackbody, synchrotron, free–free and various forms of thermal dust emission do not appear to be able to explain the majority of the AME. However, they should be considered carefully in case we are mis-understanding the emission mechanisms. Furthermore, they all contribute to the signal at some level, and therefore require accurate removal to accurately constrain AME.

3. Observations

In this section we briefly review the observational status of AME research. We begin by discussing observational results in intensity (temperature) on large scales (Section 3.1), where we mainly focus on data from CMB experiments operating on angular scales typically $\gtrsim 1^\circ$. We then move on to targeted observations of specific regions in Section 3.2, which are on angular scales typically $\lesssim 1^\circ$. We discuss extragalactic AME separately in Section 3.3 and then review current polarization constraints in Section 3.4. Section 3.5 presents a summary of the observational constraints and discusses their interpretation.

3.1. AME observations in intensity/temperature on large-scales

Until around the mid-1990s, sub-millimetre to centimetre radio emission from the Galaxy was thought to be understood, being a combination of (i) synchrotron radiation from cosmic-ray electrons spiralling in the Galactic magnetic field, (ii) free–free (thermal bremsstrahlung) emission from electrons scattering in warm ionized ($T \sim 10^4$ K) gas, and (iii) thermal (vibrational) emission from warm ($T \sim 20$ K) dust.

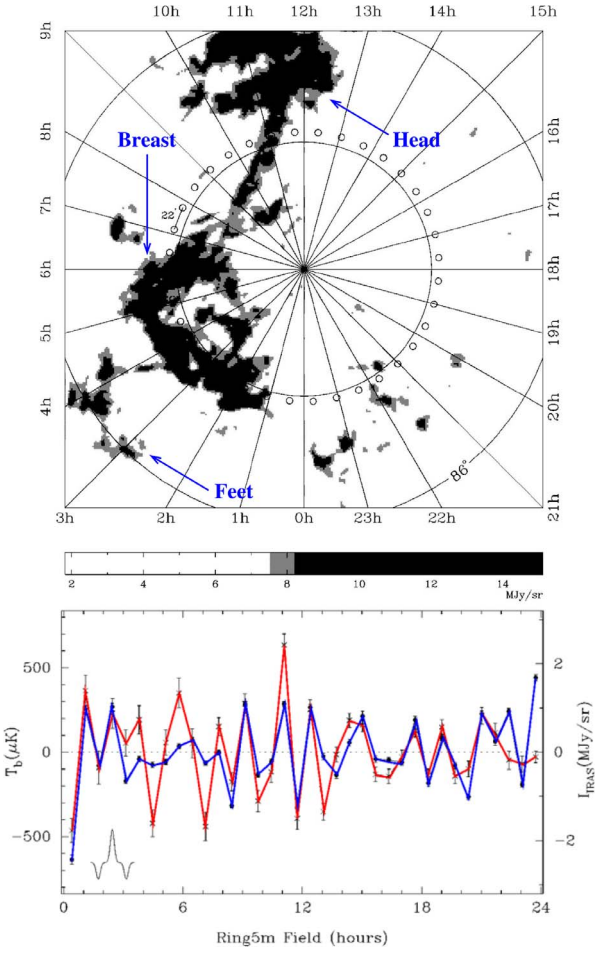

Fig. 7. *Top panel*: Far-IR 100 μm map of the NCP region. The major structure is sometimes referred to as "the duck" because of its similarity in shape. *Bottom panel*: 14.5 GHz data from the RING5M experiment (*blue*) plotted against the 100 μm map, after convolving with the triple-beam of the experiment, shown in the bottom left corner. The remarkable correlation of AME with dust emission at far-IR wavelengths is evident by eye. Figures reproduced and adapted from Leitch et al. (1997). (For interpretation of the references to colour in this figure legend, the reader is referred to the web version of this article.)

This simple picture has been complicated by mounting evidence for an additional component of emission at frequencies $\nu \sim 10$–100 GHz, spatially correlated with dust, but orders of magnitude stronger than any simple extrapolation of the thermal dust spectrum would predict. A widespread, dust-correlated component was detected in the *COBE*-DMR maps and attributed to a combination of thermal dust and free–free emission (Kogut et al., 1996). This interpretation could not be confirmed due to the lack of frequency bands and because full-sky Hα maps were still not available at that time.

The dust-correlated component was first discovered to be anomalous (and hence the term "anomalous microwave emission", or AME) by Leitch et al. (1997) at Caltech, who used the Owens Valley Radio Observatory (OVRO) 40-m and 5.5-m telescopes to observe the North Celestial Pole (NCP) region at 14.5 GHz and 32 GHz on angular scales 7–22′. They detected foreground emission that was spatially correlated with the 100 μm IRAS maps (Fig. 7) but with a microwave spectral index of $\beta \sim -2$, suggestive of free–free emission. Comparison with Hα maps of the NCP region showed that the observed signal was at least 60 times stronger than predicted free–free levels. Leitch et al. concluded that if it were free–free, it could only be emission from very hot ($T_e \gtrsim 10^6$ K) plasma. This explanation was suggested by the shock morphology of the NCP region but was subsequently shown to require implausibly high energy injection rates (Draine and Lazarian, 1998a).

Since then, "anomalous", dust-correlated emission has been seen in

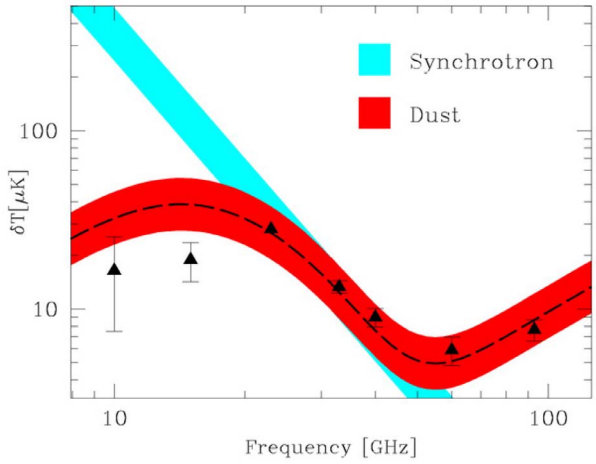

Fig. 8. Spectrum of foregrounds from WMAP data (22.8 GHz and above) and Tenerife data (10 and 15 GHz) from a template-fitting analysis at high latitudes ($|b| > 20^{\circ}$). The dust-correlated foreground appears to turn over at frequencies ≈ 15 GHz, supporting the spinning dust origin for AME. Figure taken from de Oliveira-Costa et al. (2004).

the Galaxy by numerous experiments aiming to detect CMB anisotropies. These include Saskatoon (de Oliveira-Costa et al., 1997), 19 GHz survey (de Oliveira-Costa et al., 1998), Tenerife (de Oliveira-Costa et al., 1999; Mukherjee et al., 2001), QMAP (de Oliveira-Costa et al., 2000), ACME/SP94 (Hamilton and Ganga, 2001), and Python V (Mukherjee et al., 2003), amongst others. These analyses largely relied on fitting of foreground templates to maps (Section 4), where the AME was extracted using a far-IR dust template, such as the 100 μm IRAS map. By employing multiple spatial templates for the synchrotron (low frequency data), free–free (Hα), thermal dust (FIR/IR) and CMB (the CMB data themselves), the various foreground components can be separated based on their spatial morphology. The results showed a strong, dust-correlated component of Galactic emission, that could not be easily explained by synchrotron, free–free, thermal dust or CMB radiation.

A joint analysis of *COBE*-DMR and 19 GHz data (Banday et al., 2003) provided a high S/N detection of AME through cross-correlation of foreground templates. A joint analysis of Tenerife 10/15 GHz data with *WMAP* (de Oliveira-Costa et al., 2002, 2004) showed the first evidence for a turnover at a frequency ≈ 15 GHz, supporting the spinning dust hypothesis. Fig. 8 shows the SED of diffuse emission in the high-latitude Tenerife "strip", which clearly shows the preference for a flattening and turnover of the spectrum at a frequency ≈ 15 GHz due to the mysterious "foreground X" (AME), which can be explained by spinning dust.

First results from the WMAP team using 1-year data suggested that a harder (flatter spectrum, $\beta \approx -2.5$) component of synchrotron radiation could account for AME (Bennett et al., 2003). However, their interpretation was different in later releases, where a spinning dust component was considered (e.g., Gold et al., 2011). Several other results using WMAP data showed further evidence for AME (Lagache, 2003; Finkbeiner, 2004; Dobler and Finkbeiner, 2008).

A comprehensive study of template fits to *WMAP* data was made by Davies et al. (2006). They analysed 15 regions, chosen by hand to be dominated by one specific component of either synchrotron/free–free/dust. Fig. 9 shows one of the dust-dominated regions that corresponds to the NCP region where AME was first identified (Fig. 7). The dust-correlated emission is easily discernible by eye while the other foregrounds (synchrotron traced by 408 MHz data and free–free traced by Hα data) do not correlate strongly with the K-band (22.8 GHz) data. Davies et al. (2006) also found that the brightness of the AME per unit thermal dust was remarkably constant (sometimes, confusingly, referred to as "emissivity"), with an average value of ≈ 10 μK at 30 GHz per MJy/sr at a wavelength of 100 μm. At 22.8 GHz the emissivity is ≈ 20 μK/(MJy/sr); see Table 3. This ratio varied by up to a factor of ≈ 2.5 across the sky when not including the Galactic plane, showing the apparent ubiquitous nature of AME, at least at high Galactic latitude. A more detailed work, covering 35 regions, was made by Ghosh et al. (2012). Miville-Deschênes et al. (2008) used WMAP polarization data to constrain the synchrotron spectral index and therefore separate the Galactic components, again showing a strong dust-correlated AME component.

Other large-scale data have been combined with WMAP data to extend the frequency range and improve component separation. Lu et al. (2012) re-analysed archival CMB data at 8 GHz and showed that an additional component of emission was required to explain the 23 GHz data. COSMOSOMAS data at 13–17 GHz also showed AME with a peaked spectrum around 22 GHz (Hildebrandt et al., 2007). Data from the ARCADE2 experiment at 3, 8 and 10 GHz gave a strong preference for an AME component that accounts for 40 ± 10% of the Galactic plane emission at 23 GHz (Kogut et al., 2011).

With the release of *Planck* data (Planck Collaboration et al., 2016a), a more complete picture of the spectrum of diffuse Galactic emission became available, particularly at higher frequencies. As well as the targeted analysis of the Perseus and Ophiuchus clouds (Planck Collaboration et al., 2011c), a separation of the interstellar medium components by "inversion" (Planck Collaboration et al., 2011a), which utilized multiple tracers including velocity-resolved line emission spectra thus allowing a 3-D separation to be made, showed the need for AME with an amplitude that meant that a substantial fraction (25 ± 5%) of the Galactic plane emission at 30 GHz was due to AME. A separate study of the Galactic plane components as seen by *Planck* estimated that ≈ 45% of the 30 GHz emission could be due to AME (Planck Collaboration et al., 2014c).

The *Planck* 2015 results included full-sky maps of AME based on a

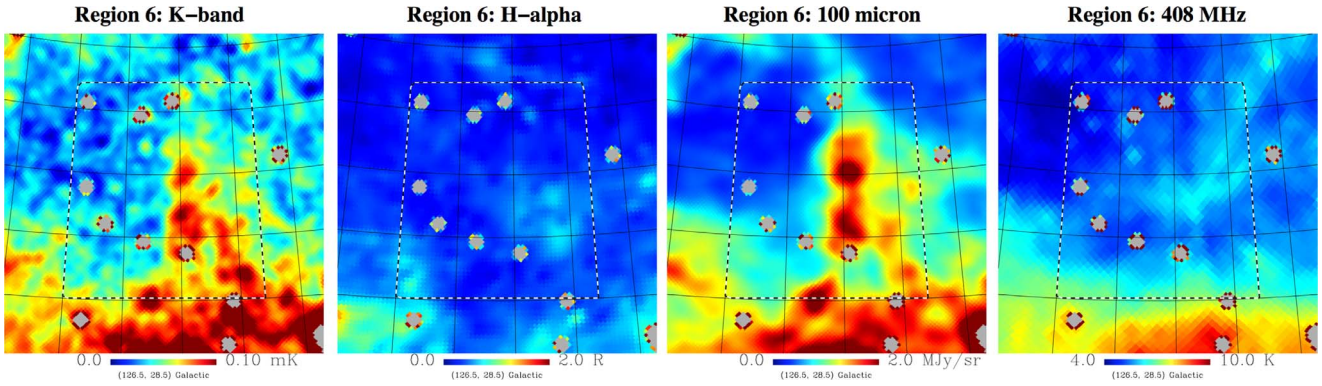

Fig. 9. Maps of a dust-dominated region centred at (l, b) = (126° 5, +28° 5), near the NCP region. From *left* to *right* are the WMAP K-band (22.8 GHz), Hα to trace free–free emission, 100 μm to trace dust emission and 408 MHz to trace synchrotron emission. All maps are smoothed to an angular resolution of 1°. There is a strong correlation of the 22.8 GHz data with dust but not the other foregrounds, indicating AME. Figure reproduced from Davies et al. (2006).

Table 3
Selected AME emissivities (correlation coefficients) at ≈ 20–30 GHz measured with various reference dust templates and regions of sky.

Sky region	Freq. (GHz)	AME emissivity	Units	Template	Reference
WMAP Kp2 mask (85% sky)	22.8	21.8 ± 1.0	μK/(MJy/sr)	100 μm (IRIS)	Davies et al. (2006)
$\|b\| > 10°$	22.8	21 ± 2	μK/(MJy/sr)	100 μm (IRIS)	Planck Collaboration et al. (2016d)
Perseus	22.8	24 ± 4	μK/(MJy/sr)	100 μm (IRIS)	Planck Collaboration et al. (2014d)
ρ Oph W	22.8	8.3 ± 1.1	μK/(MJy/sr)	100 μm (IRIS)	Planck Collaboration et al. (2014d)
32 source mean	22.8	32 ± 4	μK/(MJy/sr)	100 μm (IRIS)	Planck Collaboration et al. (2015b)
Diffuse HII regions	33	4.65 ± 0.40	μK/(MJy/sr)	100 μm (IRIS)	Todorović et al. (2010)
$\|b\| > 10°$	22.8	9.7 ± 1.0	10^6 μK	τ_{353} (*Planck*)	Planck Collaboration et al. (2016d)
Perseus	28.4	12.3 ± 1.2	10^6 μK	τ_{353} (*Planck*)	Planck Collaboration et al. (2014d)
ρ Oph W	28.4	23.9 ± 2.3	10^6 μK	τ_{353} (*Planck*)	Planck Collaboration et al. (2014d)
26% high latitude sky	30	7.9 ± 2.6	10^6 μK	τ_{353} (*Planck*)	Hensley et al. (2016)
$\|b\| > 10°$	22.8	70 ± 7	μK/(MJy/sr)	545 GHz (*Planck*)	Planck Collaboration et al. (2016d)
26% high latitude sky	30	6240 ± 1210	MJy/sr /(W/m^2/sr)	(*Planck*) ($\mathscr{R}$)	Hensley et al. (2016)
26% high latitude sky	30	271 ± 89	μK/(MJy/sr)	12 μm (WISE)	Hensley et al. (2016)

parametric SED-fitting algorithm (Planck Collaboration et al., 2016b). The fit included two AME components based on models of spinning dust with the SPDUST2 code (Ali-Haïmoud et al., 2009; Silsbee et al., 2011), one with a variable peak frequency and one with a fixed peak frequency (33.35 GHz). Two components with different peak frequencies are needed to account for the broadening of the total AME, presumably due to the presence of multiple components along the line-of-sight (which would inevitably broaden the spectrum compared to a single component model). Even using the latest *Planck, WMAP*, and ancillary data, the separation is known to be far from perfect. Due to degeneracies between parameters, caused by lack of frequency coverage particularly in the range ≈ 5–20 GHz, the data cannot always distinguish between the continuum components. The primary limitation was having to effectively fix the synchrotron spectrum in each pixel, and thus not fully accounting for spectral variations across the sky. Indeed, careful inspection of the component maps shows clear examples of aliasing of power between the various components, such as AME signal leaking into the free–free solution; see Planck Collaboration et al. (2016d) for a detailed discussion. Nevertheless, the same close correlation with dust was observed and with comparable emissivities to previous works. The emissivity defined by the thermal dust optical depth at a wavelength of 250 μm was shown to be more constant than previous estimates based on FIR brightness that was affected by variations in dust temperature (Tibbs et al., 2012b). The analysis also revealed more tentative evidence for a variable spinning dust peak frequency, where some pixels prefer a higher peak frequency. The peak frequency is typically near 30 GHz (in flux density), while some regions prefer a peak near 40–50 GHz. Such regions, including the California nebula, tend to be bright HII regions where the environment might lead to smaller and more rapidly spinning dust grains (Planck Collaboration et al., 2014d). However, as already mentioned, this requires independent confirmation given the complexity of component separation, particularly in the Galactic plane where the simple synchrotron spectral model is likely to be insufficient.

Hensley et al. (2016) examined the correlation of AME with the *Planck* 353 GHz optical depth τ_{353} and with total far-infrared radiance $\mathscr{R}$, also estimated from *Planck* data and analyses. For fixed dust size distribution, spinning dust models predict that AME should closely follow the total dust column ($\propto\tau_{353}$), but be relatively insensitive to variations in the starlight heating rate ($\propto \mathscr{R}/\tau_{353}$). Surprisingly, AME is more strongly correlated with $\mathscr{R}$ than with τ_{353}. The reason for this still remains unclear. Hensley et al. (2016) combined WISE 12 μm observations with $\mathscr{R}$ from IRAS and *Planck* to estimate the PAH abundance, which appears to show regional variations. They found that AME/$\mathscr{R}$ showed no correlation with estimated PAH abundance, suggesting that AME may be dominated by a source other than PAHs.

Various maps of Galactic dust emission have been used as spatial templates to both trace and estimate the relative brightness of dust-correlated AME. These include maps from COBE-DIRBE 100–240 μm (Banday et al., 2003), IRAS/IRIS 12–100 μm (Miville-Deschênes and Lagache, 2005; Ysard et al., 2010), combination dust model such as those of Finkbeiner et al. (1999), dust radiance (Hensley et al., 2016), and HI (Lagache, 2003) amongst others. As discussed by Finkbeiner (2004), comparisons of the various emissivity values as a function of different tracers and models has been quite confusing. Results based solely on data are easier to compare, such as the brightness in μK (or Jy/sr) per unit of MJy/sr at 100 μm, but are difficult to relate to theory. For example, Tibbs et al. (2012b) demonstrated that in warmer environments, such as HII regions, the 100 μm brightness is not a useful reference for the dust column since it varies dramatically with dust temperature. This may explain why AME in HII regions typically has a much lower (less than half) 100 μm emissivity than diffuse high-latitude emission (Dickinson, 2013) (see Table 3). Ysard et al. (2010) found that by dividing the 12 μm IRAS map by the intensity of the interstellar radiation field (G_0), a better correlation with AME was obtained on large scales, a result which has also been seen on small scales (e.g., Tibbs et al., 2011, 2012a); see Section 3.2.

Alternatively, one can choose physical properties as the AME emissivity reference, such as the column density (e.g., Jy sr^{-1} cm^2), which can (for example) be estimated from the optical depth of thermal dust emission (Planck Collaboration et al., 2014a), making it easier to compare with theoretical models (as in Fig. 2) and each other. As can be seen in Fig. 2, theoretical models yield values of $\sim 10^{-17}$ Jy sr^{-1} cm^2 at ≈ 30 GHz, although there is considerable scatter and these models are only indicative. Nevertheless, the observed emissivities are of order this level (e.g., Planck Collaboration et al., 2011c, 2014d, 2016d; Hensley et al., 2015). As an example, the mean value at high latitudes ($|b| > 15°$) of $\tau_{353}/N_{\rm H}$ is $\approx 7.3\times10^{-27}$ cm^2 (Planck Collaboration et al., 2014a) while typical observed AME emissivities are $\approx 8\times10^6$ μK/τ_{353} (Table 3). This corresponds to a brightness per unit column density of $\Delta T/N_{\rm H} \sim 6\times10^{-20}\mu$K cm^2 or 2×10^{-18} Jy sr^{-1} cm^2 at 30 GHz, which is of the same order as the theory values. Hensley et al. (2015) discuss that the observed emissivities are typically a few times 10^{-18} Jy sr^{-1} cm^2, slightly below the reference value, bringing theory and observation into better agreement. In a recent paper looking at the HI-$E(B-V)$ connection (Lenz et al., 2017), they derived $\tau_{545}/N_{\rm H} = 4.46\times10^{-26}$ cm^2. Assuming an emissivity index $\beta = +1.6$ (therefore $\tau^{1.6}$) gives 2.0×10^{-26} cm^2, which corresponds to an emissivity per τ_{353} of 1.5×10^8 Jy/sr or 5.4 K, which compares favourably to the observed values ∼ 8 K (Table 3).

In Table 3 we list a few selected AME emissivities at ≈ 23–33 GHz from the literature using various reference dust templates. It can be seen that diffuse AME emissivities have typical values of ≈ 20 μK/(MJy/sr) at 22.8 GHz relative to the 100 μm brightness (one of the most commonly used dust templates). At 30 GHz values are typically ≈ 6–10 μK/(MJy/sr). A sample of diffuse HII regions have a lower 100 μm emissivity (< 5 μK/(MJy/sr), presumably due to the higher dust temperatures that affects the 100 μm brightness; the lower value

for ρ Oph W region is also likely to be due to the warmer dust temperature (Planck Collaboration et al., 2015b). The AME emissivity relative to the optical depth at 353 GHz is $\approx 8 \times 10^6$ μK/τ_{353} for diffuse high latitude emission but is higher in the Perseus molecular cloud and, in particular, the ρ Oph W molecular cloud by a factor of ≈ 3. We also include the results from correlating with the *Planck* 545 GHz brightness, IRIS/WISE 12 μm brightness and the total dust radiance, $\mathscr{R}$, all of which have been found to be even more closely correlated with AME (Planck Collaboration et al., 2016d; Hensley et al., 2016).

On the other hand, deriving reliable column densities is difficult. First, it is model-dependent, which can make it difficult to make comparisons between different tracers. Thermal dust optical depths have been estimated at several common observing wavelengths, including 100 μm, 250 μm, and more recently with *Planck* data at 353 GHz ($\lambda = 850\,\mu$m). However, like many forms of AME emissivity, it is not straightforward to convert between the various estimates because one has to assume properties for the dust (e.g., temperature, emissivity index), while converting from a brightness at say 100 μm to an optical depth depends on empirical relations, which are known to be non-linear especially over the entire range of brightness/densities observed in the sky (Planck Collaboration et al., 2014a; Hensley et al., 2016). Second, observations of compact objects with large beams can result in artificially low values of intensity due to dilution within the beam, resulting in lower effective column densities. An example of this would be the analysis using WMAP/*Planck* using 2° diameter apertures (Planck Collaboration et al., 2014d), resulting in effective optical depths at 250 μm[10] (1200 GHz) of $\tau_{250} \sim 10^{-4}$, which corresponds to the optical depth at 353 GHz of $\tau_{353} \sim 10^{-5}$, which is below what would be expected at low latitude sight-lines ($\tau_{353} \gtrsim 10^{-4}$ typically). Ultimately, this means that one must be careful when comparing AME emissivities, particularly when using column densities. Trying to convert various observable quantities over a range of environments can lead to large (up to a factor of several) unphysical variations in AME emissivity. Nevertheless, the observed AME emissivities do appear to be the same order of magnitude across various analyses and regions in the sky and the associated column densities ($N_{\rm H}$) inferred from spinning dust models are consistent with expectations. We will discuss this further at the end of the next section.

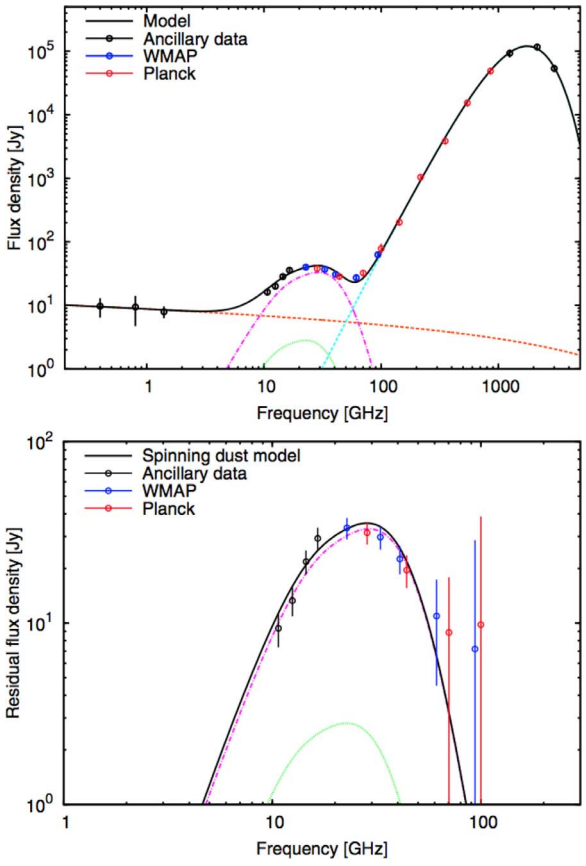

Fig. 10. The spectrum of G160.26–18.62 in the Perseus molecular cloud (*top*) and the residual spectrum showing the spinning dust component (*bottom*). The spectrum is fitted by components of free–free (*orange dashed line*), CMB (not visible), thermal dust (*dashed cyan line*) and spinning dust (*green dotted* and *magenta dot-dashed lines* for the atomic and molecular phases, respectively), which peaks at ≈ 30 GHz. The theoretical spectrum is a remarkably good fit to the data with parameters that are physically motivated. Reproduced from Planck Collaboration et al. (2011c). (For interpretation of the references to colour in this figure legend, the reader is referred to the web version of this article.)

3.2. AME on small ($\lesssim 1°$) scales

On smaller angular scales, typically on scales of $\lesssim 1°$, a number of dedicated observations have been made to study AME in more detail in specific environments and clouds.

The Green Bank 140ft telescope was used to observe 10 dust clouds at 5, 8, and 10 GHz (Finkbeiner et al., 2002). Using 1-D scans, a spectrum was estimated from 5 to 10 GHz. They found 8 with negative (falling with increasing frequency) spectral indices and 2 showing a rising spectrum, indicative of spinning dust. The first was the dark cloud LDN1622, which was confirmed later with 31 GHz data from the Cosmic Background Imager (CBI) (Casassus et al., 2006). The GBT 100-m telescope was also used to map the peak of the emission at 5 and 14 GHz, constraining the free–free emission and showing a rising spectrum from 14 to 31 GHz (Harper et al., 2015). The second source was the HII region LPH201.663 + 1.643. However, follow-up observations with the CBI at 31 GHz showed no significant excess above the expected free–free level (Dickinson et al., 2006); unpublished GBT follow-up observations (Doug Finkbeiner, priv. comm.) were also not able to reproduce the initial result. The Green Bank Galactic Plane survey was used to study the diffuse emission from the Galactic plane at 8 and 14 GHz (Finkbeiner et al., 2004). When combined with lower frequency data at 2.3 GHz and WMAP 1-year data, a rising spectrum between 8 and 14 GHz provided strong evidence for AME.

One of the most important AME detections was made towards the Perseus molecular cloud by the COSMOSOMAS experiment on angular scales of $\approx 1°$. Watson et al. (2005) combined COSMOSOMAS data at 11, 13, 17 and 19 GHz, with WMAP data to produce an AME spectrum that closely follows the prediction from spinning dust grains. This was the first time that a clear rise in the spectrum below the peak at ≈ 30 GHz had been seen, which is consistent with expectations for spinning dust. Planck Collaboration et al. (2011c) made a definitive detection by combining these data with *Planck* data, providing more data points and showing that the R-J tail of thermal dust emission was essentially negligible at frequencies ~ 30 GHz. More importantly, a physically-motivated spinning dust model, based on knowledge of the environment within the Perseus molecular cloud, provided an excellent fit to the data. Fig. 10 shows the spectrum of G160.26–18.62 on 1° scales, with synchrotron/free–free/spinning dust/thermal dust components shown. The spinning dust spectrum is a very high S/N detection and is well-fitted by 2 distinct components (low and high density), based on a plausible physical model.

Another important AME region is the ρ Ophiuchus molecular cloud. The first detection was made at 31 GHz with the CBI on arcmin scales, showing strong cm-emission associated with ρ Oph W PDR (Casassus et al., 2008). Fig. 11 shows large-scale multi-frequency maps of the region, where AME is clearly evident. Spectral modelling showed that the spinning dust model could comfortably fit the data. A more

[10] In Table 3 of Planck Collaboration et al. (2014d), the thermal dust optical depths at 250 μm are listed as multiplied by 10^5, when in fact they have been multiplied by 10^4. This results in all the τ_{250} values in their Table 3 being a factor 10 too small.

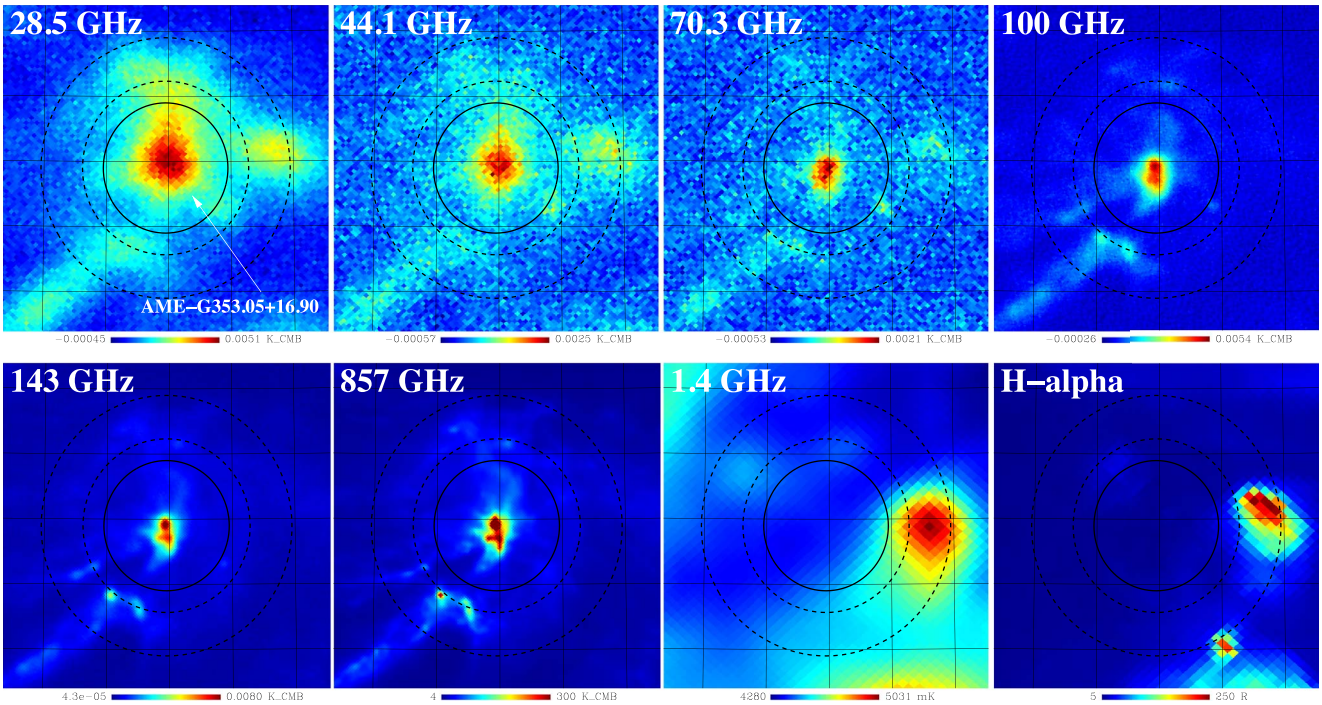

Fig. 11. Multi-frequency maps of the ρ Oph W molecular cloud region centred at (l, b) = (353.°05, +16.°90). From the *left* to *right*, from the *top* row: 28.5, 44.1, 70.3, 100, 143 and 857 GHz from *Planck*, 1.4 GHz and Hα. The maps cover 5° by 5° and the graticule has a 1° spacing. The strong AME at ≈ 20–40 GHz is evident. Note how the relatively weak HII region to the right of the main cloud is strong at low radio frequencies (1.4 GHz) and in Hα but is weak compared to AME at frequencies ≳ 20 GHz. Figure reproduced from Planck Collaboration et al. (2011c).

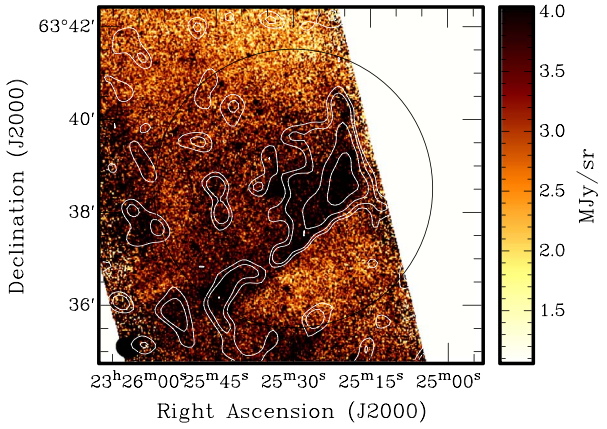

Fig. 12. AMI Large Array (AMI-LA) combined 16 GHz data shown as white contours at 1, 2, 4, 8σ of the local noise level. *Spitzer* band 4 (8 μm) map shown as greyscale in MJy/sr, saturated at both ends of the scale to emphasise the diffuse structure present. The correlation of the microwave emission with IR is evident. The AMI-LA primary beam (field-of-view) is shown as a circle and the synthesized beam (angular resolution FWHM) as a filled ellipse in the bottom left corner. Figure reproduced from Scaife et al. (2010a).

detailed picture was made with the WMAP and *Planck* data, which showed that a plausible physical model could easily explain the emission (Planck Collaboration et al., 2011c). Follow-up observations with ATCA (Casassus et al., in prep.) not only confirm the emission but, for the first time, shows a spatial shift of the spinning dust emission with frequency. This might be as expected from the varying dust properties across the PDR but requires detailed modelling. Nevertheless, this is potentially one of the strongest pieces of evidence for the spinning dust explanation.

A number of close-packed, microwave interferometers, operating either at ∼ 15 or ∼ 30 GHz, have been extensively used for AME research. In particular, the CBI at 26–36 GHz (Padin et al., 2002), the Very Small Array at 26–36 GHz (VSA; Dickinson et al. 2004), and the Arcminute Microkelvin Imager at 13–18 GHz (AMI; Zwart et al., 2008) have been used. Although they were primarily designed for CMB studies, their compact configuration resulted in good brightness sensitivities and resolutions of a few arcmin, ideal for AME research. The Combined Array for Research in Millimeter-wave Astronomy at 27–35 GHz (CARMA) has also been used.

Data from the CBI resulted in detections of AME from LDN1622 (Casassus et al., 2006) and LDN1621 (Dickinson et al., 2010), ρ Oph W (Casassus et al., 2008), the HII region RCW175 (Dickinson et al., 2009a; Tibbs et al., 2012a), the translucent cloud LDN1780 (Vidal et al., 2011), and the reflection nebula M78 (Castellanos et al., 2011). The CBI was used to refute the earlier claim of AME in the HII region LPH96 (Dickinson et al., 2006), which was shown to follow a normal optically-thin free–free spectrum. The CBI was also used to survey the brightest 6 HII regions in the southern sky (Dickinson et al., 2007) and two bright star-forming regions (Demetroullas et al., 2015), both finding little evidence for AME at 31 GHz. AME studies with the VSA revealed a flattening of the spectrum of the supernova remnant 3C396, which was interpreted as a possible signature of spinning dust. However, Cruciani et al. (2016) made follow-up observations with the Parkes 64-m telescope at 8–19 GHz and combined it with unpublished 31.2 GHz GBT data but found no evidence for AME.

The VSA was used to make a survey of the Galactic plane (l = 27°–46°, $|b| < 4°$) at 33 GHz with an angular resolution of 13′, finding an AME detection in RCW175 and statistical evidence of excess emission from the brightest sources in the sample (Todorović et al., 2010). The VSA was also used to perform the first detailed morphological analysis of AME in the Perseus cloud at 7′ resolution, identifying five regions of AME (Tibbs et al., 2010). However, the total flux density of the AME in these five regions accounted for only ∼ 10% of AME detected on degree angular scales by *Planck*, implying that the AME in Perseus is coming from a diffuse component of gas/dust and is not concentrated in the five compact regions. A similar result was found by Planck Collaboration et al. (2014d) in their sample of potential new AME candidates. Tibbs et al. (2013a) used the GBT 100-m telescope at

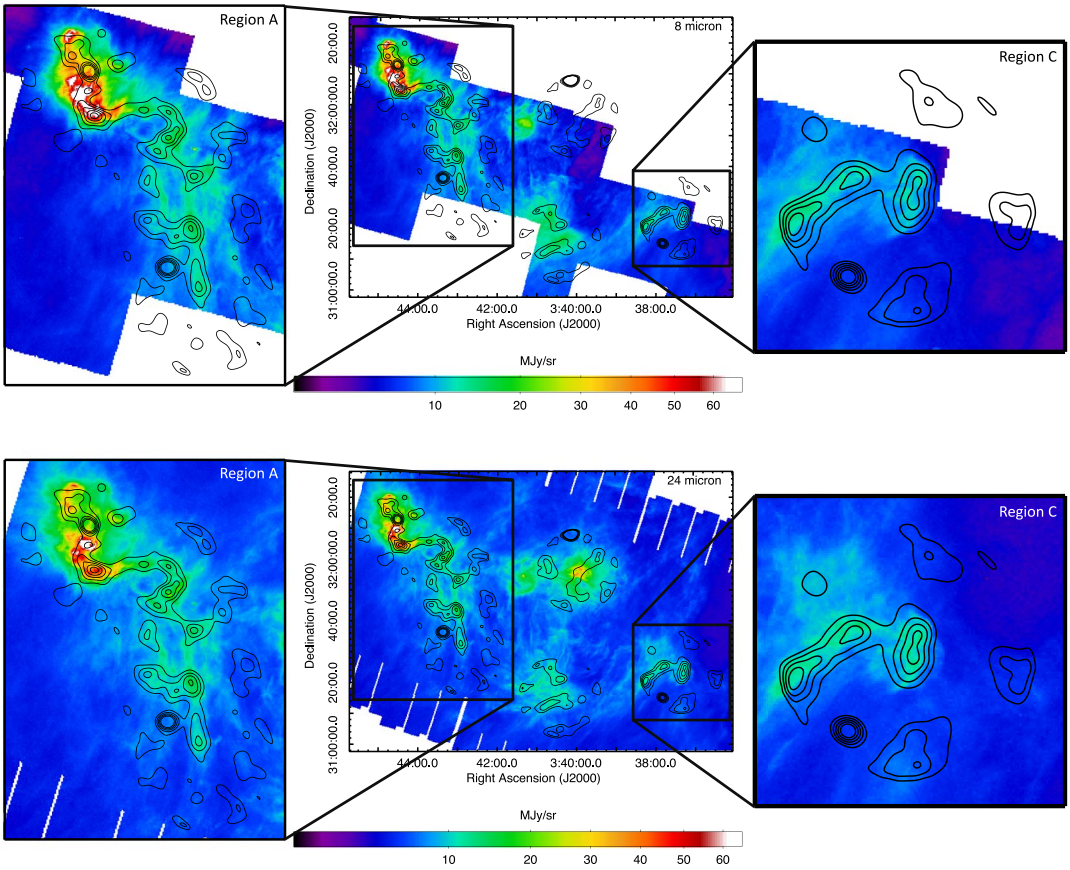

Fig. 13. *Spitzer* colour maps of the G159.6–18.5 region of the Perseus molecular cloud at 8 μm (*top*) and 24 μm (*bottom*), overlaid with AMI 16 GHz black linear contours at an angular resolution of ≈ 2′. There remains a strong correlation between AME and IR emission, with the tightest correlation being with the 24 μm band, suggesting that PAHs might not be responsible for the bulk of the AME in this region.

1.4 and 5 GHz to constrain the level of the free–free emission in Perseus on arcmin scales, confirming that the observed 33 GHz VSA data were mostly due to AME.

Several interesting results have come from high angular resolution AMI data, operating in the unique frequency band of 13–18 GHz. A survey of compact HII regions found essentially no evidence of excess emission (Scaife et al., 2008). Observations of a sample of Lynds clouds resulted in detections in LDN1111 (AMI Consortium et al., 2009) and further detections in several more Lynds clouds (Scaife et al., 2009). Of these, approximately one third of these were shown to be contaminated by optically thick free–free emission from young stellar objects (Scaife et al., 2010a). However, LDN1246 shows diffuse emission at 16 GHz on arcmin scales that is closely correlated with 8 μm maps from *Spitzer* (Scaife et al., 2010a); Fig. 12 shows the striking correlation, which remains one of the best examples of AME on scales of about an arcmin. Perrott et al. (2013) used AMI to resolve the structure of two *Planck* AME sources (G107.1 + 5.2 and G173.6 + 2.8; Planck Collaboration et al. 2011c), finding a rising spectrum in G107.1 + 5.2 that is consistent with either AME or emission from an ultra-compact HII region, but with a much lower flux density than *Planck*, consistent with AME originating on larger angular scales. Perrott et al. (2013) found no evidence for AME in G173.6 + 2.8 on angular scales ≈ 2–10′, suggesting that the bulk of AME is very diffuse. Recently, a blind survey of Sunyaev–Zoldovich clusters has revealed by accident the first blind detection of AME on scales of an arcmin (Perrott et al., 2017).

Tibbs et al. (2013b) used AMI to study the AME in the Perseus cloud in even more detail than the VSA, at a resolution of ≈ 2′, and found that the spatial correlation between AME and IR emission remained strong on these scales, as shown in Fig. 13. More interesting is that the correlation is visibly stronger with 24 μm emission than it is with 8 μm emission. This might indicate that AME is originating from a population of stochastically heated small interstellar dust grains rather than PAHs, in agreement with the conclusions from the more general analyses by Hensley et al. (2016) and Hoang et al. (2016). Although the AME-IR correlation persisted on small scales, the results also indicated that the AME intensity did not correlate with PAH abundance, but rather with the interstellar radiation field, which may be shaping the dust grain size distribution.

Using CARMA data at 31 GHz, Tibbs et al. (2015) performed the first search for AME in a sample of dense Galactic cold cores at 2′ angular resolution, finding less AME than expected. The nominal predictions from spinning dust models predicted detectable emission, providing constraints on the size distribution of dust grains and environmental conditions. Fig. 14 shows the SED of one of the sources (ECC189) with the CARMA upper limit at 30 GHz providing an upper limit on the parameter b_C, the total number of carbon atoms per H nucleus, which governs the number of small ($\lesssim$1 nm grains). As discussed by Tibbs et al. (2016), it is possible to explain these CARMA observations in terms of AME by assuming that the smallest dust grains in the dense cores are coagulating, which decreases the expected level of AME. These observations were the first time that spinning dust modelling had been used to constrain the physical properties of interstellar dust grains such as the abundance of small grains (Tibbs et al., 2016). A similar attempt was made by comparing high-resolution (1–2.4′) *Parkes* radio data with IR data (Battistelli et al., 2015) where astrophysical information was extracted from AME fits of two components, allowing both concentrated and diffuse AME to be distinguished.

A survey of bright Galactic clouds in the *Planck* data has detected a large number of potential candidates on 1° scales (Planck Collaboration

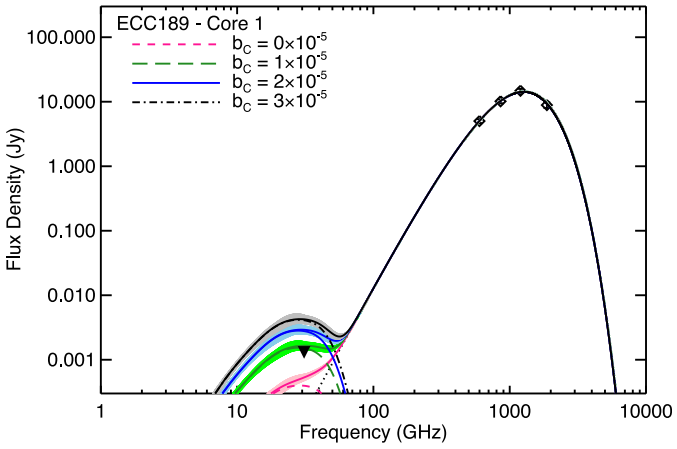

Fig. 14. SED for the cold core ECC189. The black line is the best-fitting thermal dust model while the coloured lines represent spinning dust models with different values for the total number of C atoms governing the number of very small grains responsible for spinning dust emission. The CARMA upper limit at 30 GHz is shown, which yields a limit of $b_C \leq 1 \times 10^{-5}$. Figure taken from Tibbs et al. (2016).

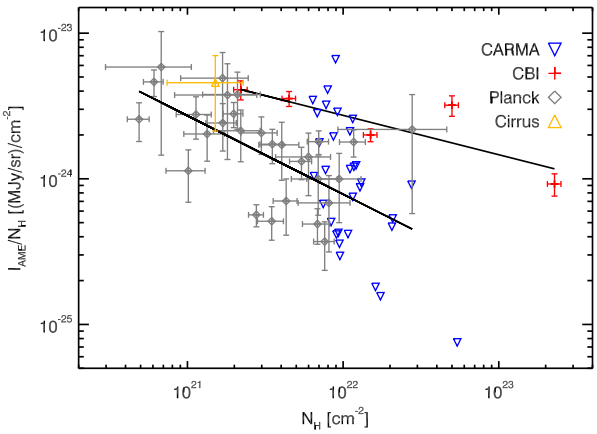

Fig. 15. AME emissivity at ≈ 30 GHz as function of column density for different Galactic objects. The *red* points represent observations of Galactic clouds with the CBI (see Vidal et al., 2011), the *grey* points are clouds measured with the *Planck* satellite (Planck Collaboration et al., 2014d) and the *blue* points are 2σ upper limits on AME emission from a sample of Galactic cold cores observed by CARMA (Tibbs et al., 2016). The *yellow* point is an average value for cirrus clouds taken from the Leitch et al. (1997) observations of AME at high Galactic latitudes.The lines represent the best-fitting power-laws to the *Planck* ($\alpha = -0.54 \pm 0.07$) and CBI ($\alpha = -0.27 \pm 0.04$) data, respectively. We did not attempt a fit to the CARMA points as these represent 2σ upper limits. The AME intensity is calculated as the mean intensity over the aperture for the integrated fluxes of the *Planck* and CARMA sources, while the CBI intensities correspond to the peak value of each source. The column densities for each point are estimated using thermal dust opacities and temperature fits. Systematic errors in this calculation can account for some of the scatter of the points. (For interpretation of the references to colour in this figure legend, the reader is referred to the web version of this article.)

et al., 2014d). Out of 98 targets, 42 were found to potentially have excess emission at frequencies ≈ 20–40 GHz, but the difficulty of detection due to overlapping sources, estimating source flux densities in the presence of bright backgrounds and optically thick sources means that some of these are likely to be false AME detections. Nevertheless, these sources tended to have similar properties (such as emissivity, peak frequency, or correlations with other datasets) to known AME sources. The most significant sources tended to be at high latitudes in regions of low free–free emission, often associated with dark clouds. Higher resolution, multi-frequency follow-up observations are needed to confirm and investigate these sources in more detail. A follow-up of some of these sources could be provided at 11, 13, 17, and 19 GHz by the Multi-Frequency Instrument (MFI) of the QUIJOTE experiment (see Rubiño-Martín et al., 2017, for an update on the status of the project). A study of the characterisation of AME toward the Taurus Molecular Cloud Complex is currently under investigation (Poidevin et al., in prep.) with 1° FWHM resolution smoothed maps obtained at these frequencies.

As discussed in Section 3.1, reliable physical emissivities relating the intensity to the gas column density (e.g., in units Jy/sr cm^2) are difficult to accurately compare. Nevertheless, a trend has been noticed by several authors that appears to corroborate the spinning dust explanation. Vidal et al. (2011) compared the emissivities of several clouds observed with the CBI at an angular resolution of ≈ 4–6′ (to reduce bias in the estimation of the average column density) and found an anti-correlation with the gas column density. A similar trend with τ_{250} (proxy for column density) was noticed by Planck Collaboration et al. (2014d) and also with dust radiance by Hensley et al. (2016).

In Fig. 15 we plot the AME emissivities for a range of objects, including the AME detections of Planck Collaboration et al. (2014d) and upper limits from cold cores by Tibbs et al. (2015). Note that the different colour points have been measured over different angular scales. For instance, the *Planck* estimates of N_H are mean values over a 2° diameter aperture, while the CBI points are peak values in a 4′ beam. This produces systematic differences for the measured column density, with the *Planck* values being typically smaller than the CARMA and CBI ones, even though one might expect them to be in the same range or larger. So we caution that the N_H values on Fig. 15 should be strictly read as relative values, only comparable for points measured with the same instrument, and not as the true (average) column density for the cloud studied. Regardless of this, there is a systematic trend that is clearly visible, where for higher column density there is less AME emissivity. However, there is considerable scatter in the data. For example, fitting only the CBI data points gives[11] $\alpha = -0.27 \pm 0.04$, but when removing the ρ Oph data point with higher emissivity (red data point at $N_H = 5 \times 10^{22}$) the slopes is − 0.34 ± 0.05. The steeper trend ($\alpha = -0.54 \pm 0.07$) found in the *Planck* data may be due to systematic errors either in the photometry or in the evaluation of N_H. Taking this trend to be real, within the spinning dust framework, the observed behaviour can be explained by a change in the dust size distribution with column density. In denser clouds the smallest grains tend to aggregate into larger ones thus reducing the number of small grains available to produce spinning dust emission (e.g., Tibbs et al., 2016). Indeed, Draine and Lazarian (1999) discussed this test as a way to discriminate between rotational emission from spinning dust and bulk magnetic dipole radiation from magnetic dust grains.

3.3. Extragalactic AME

The majority of AME detections have come from the interstellar matter and clouds in our Galaxy. Perhaps surprisingly, only a few detections from sources beyond our Galaxy have been made so far. This is partly due to the lack of high precision and high frequency ($\gtrsim$15 GHz) radio data with the required angular resolution. For example, WMAP and *Planck* data have very poor sensitivity to compact ($\lesssim$1′) sources. Peel et al. (2011) studied the integrated spectrum of three nearby bright galaxies that were detected at all WMAP/*Planck* frequency channels: M82, NGC253 and NGC4945. Almost all other galaxies are significantly weaker at these wavelengths causing flux density measurements between 10 and 300 GHz to be mostly lacking, so that no conclusion on a possible excess can be drawn at this time. They found that the bulk of the emission can be explained by synchrotron, free–free, and thermal dust emissions. No significant contribution of AME was required with upper limits ≈ 1% at 30 GHz. These limits are marginally consistent with expectations based on the AME emissivity in our own Galaxy. The

[11] In the paper by Vidal et al. (2011), the best-fitting line is correct but the quoted value ($\alpha = 0.54 \pm 0.1$) is incorrect; it should have been − 0.27 ± 0.04.

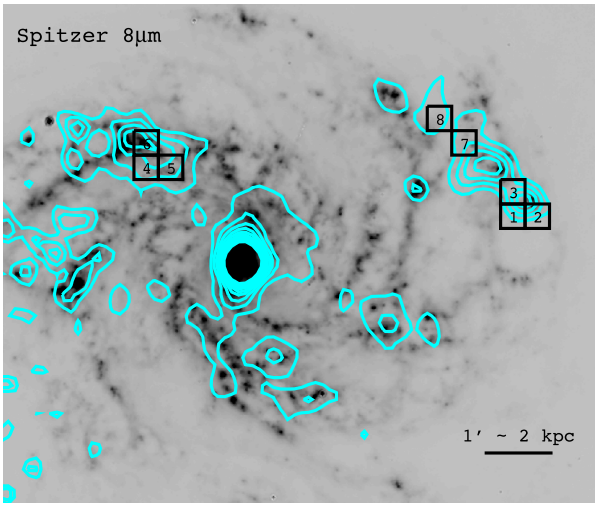

Fig. 16. From Hensley et al. (2015): 33 GHz emission contours on a *Spitzer*/IRAC 8 μm image of the face-on spiral galaxy NGC 6946, where the ten contour levels are linearly spaced between the 3σ noise level of 0.048 MJy/sr and 0.48 MJy/sr. The eight regions with significant AME detections are shown in black boxes. Boxes 1, 2, and 3 cover the location of Enuc 4 in Murphy et al. (2010), where a very significant (7 σ) AME detection was found.

brightest (ultra)-luminous infrared galaxies Arp220, Mrk231, NGC3690, and NGC6240 do have available data; although they are an order of magnitude weaker, their entire radio to far-infrared spectrum is relatively well-sampled and well-determined. None of these four galaxies shows any indication of AME (Israel, in prep.).

Murphy et al. (2010) observed 10 star-forming regions in the nearby galaxy NGC6946 at Ka-band (33 GHz) with the GBT. They found evidence for several regions having a marginal excess at 33 GHz, with one region (Enuc 4) being very significant (7 σ). This region appears to emit $\approx$ 50% AME at 33 GHz, which was confirmed by follow-up observations with the AMI telescope at 15–18 GHz (Scaife et al., 2010b). A spinning dust model for the spectrum was preferred over the free–free-only model. For the other star forming regions, the 33 GHz flux appears to be dominated by free–free emission.

Follow-up observations of NGC 6946 with CARMA, at yet higher angular resolution (21″), revealed additional regions having excess 33 GHz emission attributed to AME (Hensley et al., 2015, see Fig. 16). The strength of the excess emission in these regions was found to be correlated with the total Infrared (IR; 8–1000 μm) luminosity, lending credence to the interpretation as AME. However, no correlation with the dust mass fraction in PAHs was observed. These conclusions are consistent with later results indicating that the dust luminosity, rather than mass in PAHs, correlates more reliably with AME strength. Further, these results suggest that inferences from Galactic AME may extrapolate to extragalactic systems. In particular, measurements of IR luminosity lead to direct predictions of 30 GHz AME in external galaxies, providing an effective means of target selection for follow-up studies.

Excess emission has been detected in the Magellanic clouds. Detections of excess in the Large Magellanic Cloud (LMC) claimed by Israel et al. (2010) and Bot et al. (2010) may be largely or completely caused by a CMB (hotspot) fluctuation (Planck Collaboration et al., 2011b). Planck Collaboration et al. (2016d) show that the integrated spectrum of the LMC shows a marginal (few %) excess at $\approx$ 30 GHz with an emissivity comparable to the Milky Way. On the other hand, Planck Collaboration et al. (2011b) did find a significant excess at sub-mm wavelengths ($\sim$ 100–500 GHz) in the SMC, which extends down to $\approx$ 30 GHz (Israel et al., 2010; Bot et al., 2010; Planck Collaboration et al., 2011b). Bot et al. (2010) suggested that the 50–300 GHz excess in the SMC could be explained by spinning dust, but Draine and Hensley (2012) argued that this was inconsistent with physical conditions in the SMC, and that magnetic dipole radiation from magnetic nanoparticles (either inclusions or free-flying) could provide a more natural explanation.

Planck Collaboration et al. (2015b) found a marginal detection of AME from the integrated spectrum of the Andromeda galaxy (M31), at an amplitude of 0.7 $\pm$ 0.3 Jy (2.3 σ). The amplitude is in line with expectations from the emissivity found in our Galaxy. M31 is also the subject of high resolution microwave observations performed with the recently commissioned 64-m Sardinia Radio Telescope (SRT; Prandoni et al., 2017); detailed C-band (5.7–7.7 GHz) intensity, spectroscopic, and polarization observations have been conducted over $\approx$ 7 deg^2 around M31 (Battistelli and Fatigoni, in prep.) and K-band (18–26.5 GHz) observations are expected in 2019.

The Local group dwarf-spiral galaxy M33 has a well-defined radio to near-infrared spectrum. An in-depth analysis of its flux densities and overall spectrum (Tibbs et al., in prep.) concludes that any AME contribution at 30 GHz is less than $\approx$ 10% of the total flux density at that frequency, and almost an order of magnitude below the AME contribution expected by scaling the Milky Way results. For a few other dwarf galaxies of Magellanic type, spectra extend into the centimetre range thanks to their compactness. The spectra of Hen 2-10 and NGC4194 are still too poorly sampled to allow a conclusion, but the spectra of 2 Zw 40 and NGC5253, although needing further accurate flux density measurements in the 40–100 GHz range, at least do not yet rule out the presence of AME (Israel, in prep.).

3.4. AME observations in polarization

Extensive effort has been dedicated to the theoretical modelling of the polarization spectrum of spinning and magnetic dust emission (see Section 2 and references therein). Different physical conditions, including magnetic field strength, grain temperature, grain shape, size distribution, and alignment between the grain angular momentum and magnetic field direction, lead to different polarization levels and spectra, or even practically null polarization in cases that the quantization of energy levels produces a dramatic decrease of the alignment efficiency, as predicted by Draine and Hensley (2016). For this reason, a measurement of the polarization of AME, or the determination of stringent upper limits, is potentially a key tool for discriminating between different models, and for obtaining information about the physical parameters associated with AME environments. Note that magnetic dust models predict much higher polarization fractions ($\gtrsim$10%) than those based on spinning dust ($\lesssim$1%). Thus, polarization can in principle be crucial to determine the relative contributions of these two mechanisms, something that is complicated in intensity data due to the presence of multiple components.

Polarization is of course more difficult to observe, because the polarization signal is very weak, and also because AME must be separated in intensity to measure a polarization fraction for the AME component i.e., $\Pi_{\rm AME} = P_{\rm AME}/I_{\rm AME} \neq P_{\rm AME}/I_{\rm total}$. For this reason, observational studies of AME polarization are scarce, and so far they have only led to upper limits. Table 4, which is an update of Table 1 of Rubiño-Martín et al. (2012), summarises the current constraints. Except for the value from Casassus et al. (2008), here we list constraints on the fractional polarization relative to the AME flux density in intensity (rather than total flux density), which is derived by modelling and subtracting the other components. Note that in Battistelli et al. (2006) and in López-Caraballo et al. (2011) they referenced their polarization fractions relative to the total intensity, while here we quote the values relative to the AME intensity that were calculated by Génova-Santos et al. (2015b).

Better and more reliable limits on AME polarization come from specific Galactic clouds, which have a bright AME signal without significant contamination from other emission mechanisms. The best targets are the Perseus (specifically the dust shell G159.6–18.5) and ρ Oph molecular clouds, where AME clearly dominates the intensity spectrum

Table 4
Summary of AME polarization fraction constraints, $(P/I_{\rm AME}) \times 100$. The horizontal line separates measurements on individual non-resolved Galactic objects and on large regions of the sky. Columns 1 to 3 indicate the name of the object or region, the experiment from which the data were taken and its angular resolution, respectively. The next four columns show the constraints in different frequency ranges. Here, upper limits are referred to the 95% confidence level. The last column provides the reference. This is an updated version of Table 1 of Rubiño-Martín et al. (2012).

Target	Experiment	Angular	Polarization fraction Π [%]				Reference
		Res. [arcmin]	9–19 GHz	20–23 GHz	30–33 GHz	41 GHz	
	Galactic AME regions						
G159.6–18.5	COSMOSOMAS	60	$5.\,3^{+2.5}_{-3.1}$	...	...	...	Battistelli et al. (2006)
—"—	WMAP-7	60	...	< 1.0	< 2.6	< 4.2	López-Caraballo et al. (2011)
—"—	WMAP-7	60	...	< 1.4	< 1.9	< 4.7	Dickinson et al. (2011)
—"—	QUIJOTE	≈ 60	< 3.4	...	...	...	Génova-Santos et al. (2015b)
ρ Oph W	CBI	≈ 9	...	...	< 3.2	...	Casassus et al. (2008)
—"—	WMAP-7	60	...	< 1.7	< 1.6	< 2.6	Dickinson et al. (2011)
LDN1622	GBT	1.3	< 2.7	...	...	...	Mason et al. (2009)
—"—	WMAP-7	60	...	< 2.6	< 4.8	< 8.3	Rubiño-Martín et al. (2012)
RCW175	*Parkes* 64-m	≈ 1	...	< 2.6	...	...	Battistelli et al. (2015)
W43	QUIJOTE/WMAP	≈ 60	< 0.39	< 0.52	< 0.24	< 0.22	Génova-Santos et al. (2017)
Pleiades	WMAP-7	60	...	< 12	< 32	< 96	Génova-Santos et al. (2011)
[LPH96]201.663 + 1.643	CBI	≈ 7	...	...	< 10	...	Dickinson et al. (2006)
—"—	WMAP-7	60	...	< 1.3	< 2.5	< 7.4	Rubiño-Martín et al. (2012)
Helix nebula	CBI	≈ 9	...	...	< 8	...	Casassus et al. (2007)
	Diffuse AME						
All-sky	WMAP-3	60	...	< 1	< 1	< 1	Kogut et al. (2007)
All-sky	WMAP-5	60	...	< 5	...	...	Macellari et al. (2011)
Perseus	WMAP-9/*Planck*	60	...	0.6 ± 0.5	...	...	Planck Collaboration et al. (2016d)

at frequencies $\approx$ 10–50 GHz. Another advantage is that the emission at low frequencies is dominated by optically thin free–free emission, which is much lower than AME at frequencies near 30 GHz and is unpolarized. Also, these clouds are relatively well isolated and away from the Galactic plane, therefore avoiding contamination from diffuse Galactic emission or from nearby compact objects.

López-Caraballo et al. (2011) and Dickinson et al. (2011) obtained $\lesssim 1$ % limits on these regions at 23 GHz using WMAP observations. Previously Battistelli et al. (2006) reported in G159.6–18.5 a marginal detection of $\Pi = 3.\,4^{+1.5}_{-1.9}\%$ (or $\Pi_{\rm AME} = 5.\,3^{+2.5}_{-3.1}\%$) using data from the COSMOSOMAS experiment at 11 GHz, which has not yet been confirmed nor ruled out. Génova-Santos et al. (2015b) obtained upper limits in the same frequency range using QUIJOTE data, but they have a larger uncertainty. Reich and Reich (2009) proposed that G159.6–18.5 may be acting as a Faraday Screen, which rotates the polarization angle of background radiation, and this could be potentially contributing to this 11 GHz signal. The other reported detection by Battistelli et al. (2015) towards the HII region RCW175, at a level of $2.2 \pm 0.4\%$. However, they claim that there could be a significant contribution to the measured polarization from synchrotron emission along the line-of-sight, making this effectively an upper limit of $< 2.6\%$. Other upper limits come from well-studied regions in total intensity, like the Lynds dark cloud LDN1622. Although they are more difficult to obtain due to the weakness of the signal, some upper limits associated with the diffuse AME emission have also been derived, using either the full sky (Kogut et al., 2007; Macellari et al., 2011) or extended regions (Planck Collaboration et al., 2016d). Note that Planck Collaboration et al. (2016d) obtained a detection in the Pegasus region ($\Pi = 9 \pm 2\%$), but suggested that it was likely contaminated by polarized synchrotron emission.

More stringent upper limits on the fractional polarization require more sensitive data, or alternatively AME regions that are brighter in total intensity. The sample of 98 AME sources analysed in Planck Collaboration et al. (2015b) provides a guide to search for good candidates. One of them is the molecular complex W43, which has an AME peak flux eight times higher than G159.6–18.5, although in this case the level of free–free emission is as high as the AME in the relevant frequency range. Using a multi-frequency analysis combining QUIJOTE, WMAP and *Planck*, Génova-Santos et al. (2017) have provided the best upper limits obtained so far: < 0.22 % at 41 GHz, from WMAP data, and < 0.39 % at 17 GHz from QUIJOTE data. Génova-Santos et al. (2017) claim that the free–free level has been determined with an accuracy of around 20 % thanks to the use of low-frequency continuum and radio-recombination line data.

The constraints summarized in Table 4 are compared in Fig. 17 with various theoretical predictions for the polarization fraction of the spinning dust (Lazarian and Draine, 2000; Hoang et al., 2013, 2016) and magnetic dust emissions (Draine and Lazarian, 1999; Draine and Hensley, 2013; Hoang et al., 2016). Fig. 17 follows the same organization as Fig. 8 of Génova-Santos et al. (2015b) and of Génova-Santos et al. (2017), and depicts the same theoretical models (in the previous references predictions for different physical conditions of the AME environment than those adopted in Fig. 17 are also provided).

It can be seen that many of the upper limits fall well below early predictions of polarization for the spinning dust models. However, it must be taken into account that the models of Lazarian and Draine (2000) and Hoang et al. (2013) give, in practice, upper limits on the real spinning dust polarization due to various depolarization effects (see e.g., Génova-Santos et al., 2015b). Most of the previous constraints have been obtained at angular resolutions of $\sim 1^\circ$, so a detection of polarization would require coherence of the magnetic field over these angular scales. Similarly, a decrease of the observed polarization could be produced by the combination of different emission mechanisms along the same line-of-sight with different polarization directions. Furthermore, the observations could be affected by instrumental systematic effects, or artificially lower by depolarization, such as multiple components within a single beam ("beam depolarization").

Draine and Hensley (2016) concluded that quantization of energy levels in very small grains effectively suppresses alignment in nanoparticles that are small enough to spin at $\approx$ 20–40 GHz, leading to negligible polarization levels. In that case, only grains > 30 Å could produce polarized emission at a level comparable to the best upper limits represented in Fig. 17. Models predict the magnetic dust emission to have even higher polarization degrees, and therefore those models are also inconsistent with the measurements. However, several assumptions have been adopted while deriving some of these theoretical predictions, in particular: perfect alignment between the grain angular momentum and the magnetic field, magnetic field parallel to the plane of the sky, or dust grains ordered in a single magnetic domain (Draine and Lazarian, 1999). If any of these hypotheses does not hold

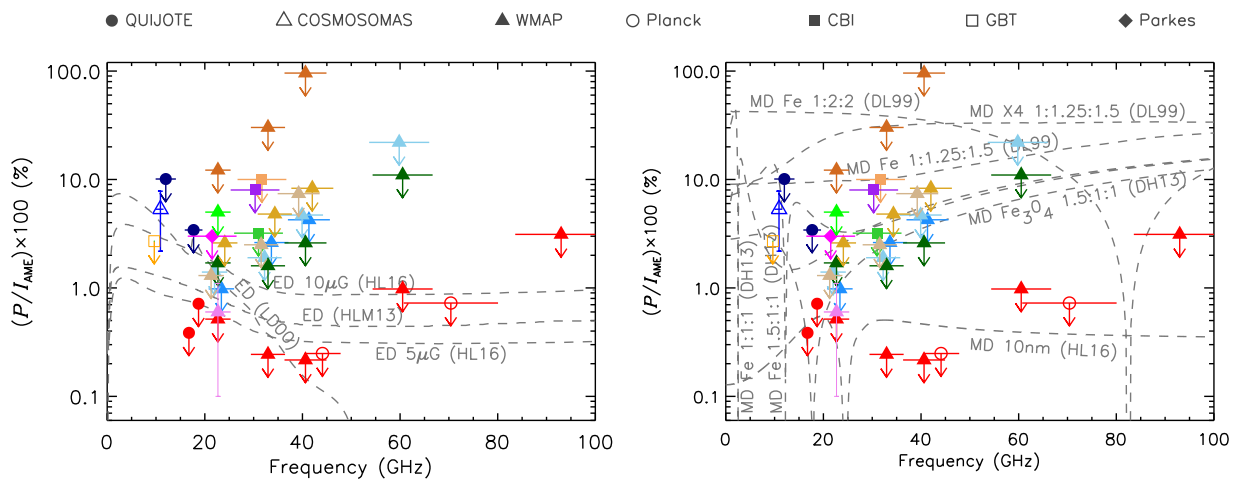

Fig. 17. Constraints on AME polarization fraction at different frequencies, from different experiments and in different regions, compared with the predictions from different models (*grey dashed lines*) based on electric dipole (ED; *left* panel) and magnetic dipole (MD; *right* panel) emissions. The horizontal lines around each data point represent the bandwidth of the corresponding detector. We have used different colours for each object and reference (see Table 4), and different symbols for each experiment, as indicated in the legend on top. In some cases, where there are many points at the same frequency (as for WMAP and CBI), for the sake of clarity, we have shifted the central frequencies in the plot. If the quantum suppression mechanism described by Draine and Hensley (2016) is in effect then the polarization fraction would be $\lesssim 0.0001\%$.

the real polarization degree may be lower. For certain extreme models – e.g., perfectly aligned grains consisting of a single ferromagnetic domain – the magnetic dipole thermal emission can be strongly polarized (Draine and Hensley, 2013), but these extreme assumptions seem unlikely to be realized even if some or all of the AME is thermal emission from ferromagnetic materials. Thermal emission from silicate grains containing randomly-oriented magnetic inclusions is predicted to have only a small degree of polarization in the 20–40 GHz region (see Fig. 10 of Draine and Hensley, 2013).

Given the abundance of free parameters (mainly related with the geometry of the grains and magnetic field, and with the physical conditions of the environment) and possible unaccounted effects (for instance, quantum suppression of the dissipation required to produce alignment) in the models, there may be multiple models consistent with any upper limit derived from the observations. However, Draine and Hensley (2016) have made the strong prediction that spinning dust emission should be unpolarized, so if AME polarization is detected, this would either require a non-spinning dust origin, or invalidate the physical arguments for quantum suppression of dissipation. For this reason, it is important to increase the angular resolution of the observations, to improve the quality of the data, and the analysis techniques, in order to try to eventually reach a detection of the polarization of AME at different frequencies. This would be important not only for constraining spinning/magnetic dust models, but also for characterising foregrounds for future high-sensitivity measurements of the CMB.

3.5. Summary of observational constraints and discussion

The first topic of discussion is simply, is AME real? i.e., is AME really a new component of emission such as spinning or magnetic dust, or is it our lack of understanding of synchrotron/free–free/thermal dust/CMB emissions?

For several years after the initial detection (Leitch et al., 1997), there was much debate whether AME was in fact real. Indeed in the first WMAP data release, the WMAP team discussed foregrounds extensively (Bennett et al., 2003). The possibility of spinning/magnetic dust was considered, yet the discussion largely rejected such alternatives. Instead, they believed that a harder (flatter spectrum) component of synchrotron emission, which was not traced by low-frequency radio surveys, was the most likely explanation for the excess. The correlation with dust was explained by the fact that hard synchrotron would be correlated with star-formation due to energy injection, which would be close to molecular clouds, and therefore dust emission. This model would also explain the flatter spectrum ($\beta \approx -2.2$) at frequencies ≈ 15 GHz but steepening to ≈ -3.0 at 30 GHz and above. At high Galactic latitudes, there appears to be no evidence for a significantly flatter component of synchrotron emission (e.g., Miville-Deschênes et al., 2008; Vidal et al., 2015), except possibly from the Galactic centre region (Planck Collaboration et al., 2013) and at low Galactic latitude (Fuskeland et al., 2014); a template-fitting analysis of WMAP data using the 2.3 GHz southern sky survey (Peel et al., 2012) showed that the AME was robust to using different radio templates.

In the early AME detections, there was concern that free–free emission could be responsible. The optical recombination line Hα is a tracer of warm ionized gas and therefore radio free–free emission, with little dependence on electron temperature for the temperatures $3000 < T_e < 15000$ K expected for photoionized gas (Dickinson et al., 2003). Earlier observations of Hα had already indicated that the free–free emission could only account for a small fraction of the total foreground signal (Gaustad et al., 1996; Leitch et al., 1997). Full-sky Hα maps (Dickinson et al., 2003; Finkbeiner, 2003) became available and quickly ruled out traditional free–free emission (e.g., Banday et al., 2003; Davies et al., 2006). Optically thick free–free emission could be contributing to the AME signal along some sight-lines, but, in general, is not a major contributor at frequencies ≈ 30 GHz and on scales of $\approx 1^\circ$ (e.g., Planck Collaboration et al., 2016d).

The major break-through came with the detection of AME from Galactic molecular clouds - the Perseus G159.6–18.5 region (Watson et al., 2005) and the ρ Oph W (Casassus et al., 2008). Both these sources contained strong dust-correlated emission that was clearly well in excess of the expected synchrotron and free–free intensity levels. There was still some doubt about the extrapolation of the thermal dust tail from higher frequencies. However, the early results paper from *Planck* (Planck Collaboration et al., 2011c) showed the peaked spectrum expected from spinning dust (on both sides), providing definitive evidence for the reality of AME, and consistent with predictions for spinning dust (see Section 2.1).

The large body of evidence for excess emission at frequencies ≈ 10–60 GHz is now difficult to refute. The recent *Planck* component separation analysis included spinning dust, which used a spectral parametric fitting code to fit each pixel seperately (Planck Collaboration et al., 2016c). They found a strong component that was correlated with dust even though this was not assumed in the analysis. Fig. 6 presents a summary of the separation on large angular scales (81–93% coverage). In this particular model, the AME is represented by a 2-component spinning dust model, which dominates the

foreground emission near 20 GHz. Although the details of the separation could be in doubt (e.g., due to the fixed synchrotron spectrum) it appears to be clear that AME (modelled as spinning dust in this case) is a significant fraction (of order half) of the total foreground signal at frequencies $\approx$ 20–40 GHz.

One potential issue relates to the absolute calibration of large-scale radio maps. Large-scale radio data, up to now, have often been taken with large radio dishes working as a total-power radiometer. The illumination of the dish is such that a significant amount of the power response of the telescope is outside of the main beam, resulting in a scale-dependent calibration that is difficult to account for (see Du et al., 2016, for a detailed discussion). For many of the large-scale radio surveys, this has resulted in a calibration scale that can be incorrect by up to tens of percent when comparing compact sources with large-scale emission over many degrees (e.g., Jonas et al., 1998). The end result is that large-scale emission on scales of 1° and larger will be enhanced relative to compact sources (which are typically used for calibration). A simple extrapolation from low to high frequencies could then yield excess emission at the higher frequencies by a similar fraction i.e. a few tens of %, which is indeed what is observed. Given this, it is difficult to account for the ubiquity of AME, even when not relying on low frequency radio maps. A number of studies have relied on such data while others have not. Furthermore, some AME sources show effectively no signal at all at low frequencies, such as ρ Oph W.

The origin of the diffuse AME found at high Galactic latitudes is still not completely settled. Although spinning dust can readily account for the bulk of the AME (e.g., Planck Collaboration et al., 2016b), other emission mechanisms could be contributing at some level (Section 2.3). Magnetic dipole radiation from fluctuations in dust grain magnetization could be significant (Draine and Lazarian, 1999; Draine and Hensley, 2013; Hensley et al., 2016), although upper limits on AME polarization (López-Caraballo et al., 2011; Dickinson et al., 2011; Macellari et al., 2011; Rubiño-Martín et al., 2012) appear to indicate that this does not account for the bulk of the signal. Similarly, a harder (flatter spectrum) component of synchrotron radiation may also be responsible for part of the AME at high latitudes, as proposed by Bennett et al. (2003) in the original *WMAP* data release. The harder spectrum would naturally explain the correlation with dust, since both are related to the process of star-formation. Furthermore, we already know that there are regions that have synchrotron spectral indices that are at $\beta \approx -2.5$ or flatter, both from supernova remnants (Onić, 2013) as well as more diffuse regions such as the *WMAP/Planck* haze (Finkbeiner, 2004; Planck Collaboration et al., 2013).

A contribution of harder synchrotron component may have been missed when applying component separation methods to microwave data. The majority of AME detections from fluctuations at high Galactic latitudes have been made using the "template fitting" technique, i.e., fitting multiple templates for each foreground component to CMB data, accounting for CMB fluctuations and noise (Kogut et al., 1996; Banday et al., 2003). The synchrotron template is traditionally the 408 MHz all-sky map (Haslam et al., 1982), or other low frequency template. However, data at these frequencies will naturally be sensitive to the softer (steeper spectrum) synchrotron emission, which has a temperature spectral index $\beta \approx -3.0$ (Davies et al., 2006; Kogut et al., 2007; Dunkley et al., 2009b; Gold et al., 2011). This leads to a significant AME signal at $\approx$ 10–60 GHz that is correlated with FIR templates, which cannot be accounted for by the R-J tail of dust emission. Peel et al. (2012) used the 2.3 GHz Southern-sky survey of Jonas et al. (1998) as a synchrotron template for the *WMAP* data and found that the dust-correlated AME component changed by only $\approx$ 7 %, compared to using the 408 MHz template. This suggests that the bulk of the diffuse high latitude synchrotron emission is indeed steep ($\beta \approx -3.0$), resulting in little change to the AME at 20–40 GHz. New data from C-BASS at 5 GHz (Dickinson et al., in prep.) have shown that synchrotron emission in the NCP region is not a major contributor to AME at 20–40 GHz and that the synchrotron emission follows a power-law with $\beta = -2.9$, from 408 MHz all the way to tens of GHz. If this is true for the entire sky, then synchrotron emission cannot explain the bulk of AME at high latitudes.

Recent works have also cast doubt on the spinning dust interpretation. A number of works have found that the small-scale morphology within AME regions does not always correlate with tracers of PAHs and/or the smallest grains (e.g., Tibbs et al., 2011, 2012a, 2013b) and, in some cases, it even tends to correlate better with far-IR/sub-mm wavelengths (e.g., Planck Collaboration et al., 2016d). More striking is that spatial variations in the PAH abundance appear to have no correlation with variations in the ratio of AME/$\mathscr{R}$ (Hensley et al., 2016), whereas a correlation was expected if AME is produced by spinning PAHs. This may indicate that the PAHs have small dipole moments, so that AME is dominated by non-PAH nanoparticles, which could be as abundant as the PAHs, but which might have suitable dipole moments. Hoang et al. (2016) showed that small silicate grains could reproduce the observed AME, and Hensley et al. (2016) demonstrated that nanosilicates could reproduce the AME without violating observational constraints on the mid-IR emission spectrum of diffuse clouds.

The lack of correlation with PAH abundance is surprising, especially because variations in PAH abundance might be expected to correlate with variations in the abundance of other nanoparticles such as nanosilicates. Nevertheless, spinning dust still appears to be the most likely of the proposed emission mechanisms, particularly given the increasingly stringent upper limits on AME polarization.

Bernstein et al. (2017) have suggested that each of the unidentified infrared (UIR) bands may be due to rotational structure from one or two relatively small molecules (i.e., less than 30 C atoms). In contrast, the PAH paradigm attributes the UIR bands to the blending of narrow spectral profiles from many (30 or more), much larger molecules (50 or more C atoms). Bernstein et al. (2017) demonstrated that the 11.2 μm UIR band profiles from multiple sources can be plausibly modelled as a vibration-rotation band of a small fullerene, C_{24}. If valid, this model offers a possible explanation for the lack of observed correlation between AME and some of the UIR features (e.g., Hensley et al., 2016). C_{24} has no dipole moment and therefore cannot produce pure rotational emission (i.e., no AME). Furthermore, it is not clear that the abundance of C_{24} should be proportional to (i.e., a tracer for) the PAH abundance. The implication is that the observed lack of correlation does not exclude PAHs as a major source of AME.

4. AME as a CMB foreground

AME has been demonstrated to be a significant component of the diffuse foreground emission at frequencies $\approx$ 10–60 GHz. Some analyses put AME as the dominant foreground in this frequency range, accounting for perhaps half of the total emission (e.g., Davies et al., 2006; Planck Collaboration et al., 2016b). It is therefore clear that AME is a major foreground for studying the CMB. Yet, CMB studies in intensity appear to not be limited by foregrounds (e.g., Dunkley et al., 2009a; Bennett et al., 2013; Planck Collaboration et al., 2016b), even though we know so little about AME. The question is how do we know that AME is not an issue?

There are two main reasons why AME does not appear to be a major problem for CMB studies. The first is that the spectrum of AME is so different from that of the CMB. AME has a steeply falling spectrum above $\approx$ 20 GHz, while the CMB is flat (in brightness temperature units). The high frequency part of the AME spectrum may be similar to that of synchrotron radiation and thus fitting for a single power-law in the WMAP data accounts for the bulk of the foreground emission (e.g., Dickinson et al., 2009b; Planck Collaboration et al., 2014e). The second reason is that because AME is so closely correlated with far-IR data, spatial templates can be used to account for most of the foreground emission, such as those used in producing the foreground-reduced maps from WMAP (e.g., Bennett et al., 2003; 2013). Thus, both spatially and spectrally, AME can be relatively easily separated from the CMB, down

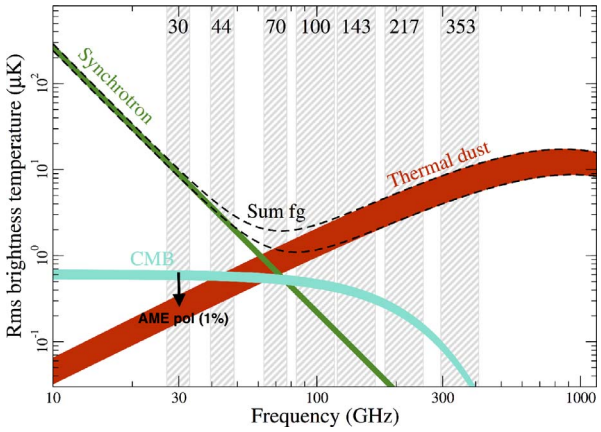

Fig. 18. Summary of the amplitude of polarized foregrounds from the *Planck* component separation 2015 results; figure taken from Planck Collaboration et al. (2016b). The brightness temperature r.m.s. against frequency, on angular scales of 40 arcmin, is plotted for each component; this figure is the same as Fig. 6 but for polarized emission. For this case, the width of the curves represents the spread when using 73% and 93% of the sky. The approximate maximum amplitude from AME polarization (assuming 1% upper limit) at 30 GHz is indicated by the downward arrow.

to levels set by cosmic variance (Planck Collaboration et al., 2016b). Nevertheless, as CMB data become more sensitive on small scales (large scales are limited by cosmic variance), dust-correlated emission will need to be removed with higher precision.

In polarization and on large angular scales ($\gtrsim 1^\circ$), the highly polarized synchrotron and thermal dust foregrounds are brighter than the CMB anisotropies over much of the sky and all frequencies. Fig. 18 depicts the average amplitude of polarized foregrounds relative to that of the total CMB polarization. The strongest polarized foregrounds are synchrotron radiation at low frequencies and thermal dust emission at high ($\gtrsim 100$ GHz) frequencies. Fortunately, AME appears to be weakly (possibly negligibly) polarized (Sections 2.1 and 3.4) and may not be a major foreground for future CMB studies; Fig. 17 shows the latest observational constraints, which nearly all are consistent with a polarization fraction of $\lesssim 1\%$. In Fig. 18 we indicate the approximate upper limit on AME polarization assuming 1% polarization fraction. It can be seen that AME is below the level of the CMB at 30 GHz and at higher frequencies will likely be much lower because of the falling spinning dust spectrum.

However, one of the major aims of current and future CMB experiments is to measure the stochastic background of gravitational waves that are a prediction of many models of inflation. This is possible with CMB polarization because these fluctuations are the only natural way to create "B-modes" on scales of a degree and larger, with an amplitude known as the tensor-to-scalar ratio, r (Seljak and Zaldarriaga, 1997; Kamionkowski et al., 1997). Current constraints are at the level of $r < 0.07$ (BICEP2 Collaboration et al., 2016) and are continuing to improve. The B-mode fluctuations at this level correspond to ~ 0.1 μK in brightness temperature but could be much lower than this. For *Planck* sensitivity levels, a 1% polarization fraction for AME has negligible impact on the recovery of the tensor-to-scalar ratio, r (Armitage-Caplan et al., 2012). Nevertheless, even a small amount of AME polarization could be problematic for component separation with future ultra-high sensitivity data that aim to constrain the tensor-to-scalar ratio at the level $r \sim 10^{-3}$ or even lower (Remazeilles et al., 2016; 2017; Alonso et al., 2017). Careful consideration of all foregrounds will be critical to achieve this level of sensitivity, including any potential spinning and magnetic dust components.

Although AME has been modelled as a single (or double) component of spinning dust, most analyses tend to reveal a residual excess at higher (> 50 GHz) frequencies (Planck Collaboration et al., 2015c). This may well be a consequence of incorrect modelling, especially since a typical spectral model for spinning dust is computed for one set of parameters; an example would be a single run of the SPDUST2 code, corresponding to a single component of spinning dust grains. In reality, there will be a distribution of dust grains and environments along the line-of-sight, which will inevitably broaden the spectrum compared to that of a single component. Indeed, this was the reasoning behind fitting for a 2-component model in the *Planck* 2015 results (Planck Collaboration et al., 2016b). It is possible that the higher frequency residuals are due to another component such as MDE, which could be more strongly polarized. Indeed, there are already hints in the *Planck* data that MDE might be contributing at frequencies ~ 100 GHz (Planck Collaboration et al., 2015c).

In summary, AME does not appear to be a major limitation for CMB studies so far. In many ways, nature has been kind to cosmologists. If all AME can be explained by spinning dust, it will probably not be a major foreground even for future CMB polarization missions. However, a highly polarized component (e.g. MDE) contributing to higher frequencies (> 50 GHz) could be problematic. It is also worth noting that on degree scales, the frequency at which foreground fluctuations are at a minimum is ≈ 70 GHz, which is not far from the peak of where spinning dust emits. For cosmologists wishing to make simulations to test their analyses, we suggest using maps of the thermal dust optical depth at 353 GHz (τ_{353}) at an angular resolution of 5′ from *Planck* (e.g., Planck Collaboration et al., 2016f) as a simple model for AME. At 30 GHz, a multiplying factor of $\approx 8 \times 10^6\,\mu\mathrm{K}/\tau_{353}$ can be used and a SPDUST2 spectrum (e.g., Planck Collaboration et al., 2016b) to give a reasonably realistic sky model. Other alternative templates include the *Planck* 545 GHz map or the total dust radiance also from *Planck* using the coefficients given in Table 3. For polarization simulations, assuming a $\approx 1\%$ average polarization fraction should provide conservative estimates of any potential AME contamination.

5. Methodology for future AME research

AME research has been progressing steadily since its initial detections (Kogut et al., 1996; Leitch et al., 1997). Nevertheless, after 2 decades, we are still not sure about the exact emission mechanism responsible, and with only a handful of reliable detections. We are even further away from using the spinning dust intensity and spectrum as a tool for studying the interstellar dust distribution and environment. So the question is where do we go from here?

There are several possible approaches. Certainly more accurate multi-frequency data (see Section 5.3) are required to make progress in AME research. In particular, the frequency coverage and quality of low frequency (few GHz up to ≈ 20 GHz) data is a major limitation. This will allow accurate spectra to be produced to more precisely discern the physics of the emission. High angular resolution ($\sim$ arcmin or better) data are required to study Galactic clouds and external galaxies in detail. More sophisticated analysis techniques are also needed. Photometric techniques are often susceptible to systematic errors, particularly for diffuse clouds. For example, aperture photometry is a well established technique, but can be problematic for diffuse sources where the background level is difficult to define and measure (Planck Collaboration et al., 2014d). Component separation techniques can also be improved upon, to better remove non-AME emission such as synchrotron, free–free, thermal dust and CMB. More high quality data would provide more AME detections for deriving statistics (e.g., emissivity, peak frequency, correlations), which would inform us about the properties of AME.

To date, most of the detections of AME have been made focusing on individual regions, with only a handful of studies focusing on larger samples of AME regions including HII regions (Dickinson et al., 2007; Scaife et al., 2008), Lynds dark clouds (Scaife et al., 2009), diffuse clouds (Planck Collaboration et al., 2014d), and cold cores (Tibbs et al., 2015). Going forward, this approach would ideally continue as a homogeneous sample of AME detections observed with the same telescope of the same environmental conditions enables us to make

accurate comparisons of the AME. Although practically this may not be possible, a more homogeneous approach would mitigate against some systematic errors and potentially provide information on the effect of environmental conditions. Even if unbiased and complete surveys are not possible, selection effects should be considered when drawing statistical conclusions.

A more focused approach is required if we are to answer specific scientific questions and provide a "smoking gun" for spinning dust and/or magnetic dust emissions. Specifically, we should have testable predictions that observations can either prove or disprove. These would ideally begin with a theoretical prediction that can be tested by observations (see Sections 5.1 and 5.5).

Although most observations of AME have been successfully fitted with a spinning dust model, the large number of parameters in the model mean that it is very difficult to test it in this manner. Therefore, to actually test the spinning dust model, we need to look at relative changes. For example, the spinning dust model predicts that, when other parameters are fixed, the amplitude and peak frequency of the spinning dust emission will increase with increasing gas density. Therefore, by observing a sample of regions covering a range of densities (e.g., cold cores), we can test this simple prediction. However, other parameters, such as the size distribution, will also be density-dependent, so it will not be easy to find ways to clearly test the predictions of spinning dust theory.

In summary, the optimal strategy that will allow moving forward with AME research is a combination of the following:

1. A set of observables and clear predictions from models, allowing to bridge the gap between theory and observations;
2. Systematic observations of statistically representative samples of astrophysical classes of sources (e.g., PDRs, cold cores, nearby galaxies) that allow investigating correlations between AME (e.g., peak intensity, peak frequency) and quantities that regulate the physics of the observed sources (e.g., radiation field intensity, density, abundance of dust grains, gas species abundance);
3. Within a given astrophysical class of objects, targeted observations of sources whose properties are well known from prior investigations and for which a plethora of ancillary data exist, thus allowing careful modelling and interpretation of the observations.

More details will be provided in the following subsections.

5.1. Future directions for Galactic AME studies

Observationally, high-density PDRs have proven to be the best targets for the search of AME. As we discussed in Section 3.2, to date the most significant AME detections are in the Perseus and ρ Oph molecular clouds, which either host PDRs or are PDR-like in nature (e.g., LDN1622, RCW175). What makes these environments ideal is the combination of high gas densities, charged PAHs, and a moderate radiation field that allows PAHs to survive, i.e., all factors that are conducive to producing spinning dust. Due to the small statistics of confirmed AME sources, the range of physical conditions in PDRs that have been probed so far is still very limited. Future observational work should focus towards expanding the currently available set of PDRs. These types of sources can be regarded as a testbed for verifying a predicted correlation between the AME peak frequency and the total gas ion column density. In particular, high-density PDRs are expected to have a high peak frequency (Draine and Lazarian, 1998b; Ali-Haïmoud et al., 2009). So far, we have only found mild evidence that the peak frequency can go higher than ~ 30 GHz, with some regions peaking at ~ 50 GHz (Planck Collaboration et al., 2014d, 2016d). An experiment that would allow testing the model prediction would entail executing pointed observation of a face-on PDR in which each pointing position would probe increasingly higher densities within the photodissociation front. If the spectral energy distributions at each pointing position showed a separation in peak frequencies, this would be a strong confirmation of the spinning dust model; modelling of the observed spatial variations of AME with frequency in the ρ Oph W PDR (Casassus et al., in prep.) might yield such a result.

Similar to PDRs are Reflection Nebulae (RN), although, in this case, the UV flux generated by nearby stars is generally less intense. An example of an AME detection in this category is represented by M78 (Section 3.2). Hoang et al. (2010) estimate that in RNs, due to fast internal relaxation, the peak emissivity and peak frequency of spinning dust are increased, respectively, by a factor $\sim$ 4 and 2. These predictions still require adequate observational vetting.

Another class of astrophysical sources that appear to be promising for studies of AME are cold molecular cores. In general terms, cores are interesting environments to explore as high densities (typically $n_H > 10^3$ cm^{-3}) make spinning dust more likely. In addition, as noted in Section 3.2, coagulation of dust particles is known to occur inside cold ($T \lesssim 15$ K) cores, as a consequence of high density, and for such a scenario clear theoretical predictions have been formulated, which can be tested. One caveat to consider, though, is the fact that many molecular cores are forming stars, and thus are found to be associated with Young Stellar Objects (YSOs). Depending on the evolutionary stage and inclination with respect to the observer's line-of-sight, YSOs can be relatively strong sources of cm radiation. Observing cores is facilitated by the large inventories that were recently made available, for the Galactic population, such as the surveys by *Planck* (Planck Collaboration et al., 2011d, 2016e) and *Herschel* (Juvela et al., 2010; André et al., 2010). Tibbs et al. (2015, 2016) observed a sample of cold cores with a range of densities ($5 \times 10^3 < n_{\rm H} < 120 \times 10^3$ H cm^{-3}) and found a lack of AME, which could be explained if AME is produced by the smallest dust grains, which are depleted due to coagulation in these dense environments. As in the case of PDRs, a more complete systematic investigation of the presence of AME in cores has yet to be conducted, which is an issue that should be addressed by future observational work (larger sample, multi-frequency observations ideally including polarization to rule out MDE). Indeed new observations, such as VLA observations of high-mass star forming region at 5 and 23 GHz (e.g., Rosero et al., 2016) that has detected rising emission with frequency (5–25 GHz) in some sources (thought to be from ionized jets), are likely able to be useful for constraining AME, even if they were not originally for that purpose.

While Galactic cold cores are showing very low levels of AME that may be indicative of very small dust grains depletion, still nothing is known about the level of AME associated to YSOs. Radio observations obtained with the Giant Metre Radio Telescope (GMRT; Ainsworth et al., 2016; Coughlan et al., 2017) are probing the free–free emission associated with the outflow of T Tau. Any detection of AME associated with such objects in the frequency range 10–60 GHz would be indicative of dust grain evolution and possibly could be used as a star-formation evolution tracer.

While the Warm Ionized Medium (WIM) is included by Draine and Lazarian (1998a) as one of the environments where one might expect to find spinning dust, hot ionized objects with compact support, such as HII regions, may not represent the best targets for shedding light on the nature of this emission. The main reason is that the interior of HII regions is notoriously devoid of dust, especially PAHs and large grains, likely due to radiation pressure drift that causes dust grains to move outwards from the location of the ionizing sources and in the direction of the HII region PDR, or, because they have been destroyed (Draine, 2011). This paradigm, which is supported by a wealth of IR data (Povich et al., 2007; Tibbs et al., 2012a), holds in particular for very bright HII regions, powered by large OB associations. In this case, the excess of cm emission that is observed could also result from the combined effect of stellar winds and shocks that are generated by the stellar cluster, rather than by spinning dust (Paladini et al., 2015). An exception with respect to this picture is represented by older, more diffuse HII regions, for which dust depletion in the ionization zone is

Table 5
Expected degrees of polarization for four molecular clouds for which the averaged magnetic field orientations with respect to the line-of-sight, α, are known. As an example the material considered here is magnetic dust of Fe with axial ratios 1: 1.25: 1.5 and with a polarization efficiency that varies between 0.9 and 1.2 between 10 and 60 GHz.

Molecular Cloud Region	α [deg.]	P_{EXP}[%] P_{MAX} = 0.09 Fe 1:1.25:1.5	P_{EXP}[%] P_{MAX} = 0.12 Fe 1:1.25:1.5
S106	[50–55]	≈ 5.7	≈ 7.6
OMC-2/3	[72–80]	≈ 8.5	≈ 11.3
W49	[50–60]	≈ 6.0	≈ 8.1
DR21	[60–70]	≈ 7.4	≈ 9.9

typically less dramatic and which are not characterized by strong wind nor shock activity.

If the carriers producing AME are magnetically aligned, with angular momenta tending to be parallel to the magnetic field, one could test the predictions for the expected range of polarization fractions provided by some models. Table 5 gives the expected maximum polarization for a small sample of molecular clouds for which averaged magnetic field orientations with respect to the line-of-sight, α, are known (Poidevin et al., 2013, and references therein). In this example, magnetic dust grains from Draine and Lazarian (1999) of Fe with axial ratios 1: 1.25: 1.5 are considered. In the case where this dust material was perfectly aligned and the magnetic field direction parallel to the plane-of-sky, Fig. 17 shows that one would expect maximum polarization P_{MAX} varying from 0.09 to 0.12 in the frequency range 10–60 GHz. Once the inclination angle of the mean field is considered one would expect the polarization degree of order the values given in columns 3 and 4 of Table 5, i.e., $P_{EXP} \approx 100 \times [1 - \cos(\alpha)^2] \times \epsilon$. Measured values of the degree of polarization associated to AME in these molecular clouds are lower than expected and this would therefore rule out the Draine and Lazarian (1999) magnetic dust model while measured values greater than about 6% would rule out almost all of the ED models displayed in Fig. 17. Precise polarization measurements will also test the prediction that quantum suppression of dissipation requires that 20–50 GHz spinning dust emission be essentially unpolarized.

The possibility of detecting AME in circumstellar disks around T Tauri ($M_* < 2\ M_\odot$) and Herbig Ae/Be ($2\ M_\odot < M_* < 10\ M_\odot$) stars has also emerged, as discussed by Rafikov (2006). Indeed, while the existence in circumstellar disks of very large, cm-size grains has long been recognized and explained through coagulation, that of PAHs is a discovery of the last ten years or so (Visser et al., 2007). At the temperatures characteristic of these environments, spinning dust is expected to peak around 30–50 GHz and, if at least 5% of C is locked up in small grains, the AME will be dominant with respect to thermal dust emission for $\nu < 50$ GHz. Broad PAH features have been detected in the pre-transitional disk around Herbig Ae star HD169142 (Seok and Li, 2016), which incidentally appears to have an excess of emission at a wavelength of 7 mm (43 GHz) relative to their thermal-dust only model, possibly due to spinning dust.

Future observational investigations of AME may also target dust-producing evolved stars, which could be used to discern the origin of this emission. For example, while there has been no clear detection of magnetised grains around evolved stars, there is some suggestion that they may exist around metal-poor evolved stars (McDonald et al., 2010, 2011). Alternatively, if PAHs are the carrier, they may be observed as a very strong feature of certain carbon-rich evolved objects but be entirely absent in comparable oxygen-rich stars. However, detecting AME around carbon-rich evolved stars is no simple matter, as strong excitation of PAHs requires an ultra-violet radiation field, and in fact the prototypical carbon-rich AGB star, IRC+10216, shows no obvious PAH features (Sloan et al., 2003) nor obvious AME feature (Wendker, 1995). For this reason, PAH features are typically best seen in post-AGB stars or planetary nebulae (Woods et al., 2011; Sloan et al., 2014; Matsuura et al., 2014). In such objects, though, the AME signal may be masked by a high background flux resulting from the high emissivity from hot dust and strong free–free emission from the ionised central cavity. In addition, the intermediate size of this type of source (often marginally resolved by mm-wavelength observatories), together with strong variation in physical conditions across each nebulae, and sometimes strong temporal variations in emission, make the detection and characterization difficult. PAH excitation will be critically dependent on UV radiation field (produced either from the interstellar medium or companion star) which is known to vary substantially in such systems (e.g., McDonald and Zijlstra, 2015).

A single, weak, tentative detection of AME has been made using a combination of *Planck* and ancillary observations of NGC 40 (Planck Collaboration et al., 2015d), a nearby carbon-rich planetary nebula (Ramos-Larios et al., 2011). While dust-producing evolved stars are naturally of interest, the overall formation site of PAHs is still quite controversial: indeed it could be stellar origin, as now described, or either molecular origin (Paradis et al., 2009; Sandstrom et al., 2010) or shattering in grain-grain collisions (Draine, 1990, 2009). We also note that PAH emission has been seen in reflection nebulae excited by cool stars, and this is consistent with theoretical models Li and Draine (2002). If PAH emission is absent in outflows from regions excited by stars with $T_{eff} > 3500$ K, then it is because small PAHs are not abundant there. A survey of such stars with a range of effective temperatures would elucidate the role of PAHs for AME.

Last of all, if AME is indeed produced by relatively small interstellar PAHs, a smoking-gun confirmation would be the detection of their line emission, as discussed in Section 2.1.3. Testing this hypothesis would require more observations, generalizing those of Ali-Haïmoud et al. (2015) to different environments and lines-of-sight.

5.2. Extragalactic AME studies

Since AME has only been detected in one or two external galaxies, it is vital that we pursue AME in extragalactic sources. It is interesting to note that in our Galaxy, the fraction of AME to total emission at frequencies near ~ 30 GHz is as much as a half. Thus, one might expect to see a similar ratio in other galaxies. There is little radio data at frequencies above ~ 10 GHz, nevertheless, AME does not appear to be this strong in extragalactic sources. For instance, Murphy et al. (2012) observed 103 galaxy nuclei and extranuclear star-forming complexes taken with the GBT as part of the Star Formation in Radio Survey (SFRS). Among the 53 sources also having ancillary far infrared and 1.7 GHz data, ≈ 10% exhibited radio spectral indices and 33 GHz to IR flux density ratios consistent with that of the source in NGC 6946 showing a strong AME signal. It appears that external star-forming galaxies emit less than a few percent of AME at frequencies ~ 30 GHz.

If the AME intensity (or emissivity) is similar to the levels we believe in our Galaxy, we would expect AME to be a significant contributor to the radio/microwave flux at rest frequencies near 30 GHz. This does not appear to be the case (at least in the few objects that have been studied) and the reason why is not clear. Possibilities include (i) the environment in the Milky Way is conducive for producing strong AME but is relatively rare among star-forming galaxies, (ii) AME is primarily a local phenomenon in the vicinity of the Sun, or (iii) we have significantly over-estimated AME in our own Galaxy (or a combination of these).

If AME is significant in external galaxies, it could have an impact on several important areas of astrophysics. For example, free–free emission has been proposed as a reliable estimator of the star-formation rate (SFR; e.g., Murphy, 2009; Murphy et al., 2011, 2017), and 30 GHz has been proposed as the ideal frequency, with it being least contaminated by synchrotron or thermal dust emission. However, this is exactly the frequency at which AME appears to be strongest (at least in our own Galaxy). Not accounting for AME would result in over-estimates of the SFR and could bias SFR estimates for a large sample.

Identifying AME candidate sources based on a coarse sampling of the radio spectrum, even with a large lever arm spanning 1.7, and 33 GHz as was done for the GBT survey of Murphy et al. (2012), is inconclusive. A much finer (i.e., better than a factor of two) sampling in frequency space, spanning $\approx$ 3–90 GHz would be ideal to measure the peak for conclusive detections. Consequently, to further investigate the impact on AME studies of star formation both at low and high redshifts, the SFR analysis has been extended to include $\approx 2''$ resolution ($\approx$ 30–300 pc) JVLA 3, 15, and 33 GHz data of 112 galaxy nuclei and extranuclear star-forming complexes to both better characterize thermal radio fractions at 33 GHz and search for discrete AME candidates in external galaxies. Any robust AME candidates can then be confirmed by more focused follow-up observations at 90 GHz.

A morphological comparison between the JVLA 33 GHz radio, Hα nebular line, and 24 μm warm dust emission shows remarkably tight similarities in their distributions suggesting that each of these emission components are indeed powered by a common source expected to be massive star-forming regions, and that the 33 GHz emission is primarily powered by free–free emission (Murphy et al., 2017a, submitted). The full multi-frequency spectral analysis to robustly measure thermal fractions and characterize AME will be presented in a future paper (Murphy et al. 2017b, in prep.). High precision and fidelity data will be essential to obtain AME detections or to place meaningful constraints.

We make a final remark that current observations may already be seeing evidence of AME, but may have been interpreted as something else. A recent example would be the 33 GHz measurements of 22 local luminous galaxies (Barcos-Muñoz et al., 2017), where some sources showed a remarkably flat ($\alpha \approx 0$) flux density spectral index. Although this may be due to self-absorption in the densest regions, it could also be indicating a (small) component of AME. Accurate multi-frequency data, with careful consideration of all contributing components, will be essential for disentangling the radio-microwave spectrum.

We note that AME for more distant, high redshift, sources will be redshifted to lower frequencies. Future high redshift observations with, for example, the SKA at frequencies $\lesssim$ 20 GHz, may need to take AME into account.

5.3. Current and future instruments and surveys

Looking to the future, what new instruments and surveys are needed to make further progress in understanding AME? Future studies will encompass detailed modelling of compact regions of the Galaxy (e.g., PDR, dark clouds, cold cores); observations of large numbers of such regions in order to gather statistics; large-scale surveys of the diffuse emission in the Galaxy; and searches for AME in other galaxies. Continuing to constrain the polarization of AME will be an important, if increasingly difficult, task. Resolving the spatial distribution of the AME on increasingly smaller scales will be limited by the maximum available resolution of the synchrotron and free–free templates available for subtracting these contributions.

Table 6 summarises some of the main current and planned astronomical facilities and surveys that will be important for AME research. To date, AME studies have relied on radio data from a disparate collection of single-dish telescopes and interferometers. Since AME is typically extended and diffuse, in order to make accurate, multi-frequency comparisons, the angular content of a map needs to be known, and ideally, contain the complete range of angular scales. For example, single-dish total power instruments typically require switching of the signal against a reference source or other form of high-pass filtering, which can reduce the sky signal on large angular scales. On the other hand, maps made using interferometers are sensitive to specific (and missing the largest) angular scales. Care must therefore be taken when constructing SEDs combining multi-frequency data from different interferometers and single-dish telescopes. It would be advantageous for AME studies if a single future instrument were able to cover the frequencies relevant to the AME itself, as well as synchrotron and free–free. The proposed next-generation VLA (ngVLA) and SKA interferometric arrays are promising in this regard (e.g., Dickinson et al., 2015), particularly if they can be supplemented with single-dish observations to fill in the missing large-scale information.

The C-Band All-Sky Survey (C-BASS; King et al. 2010) is a full-sky 5 GHz survey of intensity and polarization, at an angular resolution of $\approx 45'$. With high sensitivity ($\lesssim$ 0.1 mK) and accurate calibration, it will

Table 6
Current and future astronomical facilities and datasets that can be used for AME research. The table is separated in to different types of observational facilities (radio surveys, interferometers, IR surveys, and future). Values in parentheses are expected to be available in the future.

Telescope/ facility	Frequencies [GHz]	Angular Res. [arcmin]	Type	Status & Notes
C-BASS	5	45	Full-sky survey	Ongoing. Data to be made available
Effelsberg	$<$ 34	$\approx$ 0.3 @30 GHz	Single-dish	Available by request
GBT 100-m	$<$ 115	$\approx$ 0.3 @30 GHz	Single-dish	Available
Parkes	$<$ 24	$\approx$ 1 @21 GHz	Single-dish	Available by request
Planck	28,44,70,100 +	$\approx$ 33 @28.4 GHz	Full-sky surveys	Final data published
QUIJOTE-MFI	11,13,17,19	$\approx$ 55–36	Single-dish	Ongoing. Data to be made available
S-PASS	2.3	$\approx$ 9	Southern sky survey	Ongoing
WMAP	23,33,41,61,94	$\approx$ 50 @22.8GHz	Full-sky surveys	Final data published
ALMA	$\approx$ 30–50 (Band 1)	$\approx$ 0.1–4	Interferometer	Online and in development
AMI	13–18	$\approx$ 0.5–10	Interferometer	Available by request
ATCA	$<$ 105	$<$ 0.1	Interferometer	Available
VLA	$<$ 100	$<$ 0.1	Interferometer	Available and in development
AKARI	9–180 μm	$\approx$ 0.1–1.5	Full-sky surveys	Completed. Data to be made available
IRIS (IRAS/DIRBE)	12,25,60,100 μm	$\approx$ 2–4	Full-sky surveys	Final data published
Spitzer	3.6-160 μm	$\approx 0.02 - 0.8$	IR	Data available
WISE	3–25 μm	0.1–0.2	Full-sky surveys	Completed. Data available
CLASS	40,90,150,220	90–18	Southern sky survey	Data will be made publicly available
COMAP	26–34	$\approx$ 4	Single-dish	19 detectors, 0.2–8 MHz resolution (in prep.)
James Webb	5–28 μm (MIRI)	$<$ 0.02	Optical/IR	2018 launch
ngVLA	$\approx$ 1–116	$\approx$ 9mas–1 arcmin @30 GHz	Interferometer	Concept stage
Sardinia Radio Telescope	$<$ 26	1 @19.7 GHz	Single-dish	7-beam dual-pol array. Operational 2019
SKA	($<$ 14+)	$<$ 0.1	Interferometer	Phase 1 from $\approx$ 2023

provide a vital data point at 5 GHz. C-BASS data will be important for any component separation and large-scale studies with WMAP/*Planck* data (e.g., Irfan et al., 2015).

The Q-U-I JOint ExperimenT (QUIJOTE) is a dedicated CMB and foregrounds experiment, operating at Tenerife (Génova-Santos et al., 2015a). Although limited to $\approx 1^\circ$ resolution, and only northern sky,[12] QUIJOTE has a unique frequency coverage of 11, 13, 17 and 19 GHz, which covers the rising part of the spinning dust spectrum. QUIJOTE is primarily a polarization experiment but retains sensitivity to total-intensity, which is readily detectable at low Galactic latitudes. In combination with C-BASS, WMAP and *Planck* data, will be a powerful dataset for AME studies.

On small scales, the AMI (Zwart et al., 2008) telescope, is well-suited for studying AME. The AMI small array (AMI-SA) is a compact interferometer operating at 12–18 GHz with sensitivity to angular scales ≈ 2–$10'$ while the large array (AMI-LA) has a resolution of $\approx 0.5'$. The telescope has recently been upgraded with better receivers and a digital spectral backend (Hickish et al., 2017), resulting in better dynamic range allowing observations in the presence of bright radio frequency interference (RFI).

The available frequency range, dish size and baseline lengths makes the next-generation ngVLA, the Atacama Large Millimeter Array (ALMA), and the Square Kilometre Array (SKA), suitable for high resolution studies of compact and extended AME regions, but not for large-area surveys. ALMA is a large interferometric array located in Chile that can operate from 30 GHz up to ~ 1000 GHz and can achieve sub-arcsec angular resolution. The current capability is limited to frequencies above 84 GHz (band 3) while bands 1 (35–50 GHz) and 2 (67–90 GHz) are expected to come online around 2020.

A number of CMB experiments continue to operate from the ground with frequency channels in the tens of GHz. For example, the Cosmology Large Angular Scale Surveyor (CLASS, Essinger-Hileman et al., 2014) is focused on CMB (at multipoles $2 \lesssim \ell \lesssim 150$) and foreground characterization in intensity and in polarization. It will map around 70% of the sky from the Cerro Toco in the Atacama Desert (Chile), in frequency bands centred at 40, 90, 150 and 220 GHz with angular resolution 90, 40, 24 and 18′, respectively.

The CO Mapping Array Pathfinder (COMAP, Li et al., 2016) is an intensity mapping experiment aiming to constrain the carbon monoxide (CO) power spectrum from the epoch of reionization, but initially targeting intermediate redshifts of $z = 2.4$–3.4 with a 19-pixel focal plane array operating at 26–34 GHz. As ancillary science, COMAP will provide maps of extended AME regions with 4′ angular resolution and frequency resolution of around 8 MHz.

It is clear that for all of the above, accurate multi-frequency data are critical. However in order to be useful, the data need to be well-calibrated in terms of amplitude scale and quantification of the telescope beam. The use of existing large-scale radio maps, such as the Haslam 408 MHz (Haslam et al., 1982; Remazeilles et al., 2015), Reich 1.4 GHz (Reich and Reich, 1986; Reich et al., 2001) and HartRAO 2.3 GHz maps (Jonas et al., 1998) can be problematic. These surveys were made using general-purpose large radio telescopes that have relatively low beam efficiencies (i.e., the integrated sidelobe response represents a significant fraction of the response compared to the main beam). This means that the amplitude scale varies as a function of angular scale, often by tens of percent (see Du et al., 2016, for a discussion). For example, the full-beam to main-beam conversion factor for the Reich 1.4 GHz map is as much as a factor of 1.55. Correcting for this afterwards is not trivial. New data, such as C-BASS, should improve on this situation with improved calibration and knowledge of the full beam.

Since AME is dust-correlated, the availability of infra-red observations plays a critical role in AME studies. All-sky surveys from IRAS/IRIS and WISE are complemented by large-area surveys and observations of compact regions using the *Spitzer* Space Telescope. The AKARI satellite (Ishihara et al., 2010) made an all-sky survey with the 9 μm filter, which covers the entire PAH emission bands in the mid-IR, i.e., the bands at 6.2, 7.7, 8.6, and 11.3 μm, while the 12 μm band of IRAS and WISE do not completely cover the strong 6.2 and 7.7 μm bands and may suffer contribution from warm dust emission. Since the 6.2 and 7.7 μm bands (and the weaker 8.6 μm band) are thought to arise from ionized PAHs, and thus the 11 μm band comes from neutral PAHs, the correlation of AME with AKARI 9 μm could potentially be a better test for the spinning dust model, in which ionized PAHs contribute more significantly than neutral. However, the latest analysis of the correlation of AME with the AKARI 9 μm data do not show better correlation than with the far-IR emission (Bell et al., in prep.) in agreement with previous analyses with IRAS and WISE data (Hensley et al., 2016; Planck Collaboration et al., 2016d).

There is currently no active mid-far infra-red space telescope capability, although the airborne Sofia observatory is available. The launch of the James Webb Telescope (currently scheduled for Oct 2018) will provide space-based mid-infrared (5–28 μm) imaging and spectroscopic capability at sub-arcsec resolution, supporting detailed modelling of compact regions, but studies of larger areas will rely on existing data from IRAS/IRIS, *Spitzer* and WISE for the foreseeable future.

5.4. Laboratory studies

Laboratory studies are needed to help constrain the magnetic relaxation of small grains, which is one of the key problems relating to alignment of spinning dust grains (Lazarian and Draine, 2000). Measurements of the spin-lattice relaxation time will test theoretical models of both paramagnetic relaxation, which aligns a grain with an external magnetic field, and the alignment of the angular momentum vector with the principal axes of a wobbling grain.

For a spin to flip in a rotating grain, it is necessary for the total energy in lattice vibrations to change by $\hbar\omega$. Because the density of states is finite, it may not be possible for the lattice vibrations to absorb such energy. Indeed, the minimal bending mode frequency for grains smaller than 10^{-7} cm can be estimated to be orders of magnitude larger than $kT/\hbar$. According to Lazarian and Draine (2000) this does not mean that the spin relaxation time becomes infinite. To show this the authors considered the Raman scattering of phonons process (see Waller, 1932; Pake, 1962) where the change of the spin happens due to the scattering of phonons with energies much larger than $\hbar\omega$.

The calculations in Lazarian and Draine (2000) using the accepted approaches (see Al'tshuler and Kozyrev, 1964) provided the spin-lattice relaxation rates for the PAHs that may interfere with the resonance paramagnetic relaxation of smallest grains and can also affect the internal Barnett relaxation of energy within these particles. However, the Waller theory is known to overestimate the spin-lattice relaxation time by many orders of magnitude. Therefore, reliable estimates of the spin-lattice relaxation should be obtained through the laboratory studies of the magnetic response of suspended nano-particles.

Even more straightforward laboratory studies are required to test the expected magneto-dipole emission of magnetic grains as suggested in Lazarian and Draine (2000) and Draine and Hensley (2013). The two studies used different magnetic response expressions and none of the expressions seem to fit well to the limited available experimental data. Therefore it is important to do the corresponding laboratory studies in order to establish the magnetic response of the candidate materials at AME frequencies. For large grains the studies of the magnetic response of the bulk samples are adequate. Such studies can carried out using existing laboratory equipment.

5.5. Next steps for AME modelling

As reviewed in Section 2, theoretical models of spinning dust

[12] There are ongoing discussions about deploying the QUIJOTE instrument in South Africa, to allow a full-sky survey to be made.

emission are quite detailed in their consideration of various effects, which determine the rotational velocities and consequent microwave emission of ultrasmall interstellar grains. However, theoretical modelling faces two primary hurdles. First is that the identity of the AME carrier, and thus its material properties, are unknown. Second is that, even with perfect knowledge of the grain physics, predicting the emission from a particular interstellar environment is challenging due to the number of poorly constrained or completely unconstrained environmental parameters, such as the grain size distribution or the radiation spectrum and intensity. We address each of these hurdles in turn in this section.

Detailed calculations of rotational emission from a population of spinning grains require knowledge of: (1) the composition of the nanoparticles; (2) the distribution of sizes and shapes; (3) the electric (and perhaps magnetic) dipole moments of these particles; (4) the orientation of the dipole moment relative to the principal axes of the moment-of-inertia tensor of each particle; (5) the optical properties of the particles for absorption of optical-UV photons, and subsequent emission of infrared photons; (6) the vibrational mode spectrum of the particles, which determines the specific heat and the "temperature" of the particle as a function of internal energy; (7) the frequency-dependent magnetic polarizability of the nanoparticles, which will determine the importance of the Barnett effect, paramagnetic dissipation and "Barnett relaxation" (Purcell, 1979; Lazarian and Draine, 1999); (8) the photoelectric emission properties and (9) electron capture cross sections of the nanoparticles, which affect their electric charge; and (10) the spin-lattice relaxation times, which affect the rotational dynamics and alignment of grains. All of these physical properties are uncertain, and current theoretical modelling is based on assumptions whose validity is not always clear. Progress on these fundamental issues will be based on a combination of laboratory experiments and improved theoretical modelling of the structure of the particles, based on density functional theory, etc.

Even with perfect knowledge of the above properties, an *a priori* prediction of an AME spectrum of a specific interstellar region would be daunting due to the sensitivity of the calculations to various environmental parameters, which are typically poorly constrained. In light of this, future theoretical efforts should be directed toward what observational predictions can be made *irrespective of these modelling uncertainties*. A simple example is that the spinning dust emissivity per H atom should decrease in very high density gas where ultrasmall grains are expected to be depleted due to coagulation. Future observational efforts will be directed toward understanding systematic changes of the AME spectrum (e.g., emissivity per H atom, peak frequency, frequency width, shape) with environment. Assessing the magnitude of these changes in various idealized environments and identifying the environmental parameters inducing the largest changes will be invaluable in both selecting observational targets and for interpreting the data.

One step in this direction is continued development of the SPDUST code. In particular, porting the code to a language more amenable to integration in large simulations (e.g., Python, C, Fortran) than its native IDL would enable detailed exploration of the high-dimensional parameter space in which current models lie. Integration of such a code with models of interstellar clouds, as pioneered by Ysard et al. (2011), could identify generic predictions of spinning dust theory robust to variations in the grain properties or the specifics of the local interstellar environment.

In addition to improving the modelling of spinning dust emission and articulating generic observational predictions of how the AME spectrum should vary, theoretical efforts should also be directed toward connecting the AME to observational probes at other wavelengths. In particular, an abundance of AME carriers may have observable impact on the UV extinction, photoelectric heating, diffuse interstellar bands (see Bernstein et al., 2015), and/or MIR emission. Self consistent modelling of the AME and these phenomena may yield feasible observational tests of AME models, particularly the identity of the AME carrier(s).

Finally, while the hypothesis that the AME is predominantly rotational emission from rapidly-spinning nanoparticles is favoured at this time, the possibility remains that the AME is "thermal" emission from the "big" grains that dominate the grain mass, with the spectrum due to unusual frequency dependence of the material opacity (from either electric dipole or magnetic dipole absorption). Laboratory studies of magnetic absorption in candidate magnetic materials (e.g., metallic iron, magnetite, maghemite) are feasible and will be able to tell us whether currently-favoured phenomenological models based on the Gilbert equation (see Draine and Hensley, 2013) provide a good approximation to the actual magnetization dynamics. Laboratory studies on candidate amorphous materials at low temperatures can test whether any plausible materials exhibit a strong opacity peak in the 20–40 GHz region, possibly arising from conformational changes, as suggested by Jones (2009).

6. Concluding remarks

AME has become an important topic in astrophysics, both as a foreground for CMB observations and as a new component of the ISM. A strong, FIR-correlated component of emission has been detected at frequencies $\sim$ 10–100 GHz, which cannot be easily explained by CMB, synchrotron, free–free or thermal dust radiation. The lack of significant AME polarization appears to rule out magnetic dipole emission as the main source. The most favoured explanation is electric dipole radiation from tiny spinning dust grains. The underlying theory of spinning dust emission is well known, even if the detailed physics is not fully understood. There are at least two clear examples of high S/N detections, from the Perseus and ρ Ophiuchus molecular clouds, where the data are easily explained by a simple model of spinning dust emission.

Nevertheless, the picture is still far from settled on a number of aspects. There is a dearth of detections on very small angular scales; attempts to detect AME from compact Galactic objects (e.g., HII regions) has resulted in no clear detections. Indeed, in nearly all cases, AME is observed to have a diffuse morphology. The lack of correlation with PAHs appears to rule out PAHs as the main carriers of AME, at least along some sight-lines, even though theory would suggest that PAHs (being even smaller than the small dust "grains") are sufficiently numerous and spinning rapidly enough to naturally produce the majority of spinning dust emission, given a suitable electric dipole moment. On the other hand, the lack of AME in dense cores appears to rule out "big" dust grains as the carriers of AME. Therefore, the AME appears to be due to small spinning nano-particles containing an electric dipole moment, but the nature of these nano-particles is still undetermined.

Future AME research should continue on a number of independent fronts, including theory, laboratory measurements, as well as high-fidelity multi-frequency observations. New facilities have the capabilities to observe over a wide frequency range and at high angular resolution. New data should focus on testing specific aspects of the spinning (or magnetic) dust model predictions.

AME appears to not be a major limitation as a foreground in CMB temperature measurements. Careful component separation yields results that are not limited by foregrounds. However, CMB polarization data may be impacted. Current upper limits on AME polarization are at the level of $\approx$ 1 % and this could be non-negligible for future ultra-deep CMB polarization surveys.

Acknowledgements

We thank Chris Tibbs and colleagues at ESTEC for organising the 3rd AME workshop, held 23–24 June 2016 at ESTEC, Noordwijk, The Netherlands. CD acknowledges support from an STFC Consolidated Grants (ST/P000649/1) and an ERC Starting (Consolidator) Grant (no. 307209). BTD was supported in part by NSF grant AST-1408723. TH acknowledges the support by the Basic Science Research Program

through the National Research Foundation of Korea (NRF), funded by the Ministry of Education (2017R1D1A1B03035359). CTT acknowledges an ESA Research Fellowship. ESB acknowledges support from Sapienza Ateneo projects 2016. AB and TO are supported by JSPS and CNRS under the Japan–France Research Cooperative Program. CHLC thanks CONICYT for grant Anillo ACT-1417. MP acknowledges grant #2015/19936-1, São Paulo Research Foundation (FAPESP). YCP acknowledges support from a Trinity College JRF. FP thanks the European Commission under the Marie Sklodowska-Curie Actions within the H2020 program, Grant Agreement number: 658499-PolAME-H2020-MSCA-IF-2014. JARM acknowledges the funding from the European Union's Horizon 2020 research and innovation programme under grant agreement number 687312 (RADIOFOREGROUNDS). This work has been partially funded by the Spanish Ministry of Economy and Competitiveness (MINECO) under the project AYA2014-60438-P. MV acknowledges support from FONDECYT through grant 3160750. We thank George Bendo and Tim Pearson for helpful discussions while preparing the draft. This research was carried out in part at the Jet Propulsion Laboratory, California Institute of Technology, under a contract with the National Aeronautics and Space Administration.

Supplementary material

Supplementary material associated with this article can be found, in the online version, at doi:10.1016/j.newar.2018.02.001.

References

Agladze, N.I., Sievers, A.J., Jones, S.A., Burlitch, J.M., Beckwith, S.V.W., 1996. Laboratory results on millimeter-wave absorption in silicate grain materials at cryogenic temperatures. ApJ 462, 1026. http://dx.doi.org/10.1086/177217.

Ainsworth, R.E., Coughlan, C.P., Green, D.A., Scaife, A.M.M., Ray, T.P., 2016. A GMRT survey of regions towards the taurus molecular cloud at 323 and 608 MHz. MNRAS 462, 2904–2917. http://dx.doi.org/10.1093/mnras/stw1847.

Ali-Haïmoud, Y., 2013. Spinning dust radiation: a review of the theory. Adv. Astron. 2013, 462697. http://dx.doi.org/10.1155/2013/462697.

Ali-Haïmoud, Y., 2014. Rotational spectroscopy of interstellar PAHs. MNRAS 437, 2728–2743. http://dx.doi.org/10.1093/mnras/stt2083.

Ali-Haïmoud, Y., Hirata, C.M., Dickinson, C., 2009. A refined model for spinning dust radiation. MNRAS 395, 1055–1078. http://dx.doi.org/10.1111/j.1365-2966.2009.14599.x.

Ali-Haïmoud, Y., Pérez, L.M., Maddalena, R.J., Roshi, D.A., 2015. Search for polycyclic aromatic hydrocarbons in the Perseus molecular cloud with the Green Bank telescope. MNRAS 447, 315–324. http://dx.doi.org/10.1093/mnras/stu2476.

Alonso, D., Dunkley, J., Thorne, B., Næss, S., 2017. Simulated forecasts for primordial B -mode searches in ground-based experiments. Phys. Rev. D 95 (4), 043504. http://dx.doi.org/10.1103/PhysRevD.95.043504.

Altobelli, N., Postberg, F., Fiege, K., Trieloff, M., Kimura, H., Sterken, V.J., Hsu, H.-W., Hillier, J., Khawaja, N., Moragas-Klostermeyer, G., Blum, J., Burton, M., Srama, R., Kempf, S., Gruen, E., 2016. Flux and composition of interstellar dust at Saturn from Cassini's cosmic dust analyzer. Science 352, 312–318. http://dx.doi.org/10.1126/science.aac6397.

Al'tshuler, S.A., Kozyrev, B.M., 1964. Electron Paramagnetic Resonance. Elsevier. FTD-TT-72-1086

AMI Consortium, Scaife, A.M.M., Hurley-Walker, N., Green, D.A., Davies, M.L., Grainge, K.J.B., Hobson, M.P., Lasenby, A.N., López-Caniego, M., Pooley, G.G., Saunders, R.D.E., Scott, P.F., Titterington, D.J., Waldram, E.M., Zwart, J.T.L., 2009. An excess of emission in the dark cloud LDN1111 with the arcminute microkelvin imager. MNRAS 394, L46–L50. http://dx.doi.org/10.1111/j.1745-3933.2008.00607.x.

Andersson, B.-G., Lazarian, A., Vaillancourt, J.E., 2015. Interstellar dust grain alignment. ARA&A 53, 501–539. http://dx.doi.org/10.1146/annurev-astro-082214-122414.

André, P., Men'shchikov, A., Bontemps, S., Könyves, V., Motte, F., Schneider, N., Didelon, P., Minier, V., Saraceno, P., Ward-Thompson, D., et al., 2010. From filamentary clouds to Prestellar cores to the stellar IMF: initial highlights from the Herschel Gould belt survey. A&A 518, L102. http://dx.doi.org/10.1051/0004-6361/201014666.

Andrews, H., Boersma, C., Werner, M.W., Livingston, J., Allamandola, L.J., Tielens, A.G.G.M., 2015. PAH emission at the bright locations of PDRs: the grandpah hypothesis. ApJ 807, 99. http://dx.doi.org/10.1088/0004-637X/807/1/99.

Armitage-Caplan, C., Dunkley, J., Eriksen, H.K., Dickinson, C., 2012. Impact on the tensor-to-scalar ratio of incorrect Galactic foreground modelling. MNRAS 424, 1914–1924. http://dx.doi.org/10.1111/j.1365-2966.2012.21314.x.

Banday, A.J., Dickinson, C., Davies, R.D., Davis, R.J., Górski, K.M., 2003. Reappraising foreground contamination in the COBE-DMR data. MNRAS 345, 897–911. http://dx.doi.org/10.1046/j.1365-8711.2003.07008.x.

Barcos-Muñoz, L., Leroy, A.K., Evans, A.S., Condon, J., Privon, G.C., Thompson, T.A., Armus, L., Díaz-Santos, T., Mazzarella, J.M., Meier, D.S., Momjian, E., Murphy, E.J., Ott, J., Sanders, D.B., Schinnerer, E., Stierwalt, S., Surace, J.A., Walter, F., 2017. A 33 GHz survey of local major mergers: estimating the sizes of the energetically dominant regions from high-resolution measurements of the radio continuum. ApJ 843, 117. http://dx.doi.org/10.3847/1538-4357/aa789a.

Battistelli, E.S., Carretti, E., Cruciani, A., de Bernardis, P., Génova-Santos, R., Masi, S., Naldi, A., Paladini, R., Piacentini, F., Tibbs, C.T., Verstraete, L., Ysard, N., 2015. New radio observations of anomalous microwave emission in the H II region RCW175. ApJ 801, 111. http://dx.doi.org/10.1088/0004-637X/801/2/111.

Battistelli, E.S., Rebolo, R., Rubiño-Martín, J.A., Hildebrandt, S.R., Watson, R.A., Gutiérrez, C., Hoyland, R.J., 2006. Polarization observations of the anomalous microwave emission in the perseus molecular complex with the COSMOSOMAS experiment. ApJ 645, L141–L144. http://dx.doi.org/10.1086/506254.

Bennett, C.L., Hill, R.S., Hinshaw, G., Nolta, M.R., Odegard, N., Page, L., Spergel, D.N., Weiland, J.L., Wright, E.L., Halpern, M., Jarosik, N., Kogut, A., Limon, M., Meyer, S.S., Tucker, G.S., Wollack, E., 2003. First-year Wilkinson microwave anisotropy probe (WMAP) observations: foreground emission. ApJS 148, 97–117. http://dx.doi.org/10.1086/377252.

Bennett, C.L., Larson, D., Weiland, J.L., Jarosik, N., Hinshaw, G., Odegard, N., Smith, K.M., Hill, R.S., Gold, B., Halpern, M., Komatsu, E., Nolta, M.R., Page, L., Spergel, D.N., Wollack, E., Dunkley, J., Kogut, A., Limon, M., Meyer, S.S., Tucker, G.S., Wright, E.L., 2013. Nine-year Wilkinson microwave anisotropy probe (WMAP) observations: final maps and results. ApJS 208, 20. http://dx.doi.org/10.1088/0067-0049/208/2/20.

Bernstein, L.S., Clark, F.O., Cline, J.A., Lynch, D.K., 2015. The diffuse interstellar bands and anomalous microwave emission may originate from the same carriers. ApJ 813, 122. http://dx.doi.org/10.1088/0004-637X/813/2/122.

Bernstein, L.S., Shroll, R.M., Lynch, D.K., Clark, F.O., 2017. A small fullerene (c_{24}) may be the carrier of the 11.2 μm unidentified infrared band. ApJ 836, 229. http://dx.doi.org/10.3847/1538-4357/aa5c89.

BICEP2 Collaboration, Keck Array Collaboration, Ade, P.A.R., Ahmed, Z., Aikin, R.W., Alexander, K.D., Barkats, D., Benton, S.J., Bischoff, C.A., Bock, J.J., et al., 2016. Improved constraints on cosmology and foregrounds from BICEP2 and Keck array cosmic microwave background data with inclusion of 95 GHz band. Phys. Rev. Lett. 116 (3), 031302. http://dx.doi.org/10.1103/PhysRevLett.116.031302.

Bot, C., Ysard, N., Paradis, D., Bernard, J.P., Lagache, G., Israel, F.P., Wall, W.F., 2010. Submillimeter to centimeter excess emission from the magellanic clouds. II. On the nature of the excess. A&A 523, A20. http://dx.doi.org/10.1051/0004-6361/201014986.

Bradley, J.P., 1994. Chemically anomalous, preaccretionally irradiated grains in interplanetary dust from comets. Science 265, 925–929. http://dx.doi.org/10.1126/science.265.5174.925.

Casassus, S., Cabrera, G.F., Förster, F., Pearson, T.J., Readhead, A.C.S., Dickinson, C., 2006. Morphological analysis of the centimeter-wave continuum in the dark cloud LDN 1622. ApJ 639, 951–964. http://dx.doi.org/10.1086/499517.

Casassus, S., Dickinson, C., Cleary, K., Paladini, R., Etxaluze, M., Lim, T., White, G.J., Burton, M., Indermuehle, B., Stahl, O., Roche, P., 2008. Centimetre-wave continuum radiation from the ρ Ophiuchi molecular cloud. MNRAS 391, 1075–1090. http://dx.doi.org/10.1111/j.1365-2966.2008.13954.x.

Casassus, S., Nyman, L.-Å., Dickinson, C., Pearson, T.J., 2007. A centimetre-wave excess over free–free emission in planetary nebulae. MNRAS 382, 1607–1622. http://dx.doi.org/10.1111/j.1365-2966.2007.12366.x.

Castellanos, P., Casassus, S., Dickinson, C., Vidal, M., Paladini, R., Cleary, K., Davies, R.D., Davis, R.J., White, G.J., Taylor, A., 2011. Dust-correlated centimetre-wave radiation from the M78 reflection nebula. MNRAS 411, 1137–1150. http://dx.doi.org/10.1111/j.1365-2966.2010.17743.x.

Coughlan, C.P., Ainsworth, R.E., Eislöffel, J., Hoeft, M., Drabent, A., Scaife, A.M.M., Ray, T.P., Bell, M.E., Broderick, J.W., Corbel, S., Grießmeier, J.-M., van der Horst, A.J., van Leeuwen, J., Markoff, S., Pietka, M., Stewart, A.J., Wijers, R.A.M.J., Zarka, P., 2017. A LOFAR detection of the low-mass young star T tau at 149 MHz. ApJ 834, 206. http://dx.doi.org/10.3847/1538-4357/834/2/206.

Cruciani, A., Battistelli, E.S., Carretti, E., de Bernardis, P., Genova-Santos, R., Masi, S., Mason, B., Perera, D., Piacentini, F., Reach, B., Rubino-Martin, J.A., 2016. Detailed study of the microwave emission of the supernova remnant 3C 396. MNRAS 459, 4224–4232. http://dx.doi.org/10.1093/mnras/stw839.

Davies, R.D., Dickinson, C., Banday, A.J., Jaffe, T.R., Górski, K.M., Davis, R.J., 2006. A determination of the spectra of Galactic components observed by the Wilkinson microwave anisotropy probe. MNRAS 370, 1125–1139. http://dx.doi.org/10.1111/j.1365-2966.2006.10572.x.

Davies, R.D., Watson, R.A., Gutierrez, C.M., 1996. Galactic synchrotron emission at high frequencies. MNRAS 278, 925–939.

Davis Jr., L., Greenstein, J.L., 1951. The polarization of starlight by aligned dust grains. ApJ 114, 206. http://dx.doi.org/10.1086/145464.

de Oliveira-Costa, A., Kogut, A., Devlin, M.J., Netterfield, C.B., Page, L.A., Wollack, E.J., 1997. Galactic microwave emission at degree angular scales. ApJ 482, L17. http://dx.doi.org/10.1086/310684.

de Oliveira-Costa, A., Tegmark, M., Davies, R.D., Gutiérrez, C.M., Lasenby, A.N., Rebolo, R., Watson, R.A., 2004. The quest for microwave foreground x. ApJ 606, L89–L92. http://dx.doi.org/10.1086/421293.

de Oliveira-Costa, A., Tegmark, M., Devlin, M.J., Haffner, L.M., Herbig, T., Miller, A.D., Page, L.A., Reynolds, R.J., Tufte, S.L., 2000. Galactic contamination in the QMAP experiment. ApJ 542, L5–L8. http://dx.doi.org/10.1086/312909.

de Oliveira-Costa, A., Tegmark, M., Finkbeiner, D.P., Davies, R.D., Gutierrez, C.M., Haffner, L.M., Jones, A.W., Lasenby, A.N., Rebolo, R., Reynolds, R.J., Tufte, S.L., Watson, R.A., 2002. A new spin on galactic dust. ApJ 567, 363–369. http://dx.doi.org/10.1086/338109.

de Oliveira-Costa, A., Tegmark, M., Gutierrez, C.M., Jones, A.W., Davies, R.D., Lasenby, A.N., Rebolo, R., Watson, R.A., 1999. Cross-correlation of tenerife data with galactic

templates-evidence for spinning dust? ApJ 527, L9–L12. http://dx.doi.org/10.1086/312384.
de Oliveira-Costa, A., Tegmark, M., Page, L.A., Boughn, S.P., 1998. Galactic emission at 19 GHZ. ApJ 509, L9–L12. http://dx.doi.org/10.1086/311754.
Demetroullas, C., Dickinson, C., Stamadianos, D., Harper, S.E., Cleary, K., Jones, M.E., Pearson, T.J., Readhead, A.C.S., Taylor, A.C., 2015. Observations of galactic star-forming regions with the cosmic background imager at 31 GHz. MNRAS 453, 2082–2093. http://dx.doi.org/10.1093/mnras/stv1793.
Dickinson, C., 2013. Observations of anomalous microwave emission from HII regions. Adv. Astron. 2013, id.162478. http://dx.doi.org/10.1155/2013/162478.
Dickinson, C., Ali-Hamoud, Y., Beswick, R.J., Casassus, S., Cleary, K., Draine, B., Genova-Santos, R., Grainge, K., Hoang, T.C., Lazarian, A., Murphy, E., Paladini, R., Peel, M.W., Perrott, Y., Rubino-Martin, J.A., Scaife, A., Tibbs, C., Verstraete, L., Vidal, M., Watson, R.A., Ysard, N., 2015. Studies of anomalous microwave emission (AME) with the SKA. Advancing Astrophysics with the Square Kilometre Array (AASKA14). pp. 124.
Dickinson, C., Battye, R.A., Carreira, P., Cleary, K., Davies, R.D., Davis, R.J., Genova-Santos, R., Grainge, K., Gutiérrez, C.M., Hafez, Y.A., et al., 2004. High-sensitivity measurements of the cosmic microwave background power spectrum with the extended very small array. MNRAS 353, 732–746. http://dx.doi.org/10.1111/j.1365-2966.2004.08206.x.
Dickinson, C., Casassus, S., Davies, R.D., Allison, J.R., Bustos, R., Cleary, K., Davis, R.J., Jones, M.E., Pearson, T.J., Readhead, A.C.S., Reeves, R., Taylor, A.C., Tibbs, C.T., Watson, R.A., 2010. Infrared-correlated 31-GHz radio emission from Orion East. MNRAS 407, 2223–2229. http://dx.doi.org/10.1111/j.1365-2966.2010.17079.x.
Dickinson, C., Casassus, S., Pineda, J.L., Pearson, T.J., Readhead, A.C.S., Davies, R.D., 2006. An upper limit on anomalous dust emission at 31 GHz in the diffuse cloud [LPH96] 201.663 + 1.643. ApJ 643, L111–L114. http://dx.doi.org/10.1086/505299.
Dickinson, C., Davies, R.D., Allison, J.R., Bond, J.R., Casassus, S., Cleary, K., Davis, R.J., Jones, M.E., Mason, B.S., Myers, S.T., Pearson, T.J., Readhead, A.C.S., Sievers, J.L., Taylor, A.C., Todorović, M., White, G.J., Wilkinson, P.N., 2009. Anomalous microwave emission from the H II region RCW175. ApJ 690, 1585–1589. http://dx.doi.org/10.1088/0004-637X/690/2/1585.
Dickinson, C., Davies, R.D., Bronfman, L., Casassus, S., Davis, R.J., Pearson, T.J., Readhead, A.C.S., Wilkinson, P.N., 2007. CBI limits on 31GHz excess emission in southern HII regions. MNRAS 379, 297–307. http://dx.doi.org/10.1111/j.1365-2966.2007.11967.x.
Dickinson, C., Davies, R.D., Davis, R.J., 2003. Towards a free–free template for CMB foregrounds. MNRAS 341, 369–384. http://dx.doi.org/10.1046/j.1365-8711.2003.06439.x.
Dickinson, C., Eriksen, H.K., Banday, A.J., Jewell, J.B., Górski, K.M., Huey, G., Lawrence, C.R., O'Dwyer, I.J., Wandelt, B.D., 2009. Bayesian component separation and cosmic microwave background estimation for the five-year WMAP temperature data. ApJ 705, 1607–1623. http://dx.doi.org/10.1088/0004-637X/705/2/1607.
Dickinson, C., Paladini, R., Verstraete, L., 2013. Anomalous microwave emission: theory, modeling, and observations. Adv. Astron. 2013. http://dx.doi.org/10.1155/2013/134979. 1–1
Dickinson, C., Peel, M., Vidal, M., 2011. New constraints on the polarization of anomalous microwave emission in nearby molecular clouds. MNRAS 418, L35–L39. http://dx.doi.org/10.1111/j.1745-3933.2011.01138.x.
Dobler, G., Finkbeiner, D.P., 2008. Extended anomalous foreground emission in the WMAP three-year data. ApJ 680, 1222–1234. http://dx.doi.org/10.1086/587862.
Draine, B.T., 1990. Evolution of interstellar dust. In: Blitz, L. (Ed.), The Evolution of the Interstellar Medium. Astronomical Society of the Pacific Conference Series 12. pp. 193–205.
Draine, B.T., 2009. Interstellar Dust Models and Evolutionary Implications. In: Henning, T., Grün, E., Steinacker, J. (Eds.), Cosmic Dust - Near and Far. Astronomical Society of the Pacific Conference Series 414. pp. 453.
Draine, B.T., 2011. Physics of the Interstellar and Intergalactic Medium. Princeton University Press.
Draine, B.T., Hensley, B., 2012. The submillimeter and millimeter excess of the small magellanic cloud: magnetic dipole emission from magnetic nanoparticles? ApJ 757, 103. http://dx.doi.org/10.1088/0004-637X/757/1/103.
Draine, B.T., Hensley, B., 2013. Magnetic nanoparticles in the interstellar medium: emission spectrum and polarization. ApJ 765, 159. http://dx.doi.org/10.1088/0004-637X/765/2/159.
Draine, B.T., Hensley, B.S., 2016. Quantum suppression of alignment in ultrasmall grains: microwave emission from spinning dust will be negligibly polarized. ApJ 831, 59. http://dx.doi.org/10.3847/0004-637X/831/1/59.
Draine, B.T., Lazarian, A., 1998a. Diffuse galactic emission from spinning dust grains. ApJ 494, L19–L22. http://dx.doi.org/10.1086/311167.
Draine, B.T., Lazarian, A., 1998b. Electric dipole radiation from spinning dust grains. ApJ 508, 157–179. http://dx.doi.org/10.1086/306387.
Draine, B.T., Lazarian, A., 1999. Magnetic dipole microwave emission from dust grains. ApJ 512, 740–754. http://dx.doi.org/10.1086/306809.
Du, X., Landecker, T.L., Robishaw, T., Gray, A.D., Douglas, K.A., Wolleben, M., 2016. Gain and polarization properties of a large radio telescope from calculation and measurement: the john a. galt telescope. PASP 128 (11), 115006. http://dx.doi.org/10.1088/1538-3873/128/969/115006.
Dunkley, J., Amblard, A., Baccigalupi, C., Betoule, M., Chuss, D., Cooray, A., Delabrouille, J., Dickinson, C., Dobler, G., Dotson, J., et al., 2009a. Prospects for polarized foreground removal. American Institute of Physics Conference Series 1141. pp. 222–264. http://dx.doi.org/10.1063/1.3160888.
Dunkley, J., Spergel, D.N., Komatsu, E., Hinshaw, G., Larson, D., Nolta, M.R., Odegard, N., Page, L., Bennett, C.L., Gold, B., Hill, R.S., Jarosik, N., Weiland, J.L., Halpern, M., Kogut, A., Limon, M., Meyer, S.S., Tucker, G.S., Wollack, E., Wright, E.L., 2009. Five-year Wilkinson microwave anisotropy probe (WMAP) observations: Bayesian estimation of cosmic microwave background polarization maps. ApJ 701, 1804–1813. http://dx.doi.org/10.1088/0004-637X/701/2/1804.
Erickson, W.C., 1957. A mechanism of non-thermal radio-noise origin. ApJ 126, 480. http://dx.doi.org/10.1086/146421.
Essinger-Hileman, T., Ali, A., Amiri, M., Appel, J.W., Araujo, D., Bennett, C.L., Boone, F., Chan, M., Cho, H.-M., Chuss, D.T., et al., 2014. CLASS: the cosmology large angular scale surveyor. Millimeter, Submillimeter, and Far-Infrared Detectors and Instrumentation for Astronomy VII. Proceedings of SPIE 9153. pp. 91531I. http://dx.doi.org/10.1117/12.2056701.
Ferrara, A., Dettmar, R.-J., 1994. Radio-emitting dust in the free electron layer of spiral galaxies: testing the disk/halo interface. ApJ 427, 155–159. http://dx.doi.org/10.1086/174128.
Finkbeiner, D.P., 2003. A full-sky hα template for microwave foreground prediction. ApJS 146, 407–415. http://dx.doi.org/10.1086/374411.
Finkbeiner, D.P., 2004. Microwave interstellar medium emission observed by the Wilkinson microwave anisotropy probe. ApJ 614, 186–193. http://dx.doi.org/10.1086/423482.
Finkbeiner, D.P., Davis, M., Schlegel, D.J., 1999. Extrapolation of galactic dust emission at 100 microns to cosmic microwave background radiation frequencies using FIRAS. ApJ 524, 867–886. http://dx.doi.org/10.1086/307852.
Finkbeiner, D.P., Langston, G.I., Minter, A.H., 2004. Microwave interstellar medium emission in the green bank galactic plane survey: evidence for spinning dust. ApJ 617, 350–359. http://dx.doi.org/10.1086/425165.
Finkbeiner, D.P., Schlegel, D.J., Frank, C., Heiles, C., 2002. Tentative detection of electric dipole emission from rapidly rotating dust grains. ApJ 566, 898–904. http://dx.doi.org/10.1086/338225.
Fuskeland, U., Wehus, I.K., Eriksen, H.K., Næss, S.K., 2014. Spatial variations in the spectral index of polarized synchrotron emission in the 9 yr WMAP sky maps. ApJ 790, 104. http://dx.doi.org/10.1088/0004-637X/790/2/104.
Gaustad, J.E., McCullough, P.R., van Buren, D., 1996. An upper limit on the contribution of galactic free–free emission to the cosmic microwave background near the north celestial pole. PASP 108, 351. http://dx.doi.org/10.1086/133729.
Génova-Santos, R., Rebolo, R., Rubiño-Martín, J.A., López-Caraballo, C.H., Hildebrandt, S.R., 2011. Detection of anomalous microwave emission in the pleiades reflection nebula with wilkinson microwave anisotropy probe and the COSMOSOMAS experiment. ApJ 743, 67. http://dx.doi.org/10.1088/0004-637X/743/1/67.
Génova-Santos, R., Rubiño-Martín, J.A., Peláez-Santos, A., Poidevin, F., Rebolo, R., Vignaga, R., Artal, E., Harper, S., Hoyland, R., Lasenby, A., Martínez-González, E., Piccirillo, L., Tramonte, D., Watson, R.A., 2017. QUIJOTE scientific results - II. Polarisation measurements of the microwave emission in the Galactic molecular complexes W43 and W47 and supernova remnant W44. MNRAS 464, 4107–4132. http://dx.doi.org/10.1093/mnras/stw2503.
Génova-Santos, R., Rubiño-Martín, J.A., Rebolo, R., Aguiar, M., Gómez-Reñasco, F., Gutiérrez, C., Hoyland, R.J., López-Caraballo, C., Peláez-Santos, A.E., Pérez-de-Taoro, M.R., et al., 2015. The QUIJOTE experiment: project overview and first results. In: Cenarro, A.J., Figueras, F., Hernández-Monteagudo, C., Trujillo Bueno, J., Valdivielso, L. (Eds.), Highlights of Spanish Astrophysics VIII, pp. 207–212. [arXiv:1504.03514].
Génova-Santos, R., Rubiño-Martín, J.A., Rebolo, R., Peláez-Santos, A., López-Caraballo, C.H., Harper, S., Watson, R.A., Ashdown, M., Barreiro, R.B., Casaponsa, B., Dickinson, C., et al., 2015. QUIJOTE scientific results - I. Measurements of the intensity and polarisation of the anomalous microwave emission in the Perseus molecular complex. MNRAS 452, 4169–4182. http://dx.doi.org/10.1093/mnras/stv1405.
Ghosh, T., Banday, A.J., Jaffe, T., Dickinson, C., Davies, R., Davis, R., Gorski, K., 2012. Foreground analysis using cross-correlations of external templates on the 7-year Wilkinson Microwave Anisotropy Probe data. MNRAS 422, 3617–3642. http://dx.doi.org/10.1111/j.1365-2966.2012.20875.x.
Gilbert, T.L., 2004. Classics in magnetics a phenomenological theory of damping in ferromagnetic materials. IEEE Trans Magn 40, 3443–3449. http://dx.doi.org/10.1109/TMAG.2004.836740.
Gold, B., Odegard, N., Weiland, J.L., Hill, R.S., Kogut, A., Bennett, C.L., Hinshaw, G., Chen, X., Dunkley, J., Halpern, M., Jarosik, N., Komatsu, E., Larson, D., Limon, M., Meyer, S.S., Nolta, M.R., Page, L., Smith, K.M., Spergel, D.N., Tucker, G.S., Wollack, E., Wright, E.L., 2011. Seven-year Wilkinson microwave anisotropy probe (WMAP) observations: galactic foreground emission. ApJS 192, 15. http://dx.doi.org/10.1088/0067-0049/192/2/15.
Hamilton, J.-C., Ganga, K.M., 2001. Correlation of the South Pole 94 data with 100 μm and 408 MHz maps. A&A 368, 760–765. http://dx.doi.org/10.1051/0004-6361:20010061.
Harper, S.E., Dickinson, C., Cleary, K., 2015. Observations of free–free and anomalous microwave emission from LDN 1622 with the 100 m Green Bank telescope. MNRAS 453, 3375–3385. http://dx.doi.org/10.1093/mnras/stv1863.
Haslam, C.G.T., Salter, C.J., Stoffel, H., Wilson, W.E., 1982. A 408 MHz all-sky continuum survey. II – the atlas of contour maps. A&AS 47, 1.
Hensley, B., Murphy, E., Staguhn, J., 2015. Characterizing extragalactic anomalous microwave emission in NGC 6946 with CARMA. MNRAS 449, 809–819. http://dx.doi.org/10.1093/mnras/stv287.
Hensley, B.S., Draine, B.T., 2017. Modeling the anomalous microwave emission with spinning nanoparticles: no PAHs required. ApJ 836, 179. http://dx.doi.org/10.3847/1538-4357/aa5c37.
Hensley, B.S., Draine, B.T., Meisner, A.M., 2016. A case against spinning PAHs as the source of the anomalous microwave emission. ApJ 827, 45. http://dx.doi.org/10.3847/0004-637X/827/1/45.
Hickish, J., Razavi-Ghods, N., Perrott, Y.C., Titterington, D.J., Carey, S.H., Scott, P.F., Grainge, K.J.B., Scaife, A.M.M., Alexander, P., Saunders, R.D.E., Crofts, M., Javid, K.,

Rumsey, C., Jin, T.Z., Ely, J.A., Shaw, C., Northrop, I.G., Pooley, G., D'Alessandro, R., Doherty, P., Willatt, G.P., 2017. A digital correlator upgrade for the arcminute microkelvin imager. Submitted to Instrum. Methods Astrophys. arXiv:1707.04237.
Hildebrandt, S.R., Rebolo, R., Rubiño-Martín, J.A., Watson, R.A., Gutiérrez, C.M., Hoyland, R.J., Battistelli, E.S., 2007. COSMOSOMAS observations of the cosmic microwave background and galactic foregrounds at 11 GHz: evidence for anomalous microwave emission at high galactic latitude. MNRAS 382, 594–608. http://dx.doi.org/10.1111/j.1365-2966.2007.12380.x.
Hoang, T., 2017. Effect of alignment on polarized infrared emission from polycyclic aromatic hydrocarbons. ApJ 838, 112. http://dx.doi.org/10.3847/1538-4357/aa65cf.
Hoang, T., Draine, B.T., Lazarian, A., 2010. Improving the model of emission from spinning dust: effects of grain wobbling and transient spin-up. ApJ 715, 1462–1485. http://dx.doi.org/10.1088/0004-637X/715/2/1462.
Hoang, T., Lazarian, A., 2016a. A unified model of grain alignment: radiative alignment of interstellar grains with magnetic inclusions. ApJ 831, 159. http://dx.doi.org/10.3847/0004-637X/831/2/159.
Hoang, T., Lazarian, A., 2016b. Polarization of magnetic dipole emission and spinning dust emission from magnetic nanoparticles. ApJ 821, 91. http://dx.doi.org/10.3847/0004-637X/821/2/91.
Hoang, T., Lazarian, A., Draine, B.T., 2011. Spinning dust emission: effects of irregular grain shape, transient heating, and comparison with Wilkinson microwave anisotropy probe results. ApJ 741, 87. http://dx.doi.org/10.1088/0004-637X/741/2/87.
Hoang, T., Lazarian, A., Martin, P.G., 2013. Constraint on the polarization of electric dipole emission from spinning dust. ApJ 779, 152. http://dx.doi.org/10.1088/0004-637X/779/2/152.
Hoang, T., Vinh, N.-A., Quynh Lan, N., 2016. Spinning dust emission from ultra-small silicates: emissivity and polarization spectrum. ApJ 824, 18. http://dx.doi.org/10.3847/0004-637X/824/1/18.
Hoyle, F., Wickramasinghe, N.C., 1970. Radio waves from grains in HII regions. Nature 227, 473–474. http://dx.doi.org/10.1038/227473a0.
Hudgins, D.M., Bauschlicher Jr., C.W., Allamandola, L.J., 2005. Variations in the peak position of the 6.2 μm interstellar emission feature: a tracer of n in the interstellar polycyclic aromatic hydrocarbon population. ApJ 632, 316–332. http://dx.doi.org/10.1086/432495.
Irfan, M.O., Dickinson, C., Davies, R.D., Copley, C., Davis, R.J., Ferreira, P.G., Holler, C.M., Jonas, J.L., Jones, M.E., King, O.G., Leahy, J.P., Leech, J., Leitch, E.M., Muchovej, S.J.C., Pearson, T.J., Peel, M.W., Readhead, A.C.S., Stevenson, M.A., Sutton, D., Taylor, A.C., Zuntz, J., 2015. C-band all-sky survey: a first look at the galaxy. MNRAS 448, 3572–3586. http://dx.doi.org/10.1093/mnras/stv212.
Ishihara, D., Onaka, T., Kataza, H., Salama, A., Alfageme, C., Cassatella, A., Cox, N., García-Lario, P., Stephenson, C., Cohen, M., et al., 2010. The AKARI/IRC mid-infrared all-sky survey. A&A 514, A1. http://dx.doi.org/10.1051/0004-6361/200913811.
Israel, F.P., Wall, W.F., Raban, D., Reach, W.T., Bot, C., Oonk, J.B.R., Ysard, N., Bernard, J.P., 2010. Submillimeter to centimeter excess emission from the magellanic clouds. I. Global spectral energy distribution. A&A 519, A67. http://dx.doi.org/10.1051/0004-6361/201014073.
Jenkins, E.B., 2009. A unified representation of gas-phase element depletions in the interstellar medium. ApJ 700, 1299–1348. http://dx.doi.org/10.1088/0004-637X/700/2/1299.
Jonas, J.L., Baart, E.E., Nicolson, G.D., 1998. The Rhodes/Hartrao 2326-MHz radio continuum survey. MNRAS 297, 977–989. http://dx.doi.org/10.1046/j.1365-8711.1998.01367.x.
Jones, A.P., 2009. Microwave emission from dust revisited. A&A 506, 797–798. http://dx.doi.org/10.1051/0004-6361/200810621.
Juvela, M., Ristorcelli, I., Montier, L.A., Marshall, D.J., Pelkonen, V.-M., Malinen, J., Ysard, N., Tóth, L.V., Harju, J., Bernard, J.-P., et al., 2010. Galactic cold cores: Herschel study of first planck detections. A&A 518, L93. http://dx.doi.org/10.1051/0004-6361/201014619.
Kamionkowski, M., Kosowsky, A., Stebbins, A., 1997. A probe of primordial gravity waves and vorticity. Phys. Rev. Lett. 78, 2058–2061. http://dx.doi.org/10.1103/PhysRevLett.78.2058.
King, O.G., Copley, C., Davies, R., Davis, R., Dickinson, C., Hafez, Y.A., Holler, C., John, J.J., Jonas, J.L., Jones, M.E., Leahy, J.P., Muchovej, S.J.C., Pearson, T.J., Readhead, A.C.S., Stevenson, M.A., Taylor, A.C., 2010. The C-band all-sky survey: instrument design, status, and first-look data. Society of Photo-Optical Instrumentation Engineers (SPIE) Conference Series 7741http://dx.doi.org/10.1117/12.858011.
Kogut, A., Banday, A.J., Bennett, C.L., Gorski, K.M., Hinshaw, G., Smoot, G.F., Wright, E.I., 1996. Microwave emission at high galactic latitudes in the four-year DMR sky maps. ApJ 464, L5. http://dx.doi.org/10.1086/310072.
Kogut, A., Dunkley, J., Bennett, C.L., Doré, O., Gold, B., Halpern, M., Hinshaw, G., Jarosik, N., Komatsu, E., Nolta, M.R., Odegard, N., Page, L., Spergel, D.N., Tucker, G.S., Weiland, J.L., Wollack, E., Wright, E.L., 2007. Three-year Wilkinson microwave anisotropy probe (WMAP) observations: foreground polarization. ApJ 665, 355–362. http://dx.doi.org/10.1086/519754.
Kogut, A., Fixsen, D.J., Levin, S.M., Limon, M., Lubin, P.M., Mirel, P., Seiffert, M., Singal, J., Villela, T., Wollack, E., Wuensche, C.A., 2011. ARCADE 2 observations of galactic radio emission. ApJ 734, 4. http://dx.doi.org/10.1088/0004-637X/734/1/4.
Kurtz, S., 2002. Ultracompact HII regions. In: Crowther, P. (Ed.), Hot Star Workshop III: The Earliest Phases of Massive Star Birth. Astronomical Society of the Pacific Conference Series 267. pp. 81.
Kurtz, S., 2005. Hypercompact HII regions. In: Cesaroni, R., Felli, M., Churchwell, E., Walmsley, M. (Eds.), Massive Star Birth: A Crossroads of Astrophysics. IAU Symposium 227. pp. 111–119. http://dx.doi.org/10.1017/S1743921305004424.
Kurtz, S., Churchwell, E., Wood, D.O.S., 1994. Ultracompact H II regions. 2: new high-resolution radio images. ApJS 91, 659–712. http://dx.doi.org/10.1086/191952.
Lagache, G., 2003. The large-scale anomalous microwave emission revisited by WMAP. A&A 405, 813–819. http://dx.doi.org/10.1051/0004-6361:20030545.
Lazarian, A., Draine, B.T., 1999. Thermal flipping and thermal trapping: new elements in grain dynamics. ApJ 516, L37–L40. http://dx.doi.org/10.1086/311986.
Lazarian, A., Draine, B.T., 2000. Resonance paramagnetic relaxation and alignment of small grains. ApJ 536, L15–L18. http://dx.doi.org/10.1086/312720.
Leitch, E.M., Readhead, A.C.S., Pearson, T.J., Myers, S.T., 1997. An anomalous component of galactic emission. ApJ 486, L23. http://dx.doi.org/10.1086/310823.
Lenz, D., Hensley, B.S., Doré, O., 2017. A new, large-scale map of interstellar reddening derived from HI emission. Submitted to ApJ. arXiv:1706.00011.
Li, A., Draine, B.T., 2002. Do the infrared emission features need ultraviolet excitation? The polycyclic aromatic hydrocarbon model in UV-poor reflection nebulae. ApJ 572, 232–237. http://dx.doi.org/10.1086/340285.
Li, T.Y., Wechsler, R.H., Devaraj, K., Church, S.E., 2016. Connecting CO intensity mapping to molecular gas and star formation in the epoch of galaxy assembly. ApJ 817, 169. http://dx.doi.org/10.3847/0004-637X/817/2/169.
López-Caraballo, C.H., Rubiño-Martín, J.A., Rebolo, R., Génova-Santos, R., 2011. Constraints on the polarization of the anomalous microwave emission in the Perseus molecular complex from seven-year WMAP data. ApJ 729, 25. http://dx.doi.org/10.1088/0004-637X/729/1/25.
Lu, M., Dunkley, J., Page, L., 2012. Evidence for anomalous dust-correlated emission at 8 GHz. ApJ 749, 165. http://dx.doi.org/10.1088/0004-637X/749/2/165.
Macellari, N., Pierpaoli, E., Dickinson, C., Vaillancourt, J.E., 2011. Galactic foreground contributions to the 5-year Wilkinson microwave anisotropy probe maps. MNRAS 418, 888–905. http://dx.doi.org/10.1111/j.1365-2966.2011.19542.x.
Martin, P.G., Clayton, G.C., Wolff, M.J., 1999. Ultraviolet interstellar linear polarization. V. Analysis of the final data set. ApJ 510, 905–914. http://dx.doi.org/10.1086/306613.
Martin, P.G., Roy, A., Bontemps, S., Miville-Deschênes, M.-A., Ade, P.A.R., Bock, J.J., Chapin, E.L., Devlin, M.J., Dicker, S.R., Griffin, M., et al., 2012. Evidence for environmental changes in the submillimeter dust opacity. ApJ 751, 28. http://dx.doi.org/10.1088/0004-637X/751/1/28.
Mason, B.S., Robishaw, T., Heiles, C., Finkbeiner, D., Dickinson, C., 2009. A limit on the polarized anomalous microwave emission of Lynds 1622. ApJ 697, 1187–1193. http://dx.doi.org/10.1088/0004-637X/697/2/1187.
Matsuura, M., Bernard-Salas, J., Lloyd Evans, T., Volk, K.M., Hrivnak, B.J., Sloan, G.C., Chu, Y.-H., Gruendl, R., Kraemer, K.E., Peeters, E., et al., 2014. Spitzer space telescope spectra of post-AGB stars in the large magellanic cloud - polycyclic aromatic hydrocarbons at low metallicities. MNRAS 439, 1472–1493. http://dx.doi.org/10.1093/mnras/stt2495.
McDonald, I., Sloan, G.C., Zijlstra, A.A., Matsunaga, N., Matsuura, M., Kraemer, K.E., Bernard-Salas, J., Markwick, A.J., 2010. Rusty old stars: a source of the missing interstellar iron? ApJ 717, L92–L97. http://dx.doi.org/10.1088/2041-8205/717/2/L92.
McDonald, I., van Loon, J.T., Sloan, G.C., Dupree, A.K., Zijlstra, A.A., Boyer, M.L., Gehrz, R.D., Evans, A., Woodward, C.E., Johnson, C.I., 2011. Spitzer spectra of evolved stars in ω Centauri and their low-metallicity dust production. MNRAS 417, 20–31. http://dx.doi.org/10.1111/j.1365-2966.2011.18963.x.
McDonald, I., Zijlstra, A.A., 2015. Globular cluster interstellar media: ionized and ejected by white dwarfs. MNRAS 446, 2226–2242. http://dx.doi.org/10.1093/mnras/stu2202.
Meny, C., Gromov, V., Boudet, N., Bernard, J.-P., Paradis, D., Nayral, C., 2007. Far-infrared to millimeter astrophysical dust emission. I. A model based on physical properties of amorphous solids. A&A 468, 171–188. http://dx.doi.org/10.1051/0004-6361:20065771.
Miville-Deschênes, M., Lagache, G., 2005. IRIS: a new generation of IRAS maps. ApJS 157, 302–323. http://dx.doi.org/10.1086/427938.
Miville-Deschênes, M., Ysard, N., Lavabre, A., Ponthieu, N., Macías-Pérez, J.F., Aumont, J., Bernard, J.P., 2008. Separation of anomalous and synchrotron emissions using WMAP polarization data. A&A 490, 1093–1102. http://dx.doi.org/10.1051/0004-6361:200809484.
Morrish, A.H., 2001. The Physical Principles of Magnetism. Wiley-VCH.
Mukherjee, P., Coble, K., Dragovan, M., Ganga, K., Kovac, J., Ratra, B., Souradeep, T., 2003. Galactic foreground constraints from the Python V cosmic microwave background anisotropy data. ApJ 592, 692–698. http://dx.doi.org/10.1086/375860.
Mukherjee, P., Jones, A.W., Kneissl, R., Lasenby, A.N., 2001. On dust-correlated galactic emission in the tenerife data. MNRAS 320, 224–234. http://dx.doi.org/10.1046/j.1365-8711.2001.03961.x.
Murphy, E.J., 2009. The far-infrared-radio correlation at high redshifts: physical considerations and prospects for the square kilometer array. ApJ 706, 482–496. http://dx.doi.org/10.1088/0004-637X/706/1/482.
Murphy, E.J., Bremseth, J., Mason, B.S., Condon, J.J., Schinnerer, E., Aniano, G., Armus, L., Helou, G., Turner, J.L., Jarrett, T.H., 2012. The star formation in radio survey: GBT 33 GHz observations of nearby galaxy nuclei and extranuclear star-forming regions. ApJ 761, 97. http://dx.doi.org/10.1088/0004-637X/761/2/97.
Murphy, E.J., Condon, J.J., Schinnerer, E., Kennicutt, R.C., Calzetti, D., Armus, L., Helou, G., Turner, J.L., Aniano, G., Beirão, P., et al., 2011. Calibrating extinction-free star formation rate diagnostics with 33 GHz free–free emission in NGC 6946. ApJ 737, 67. http://dx.doi.org/10.1088/0004-637X/737/2/67.
Murphy, E.J., Helou, G., Condon, J.J., Schinnerer, E., Turner, J.L., Beck, R., Mason, B.S., Chary, R., Armus, L., 2010. The detection of anomalous dust emission in the nearby galaxy NGC 6946. ApJ 709, L108–L113. http://dx.doi.org/10.1088/2041-8205/709/2/L108.
Murphy, E.J., Momjian, E., Condon, J.J., Chary, R.-R., Dickinson, M., Inami, H., Taylor, A.R., Weiner, B.J., 2017. The GOODS-N Jansky VLA 10 GHz pilot survey: sizes of star-

forming μJY radio sources. ApJ 839, 35. http://dx.doi.org/10.3847/1538-4357/aa62fd.
Onić, D., 2013. On the supernova remnants with flat radio spectra. Ap&SS 346, 3–13. http://dx.doi.org/10.1007/s10509-013-1444-z.
Padin, S., Shepherd, M.C., Cartwright, J.K., Keeney, R.G., Mason, B.S., Pearson, T.J., Readhead, A.C.S., Schaal, W.A., Sievers, J., Udomprasert, P.S., Yamasaki, J.K., Holzapfel, W.L., Carlstrom, J.E., Joy, M., Myers, S.T., Otarola, A., 2002. The cosmic background imager. PASP 114, 83–97. http://dx.doi.org/10.1086/324786.
Pake, G., 1962. Paramagnetic resonance: an introductory monograph. Frontiers in Physics. W.A. Benjamin.
Paladini, R., Ingallinera, A., Agliozzo, C., Tibbs, C.T., Noriega-Crespo, A., Umana, G., Dickinson, C., Trigilio, C., 2015. Anomalous microwave emission in HII regions: is it really anomalous? The case of RCW 49. ApJ 813, 24. http://dx.doi.org/10.1088/0004-637X/813/1/24.
Paradis, D., Reach, W.T., Bernard, J.-P., Block, M., Engelbracht, C.W., Gordon, K., Hora, J.L., Indebetouw, R., Kawamura, A., Meade, M., Meixner, M., Sewilo, M., Vijh, U.P., Volk, K., 2009. Spatial variations of dust abundances across the large magellanic cloud. AJ 138, 196–209. http://dx.doi.org/10.1088/0004-6256/138/1/196.
Peel, M.W., Dickinson, C., Davies, R.D., Banday, A.J., Jaffe, T.R., Jonas, J.L., 2012. Template fitting of WMAP 7-year data: anomalous dust or flattening synchrotron emission? MNRAS 424, 2676–2685. http://dx.doi.org/10.1111/j.1365-2966.2012.21358.x.
Peel, M.W., Dickinson, C., Davies, R.D., Clements, D.L., Beswick, R.J., 2011. Radio to infrared spectra of late-type galaxies with Planck and Wilkinson microwave anisotropy probe data. MNRAS 416, L99–L103. http://dx.doi.org/10.1111/j.1745-3933.2011.01108.x.
Perrott, Y.C., Cantwell, T.M., Carey, S.H., Elwood, P.J., Feroz, F., Grainge, K.J.B., Green, D.A., Hobson, M.P., Javid, K., Jin, T.Z., Pooley, G.G., Razavi-Ghods, N., Rumsey, C., Saunders, R.D.E., Scaife, A.M.M., Schammel, M.P., Scott, P.F., Shimwell, T.W., Titterington, D.J., Waldram, E.M., 2017. AMI-CL J0300 + 2613: a Galactic anomalous-microwave-emission ring masquerading as a galaxy cluster. MNRAS, submitted. arXiv:1709.05136.
Perrott, Y.C., Scaife, A.M.M., Hurley-Walker, N., Grainge, K.J.B., 2013. Investigating the source of planck-detected AME: high-resolution observations at 15 GHz. Adv. Astron. 2013, 354259. http://dx.doi.org/10.1155/2013/354259.
Phillips, W.A., 1973. Tunneling states and the low-temperature thermal expansion of glasses. J. Low Temp. Phys. 11, 757–763. http://dx.doi.org/10.1007/BF00654457.
Planck Collaboration, Abergel, A., Ade, P.A.R., Aghanim, N., Alves, M.I.R., Aniano, G., Armitage-Caplan, C., Arnaud, M., Ashdown, M., Atrio-Barandela, F., et al., 2014a. Planck 2013 results. XI. All-sky model of thermal dust emission. A&A 571, A11. http://dx.doi.org/10.1051/0004-6361/201323195.
Planck Collaboration, Abergel, A., Ade, P.A.R., Aghanim, N., Alves, M.I.R., Aniano, G., Arnaud, M., Ashdown, M., Aumont, J., Baccigalupi, C., et al., 2014b. Planck intermediate results. XVII. Emission of dust in the diffuse interstellar medium from the far-infrared to microwave frequencies. A&A 566, A55. http://dx.doi.org/10.1051/0004-6361/201323270.
Planck Collaboration, Abergel, A., Ade, P.A.R., Aghanim, N., Arnaud, M., Ashdown, M., Aumont, J., Baccigalupi, C., Balbi, A., Banday, A.J., et al., 2011a. Planck early results. XXI. Properties of the interstellar medium in the Galactic plane. A&A 536, A21. http://dx.doi.org/10.1051/0004-6361/201116455.
Planck Collaboration, Adam, R., Ade, P.A.R., Aghanim, N., Akrami, Y., Alves, M.I.R., Argüeso, F., Arnaud, M., Arroja, F., Ashdown, M., et al., 2016a. Planck 2015 results. I. Overview of products and scientific results. A&A 594, A1. http://dx.doi.org/10.1051/0004-6361/201527101.
Planck Collaboration, Adam, R., Ade, P.A.R., Aghanim, N., Alves, M.I.R., Arnaud, M., Ashdown, M., Aumont, J., Baccigalupi, C., Banday, A.J., et al., 2016b. Planck 2015 results. X. Diffuse component separation: foreground maps. A&A 594, A10. http://dx.doi.org/10.1051/0004-6361/201525967.
Planck Collaboration, Adam, R., Ade, P.A.R., Aghanim, N., Arnaud, M., Ashdown, M., Aumont, J., Baccigalupi, C., Banday, A.J., Barreiro, R.B., et al., 2016c. Planck 2015 results. IX. Diffuse component separation: CMB maps. A&A 594, A9. http://dx.doi.org/10.1051/0004-6361/201525936.
Planck Collaboration, Ade, P.A.R., Aghanim, N., Alina, D., Alves, M.I.R., Armitage-Caplan, C., Arnaud, M., Arzoumanian, D., Ashdown, M., Atrio-Barandela, F., et al., 2015a. Planck intermediate results. XIX. An overview of the polarized thermal emission from Galactic dust. A&A 576, A104. http://dx.doi.org/10.1051/0004-6361/201424082.
Planck Collaboration, Ade, P. A. R., Aghanim, N., Alves, M. I. R., Arnaud, M., Ashdown, M., Atrio-Barandela, F., Aumont, J., Baccigalupi, C., Banday, A. J., et al. 2014c. Planck intermediate results. XXIII. Galactic plane emission components derived from Planck with ancillary data. ArXiv e-prints.
Planck Collaboration, Ade, P.A.R., Aghanim, N., Alves, M.I.R., Arnaud, M., Ashdown, M., Aumont, J., Baccigalupi, C., Banday, A.J., Barreiro, R.B., et al., 2016d. Planck 2015 results. XXV. Diffuse low-frequency Galactic foregrounds. A&A 594, A25. http://dx.doi.org/10.1051/0004-6361/201526803.
Planck Collaboration, Ade, P.A.R., Aghanim, N., Alves, M.I.R., Arnaud, M., Atrio-Barandela, F., Aumont, J., Baccigalupi, C., Banday, A.J., Barreiro, R.B., et al., 2014d. Planck intermediate results. XV. A study of anomalous microwave emission in Galactic clouds. A&A 565, A103. http://dx.doi.org/10.1051/0004-6361/201322612.
Planck Collaboration, Ade, P.A.R., Aghanim, N., Armitage-Caplan, C., Arnaud, M., Ashdown, M., Atrio-Barandela, F., Aumont, J., Baccigalupi, C., Banday, A.J., et al., 2014e. Planck 2013 results. XII. Diffuse component separation. A&A 571, A12. http://dx.doi.org/10.1051/0004-6361/201321580.
Planck Collaboration, Ade, P.A.R., Aghanim, N., Arnaud, M., Ashdown, M., Atrio-Barandela, F., Aumont, J., Baccigalupi, C., Balbi, A., Banday, A.J., et al., 2013. Planck intermediate results. IX. Detection of the Galactic haze with Planck. A&A 554, A139. http://dx.doi.org/10.1051/0004-6361/201220271.
Planck Collaboration, Ade, P.A.R., Aghanim, N., Arnaud, M., Ashdown, M., Aumont, J., Baccigalupi, C., Balbi, A., Banday, A.J., Barreiro, R.B., et al., 2011b. Planck early results. XVII. Origin of the submillimetre excess dust emission in the magellanic clouds. A&A 536, A17. http://dx.doi.org/10.1051/0004-6361/201116473.
Planck Collaboration, Ade, P.A.R., Aghanim, N., Arnaud, M., Ashdown, M., Aumont, J., Baccigalupi, C., Balbi, A., Banday, A.J., Barreiro, R.B., et al., 2011c. Planck early results. XX. New light on anomalous microwave emission from spinning dust grains. A&A 536, A20. http://dx.doi.org/10.1051/0004-6361/201116470.
Planck Collaboration, Ade, P.A.R., Aghanim, N., Arnaud, M., Ashdown, M., Aumont, J., Baccigalupi, C., Balbi, A., Banday, A.J., Barreiro, R.B., et al., 2011d. Planck early results. XXIII. The first all-sky survey of Galactic cold clumps. A&A 536, A23. http://dx.doi.org/10.1051/0004-6361/201116472.
Planck Collaboration, Ade, P.A.R., Aghanim, N., Arnaud, M., Ashdown, M., Aumont, J., Baccigalupi, C., Banday, A.J., Barreiro, R.B., Bartolo, N., et al., 2015b. Planck intermediate results. XXV. The Andromeda galaxy as seen by Planck. A&A 582, A28. http://dx.doi.org/10.1051/0004-6361/201424643.
Planck Collaboration, Ade, P.A.R., Aghanim, N., Arnaud, M., Ashdown, M., Aumont, J., Baccigalupi, C., Banday, A.J., Barreiro, R.B., Bartolo, N., et al., 2016e. Planck 2015 results. XXVIII. The Planck catalogue of galactic cold clumps. A&A 594, A28. http://dx.doi.org/10.1051/0004-6361/201525819.
Planck Collaboration, Ade, P.A.R., Alves, M.I.R., Aniano, G., Armitage-Caplan, C., Arnaud, M., Atrio-Barandela, F., Aumont, J., Baccigalupi, C., Banday, A.J., et al., 2015c. Planck intermediate results. XXII. Frequency dependence of thermal emission from Galactic dust in intensity and polarization. A&A 576, A107. http://dx.doi.org/10.1051/0004-6361/201424088.
Planck Collaboration, Aghanim, N., Ashdown, M., Aumont, J., Baccigalupi, C., Ballardini, M., Banday, A.J., Barreiro, R.B., Bartolo, N., Basak, S., et al., 2016f. Planck intermediate results. XLVIII. Disentangling Galactic dust emission and cosmic infrared background anisotropies. A&A 596, A109. http://dx.doi.org/10.1051/0004-6361/201629022.
Planck Collaboration, Arnaud, M., Atrio-Barandela, F., Aumont, J., Baccigalupi, C., Banday, A.J., Barreiro, R.B., Battaner, E., Benabed, K., Benoit-Lévy, A., et al., 2015d. Planck intermediate results. XVIII. The millimetre and sub-millimetre emission from planetary nebulae. A&A 573, A6. http://dx.doi.org/10.1051/0004-6361/201423836.
Poidevin, F., Falceta-Gonçalves, D., Kowal, G., de Gouveia Dal Pino, E., Mário Magalhães, A., 2013. Magnetic field components analysis of the SCUPOL 850 μm polarization data catalog. ApJ 777, 112. http://dx.doi.org/10.1088/0004-637X/777/2/112.
Povich, M.S., Stone, J.M., Churchwell, E., Zweibel, E.G., Wolfire, M.G., Babler, B.L., Indebetouw, R., Meade, M.R., Whitney, B.A., 2007. A multiwavelength study of M17: the spectral energy distribution and PAH emission morphology of a massive star formation region. ApJ 660, 346–362. http://dx.doi.org/10.1086/513073.
Prandoni, I., Murgia, M., Tarchi, A., Burgay, M., Castangia, P., Egron, E., Govoni, F., Pellizzoni, A., Ricci, R., Righini, S., et al., 2017. The Sardinia radio telescope: from a technological project to a radio observatory. Astron. Astrophys., accepted. arXiv:1703.09673.
Purcell, C.R., Hoare, M.G., Cotton, W.D., Lumsden, S.L., Urquhart, J.S., Chandler, C., Churchwell, E.B., Diamond, P., Dougherty, S.M., Fender, R.P., et al., 2013. The co-ordinated radio and infrared survey for high-mass star formation. II. Source catalog. ApJS 205, 1. http://dx.doi.org/10.1088/0067-0049/205/1/1.
Purcell, E.M., 1969. On the absorption and emission of light by interstellar grains. ApJ 158, 433. http://dx.doi.org/10.1086/150207.
Purcell, E.M., 1979. Suprathermal rotation of interstellar grains. ApJ 231, 404–416.
Rafikov, R.R., 2006. Microwave emission from spinning dust in circumstellar disks. ApJ 646, 288–296. http://dx.doi.org/10.1086/504793.
Ramos-Larios, G., Phillips, J.P., Cuesta, L.C., 2011. The halo and rings of the planetary Nebula NGC 40 in the mid-infrared. MNRAS 411, 1245–1257. http://dx.doi.org/10.1111/j.1365-2966.2010.17756.x.
Reich, P., Reich, W., 1986. A radio continuum survey of the northern sky at 1420 MHz. II. A&AS 63, 205–288.
Reich, P., Reich, W., 1988. A map of spectral indices of the Galactic radio continuum emission between 408 MHz and 1420 MHz for the entire northern sky. A&AS 74, 7–20.
Reich, P., Testori, J.C., Reich, W., 2001. A radio continuum survey of the southern sky at 1420 MHz. The atlas of contour maps. A&A 376, 861–877. http://dx.doi.org/10.1051/0004-6361:20011000.
Reich, W., Reich, P., 2009. Measuring and calibrating galactic synchrotron emission. In: Strassmeier, K.G., Kosovichev, A.G., Beckman, J.E. (Eds.), Cosmic Magnetic Fields: From Planets, to Stars and Galaxies. IAU Symposium 259. pp. 603–612. http://dx.doi.org/10.1017/S1743921309031433.
Remazeilles, M., Banday, A.J., Baccigalupi, C., Basak, S., Bonaldi, A., De Zotti, G., Delabrouille, J., Dickinson, C., Eriksen, H.K., Errard, J., et al., 2017. Exploring cosmic origins with CORE: B-mode component separation. JCAP, accepted. arXiv:1704.04501.
Remazeilles, M., Dickinson, C., Banday, A.J., Bigot-Sazy, M.-A., Ghosh, T., 2015. An improved source-subtracted and destriped 408-MHz all-sky map. MNRAS 451, 4311–4327. http://dx.doi.org/10.1093/mnras/stv1274.
Remazeilles, M., Dickinson, C., Eriksen, H.K.K., Wehus, I.K., 2016. Sensitivity and foreground modelling for large-scale cosmic microwave background B-mode polarization satellite missions. MNRAS 458, 2032–2050. http://dx.doi.org/10.1093/mnras/stw441.
Rosero, V., Hofner, P., Claussen, M., Kurtz, S., Cesaroni, R., Araya, E.D., Carrasco-González, C., Rodríguez, L.F., Menten, K.M., Wyrowski, F., Loinard, L., Ellingsen, S.P., 2016. Weak and compact radio emission in early high-mass star-forming regions. I. VLA observations. ApJS 227, 25. http://dx.doi.org/10.3847/1538-4365/

227/2/25.
Rubiño-Martín, J.A., Génova-Santos, R., Rebolo, R., Aguiar, C.-C., J.M., Gómez-Reñasco, F., Gutiérrez, C., Hoyland, R.J., López-Caraballo, C., Peláez-Santos, A.E., Pérez-de-Taoro, M.R., et al., 2017. The QUIJOTE experiment: project status and first scientific results. In: Arribas, S., Alonso-Herrero, A., Figueras, F., Hernández-Monteagudo, C., Sánchez-Lavega, A., Pérez-Hoyos, S. (Eds.), Highlights on Spanish Astrophysics IX, pp. 99–107.
Rubiño-Martín, J.A., López-Caraballo, C.H., Génova-Santos, R., Rebolo, R., 2012. Observations of the polarisation of the anomalous microwave emission: a review. Adv. Astron. 2012. http://dx.doi.org/10.1155/2012/351836.
Sandstrom, K.M., Bolatto, A.D., Draine, B.T., Bot, C., Stanimirović, S., 2010. The spitzer survey of the small magellanic cloud (s^3MC): insights into the life cycle of polycyclic aromatic hydrocarbons. ApJ 715, 701–723. http://dx.doi.org/10.1088/0004-637X/715/2/701.
Scaife, A.M.M., Green, D.A., Pooley, G.G., Davies, M.L., Franzen, T.M.O., Grainge, K.J.B., Hobson, M.P., Hurley-Walker, N., Lasenby, A.N., Olamaie, M., Richer, J.S., Rodríguez-Gonzálvez, C., Saunders, R.D.E., Scott, P.F., Shimwell, T.W., Titterington, D.J., Waldram, E.M., Zwart, J.T.L., 2010. High-resolution AMI large array imaging of spinning dust sources: spatially correlated 8 μm emission and evidence of a stellar wind in L675. MNRAS 403, L46–L50. http://dx.doi.org/10.1111/j.1745-3933.2010.00812.x.
Scaife, A.M.M., Hurley-Walker, N., Davies, M.L., Duffett-Smith, P.J., Feroz, F., Grainge, K.J.B., Green, D.A., Hobson, M.P., Kaneko, T., Lasenby, A.N., Pooley, G.G., Saunders, R.D.E., Scott, P.F., Titterington, D.J., Waldram, E.M., Zwart, J., 2008. AMI limits on 15-GHz excess emission in northern HII regions. MNRAS 385, 809–822. http://dx.doi.org/10.1111/j.1365-2966.2007.12743.x.
Scaife, A.M.M., Hurley-Walker, N., Green, D.A., Davies, M.L., Franzen, T.M.O., Grainge, K.J.B., Hobson, M.P., Lasenby, A.N., Pooley, G.G., Rodríguez-Gonzálvez, C., Saunders, R.D.E., Scott, P.F., Shimwell, T.W., Titterington, D.J., Waldram, E.M., Zwart, J.T.L., 2009. AMI observations of Lynds dark nebulae: further evidence for anomalous cm-wave emission. MNRAS 400, 1394–1412. http://dx.doi.org/10.1111/j.1365-2966.2009.15542.x.
Scaife, A.M.M., Nikolic, B., Green, D.A., Beck, R., Davies, M.L., Franzen, T.M.O., Grainge, K.J.B., Hobson, M.P., Hurley-Walker, N., Lasenby, A.N., Olamaie, M., Pooley, G.G., Rodríguez-Gonzálvez, C., Saunders, R.D.E., Scott, P.F., Shimwell, T.W., Titterington, D.J., Waldram, E.M., Zwart, J.T.L., 2010. Microwave observations of spinning dust emission in NGC6946. MNRAS 406, L45–L49. http://dx.doi.org/10.1111/j.1745-3933.2010.00878.x.
Seljak, U., Zaldarriaga, M., 1997. Signature of gravity waves in the polarization of the microwave background. Phys. Rev. Lett. 78, 2054–2057. http://dx.doi.org/10.1103/PhysRevLett.78.2054.
Seok, J.Y., Li, A., 2016. Dust and polycyclic aromatic hydrocarbon in the pre-transitional disk around HD 169142. ApJ 818, 2. http://dx.doi.org/10.3847/0004-637X/818/1/2.
Silsbee, K., Ali-Haïmoud, Y., Hirata, C.M., 2011. Spinning dust emission: the effect of rotation around a non-principal axis. MNRAS 411, 2750–2769. http://dx.doi.org/10.1111/j.1365-2966.2010.17882.x.
Sloan, G.C., Kraemer, K.E., Price, S.D., Shipman, R.F., 2003. A uniform database of 2.4–45.4 micron spectra from the infrared space observatory short wavelength spectrometer. ApJS 147, 379–401. http://dx.doi.org/10.1086/375443.
Sloan, G.C., Lagadec, E., Zijlstra, A.A., Kraemer, K.E., Weis, A.P., Matsuura, M., Volk, K., Peeters, E., Duley, W.W., Cami, J., Bernard-Salas, J., Kemper, F., Sahai, R., 2014. Carbon-rich dust past the asymptotic giant branch: aliphatics, aromatics, and fullerenes in the magellanic clouds. ApJ 791, 28. http://dx.doi.org/10.1088/0004-637X/791/1/28.
Strong, A.W., Orlando, E., Jaffe, T.R., 2011. The interstellar cosmic-ray electron spectrum from synchrotron radiation and direct measurements. A&A 534, A54. http://dx.doi.org/10.1051/0004-6361/201116828.
Tibbs, C.T., Flagey, N., Paladini, R., Compiègne, M., Shenoy, S., Carey, S., Noriega-Crespo, A., Dickinson, C., Ali-Haïmoud, Y., Casassus, S., Cleary, K., Davies, R.D., Davis, R.J., Hirata, C.M., Watson, R.A., 2011. Spitzer characterization of dust in an anomalous emission region: the Perseus cloud. MNRAS 418, 1889–1900. http://dx.doi.org/10.1111/j.1365-2966.2011.19605.x.
Tibbs, C.T., Paladini, R., Cleary, K., Muchovej, S.J.C., Scaife, A.M.M., Stevenson, M.A., Laureijs, R.J., Ysard, N., Grainge, K.J.B., Perrott, Y.C., Rumsey, C., Villadsen, J., 2015. CARMA observations of Galactic cold cores: searching for spinning dust emission. MNRAS 453, 3356–3374. http://dx.doi.org/10.1093/mnras/stv1760.
Tibbs, C.T., Paladini, R., Cleary, K., Muchovej, S.J.C., Scaife, A.M.M., Stevenson, M.A., Laureijs, R.J., Ysard, N., Grainge, K.J.B., Perrott, Y.C., Rumsey, C., Villadsen, J., 2016. Using cm observations to constrain the abundance of very small dust grains in Galactic cold cores. MNRAS 456, 2290–2300. http://dx.doi.org/10.1093/mnras/stv2759.
Tibbs, C.T., Paladini, R., Compiègne, M., Dickinson, C., Alves, M.I.R., Flagey, N., Shenoy, S., Noriega-Crespo, A., Carey, S., Casassus, S., Davies, R.D., Davis, R.J., Molinari, S., Elia, D., Pestalozzi, M., Schisano, E., 2012. A multi-wavelength investigation of RCW175: an H II region harboring spinning dust emission. ApJ 754, 94. http://dx.doi.org/10.1088/0004-637X/754/2/94.
Tibbs, C.T., Paladini, R., Dickinson, C., 2012. On the limitations of the anomalous microwave emission emissivity. Adv. Astron. http://dx.doi.org/10.1155/2012/124931.
Tibbs, C.T., Paladini, R., Dickinson, C., Mason, B.S., Casassus, S., Cleary, K., Davies, R.D., Davis, R.J., Watson, R.A., 2013. Constraints on free–free emission from anomalous microwave emission sources in the perseus molecular cloud. ApJ 770, 122. http://dx.doi.org/10.1088/0004-637X/770/2/122.
Tibbs, C.T., Scaife, A.M.M., Dickinson, C., Paladini, R., Davies, R.D., Davis, R.J., Grainge, K.J.B., Watson, R.A., 2013. AMI observations of the anomalous microwave emission in the perseus molecular cloud. ApJ 768, 98. http://dx.doi.org/10.1088/0004-637X/768/2/98.
Tibbs, C.T., Watson, R.A., Dickinson, C., Davies, R.D., Davis, R.J., Buckmaster, S., Del Burgo, C., Franzen, T.M.O., Génova-Santos, R., Grainge, K., Hobson, M.P., Padilla-Torres, C.P., Rebolo, R., Rubiño-Martín, J.A., Saunders, R.D.E., Scaife, A.M.M., Scott, P.F., 2010. Very small array observations of the anomalous microwave emission in the perseus region. MNRAS 402, 1969–1979. http://dx.doi.org/10.1111/j.1365-2966.2009.16023.x.
Tielens, A.G.G.M., 2010. The Physics and Chemistry of the Interstellar Medium. Cambridge University Press.
Tielens, A.G.G.M., 2013. The molecular universe. Rev. Mod. Phys. 85, 1021–1081. http://dx.doi.org/10.1103/RevModPhys.85.1021.
Todorović, M., Davies, R.D., Dickinson, C., Davis, R.J., Cleary, K.A., Génova-Santos, R., Grainge, K.J.B., Hafez, Y.A., Hobson, M.P., Jones, M.E., Lancaster, K., Rebolo, R., Reich, W., Rubiño-Martín, J.A., Saunders, R.D.E., Savage, R.S., Scott, P.F., Slosar, A., Taylor, A.C., Watson, R.A., 2010. A 33-GHz very small array survey of the galactic plane from l = 27 deg to 46 deg. MNRAS 406, 1629–1643. http://dx.doi.org/10.1111/j.1365-2966.2010.16809.x.
Vidal, M., Casassus, S., Dickinson, C., Witt, A.N., Castellanos, P., Davies, R.D., Davis, R.J., Cabrera, G., Cleary, K., Allison, J.R., Bond, J.R., Bronfman, L., Bustos, R., Jones, M.E., Paladini, R., Pearson, T.J., Readhead, A.C.S., Reeves, R., Sievers, J.L., Taylor, A.C., 2011. Dust-correlated cm wavelength continuum emission from translucent clouds ζ Oph and LDN 1780. MNRAS 414, 2424–2435. http://dx.doi.org/10.1111/j.1365-2966.2011.18562.x.
Vidal, M., Dickinson, C., Davies, R.D., Leahy, J.P., 2015. Polarized radio filaments outside the galactic plane. MNRAS 452, 656–675. http://dx.doi.org/10.1093/mnras/stv1328.
Visser, R., Geers, V.C., Dullemond, C.P., Augereau, J.-C., Pontoppidan, K.M., van Dishoeck, E.F., 2007. PAH chemistry and IR emission from circumstellar disks. A&A 466, 229–241. http://dx.doi.org/10.1051/0004-6361:20066829.
Waller, I., 1932. Über die magnetisierung von paramagnetischen Kristallen in wechselfeldern. Z. Angew. Phys. 79, 370–388. http://dx.doi.org/10.1007/BF01349398.
Watson, R.A., Rebolo, R., Rubiño-Martín, J.A., Hildebrandt, S., Gutiérrez, C.M., Fernández-Cerezo, S., Hoyland, R.J., Battistelli, E.S., 2005. Detection of anomalous microwave emission in the perseus molecular cloud with the COSMOSOMAS experiment. ApJ 624, L89–L92. http://dx.doi.org/10.1086/430519.
Wendker, H.J., 1995. Radio continuum emission from stars: a catalogue update. A&AS 109.
Westphal, A.J., Stroud, R.M., Bechtel, H.A., Brenker, F.E., Butterworth, A.L., Flynn, G.J., Frank, D.R., Gainsforth, Z., Hillier, J.K., Postberg, F., et al., 2014. Evidence for interstellar origin of seven dust particles collected by the stardust spacecraft. Science 345, 786–791. http://dx.doi.org/10.1126/science.1252496.
Woods, P.M., Oliveira, J.M., Kemper, F., van Loon, J.T., Sargent, B.A., Matsuura, M., Szczerba, R., Volk, K., Zijlstra, A.A., Sloan, G.C., et al., 2011. The SAGE-spec spitzer legacy programme: the life-cycle of dust and gas in the large magellanic cloud - point source classification I. MNRAS 411, 1597–1627. http://dx.doi.org/10.1111/j.1365-2966.2010.17794.x.
Ysard, N., Juvela, M., Verstraete, L., 2011. Modelling the spinning dust emission from dense interstellar clouds. A&A 535, A89. http://dx.doi.org/10.1051/0004-6361/201117394.
Ysard, N., Miville-Deschênes, M.A., Verstraete, L., 2010. Probing the origin of the microwave anomalous foreground. A&A 509, L1. http://dx.doi.org/10.1051/0004-6361/200912715.
Ysard, N., Verstraete, L., 2010. The long-wavelength emission of interstellar PAHs: characterizing the spinning dust contribution. A&A 509, A12. http://dx.doi.org/10.1051/0004-6361/200912708.
Zhang, H., Telesco, C.M., Hoang, T., Li, A., Pantin, E., Wright, C.M., Li, D., Barnes, P., 2017. Detection of polarized infrared emission by polycyclic aromatic hydrocarbons in the MWC 1080 nebula. ApJ 844, 6. http://dx.doi.org/10.3847/1538-4357/aa77ff.
Zwart, J.T.L., Barker, R.W., Biddulph, P., Bly, D., Boysen, R.C., Brown, A.R., Clementson, C., Crofts, M., Culverhouse, T.L., Czeres, J., et al., 2008. The arcminute microkelvin imager. MNRAS 391, 1545–1558. http://dx.doi.org/10.1111/j.1365-2966.2008.13953.x.